University of Stavanger

Faculty of Science and Technology

MASTER'S THESIS

Study program/ Specialization: Petroleum Engineering Reservoir technology	Spring semester, 2012 Open
Writer: Ole Andreas Knappskog	…… (Writer's signature)
Faculty supervisor: Hans Kleppe (University of Stavanger) External supervisor: Robert W. Moe (ConocoPhillips)	
Title of thesis: Evaluation of WAG injection at Ekofisk	
Credits (ECTS): 30	
Key words: -HC WAG -SORM -Trapped gas -Hysteresis effect -Minimum miscibility pressure -Minimum miscibility enrichment	Pages: …… + enclosure: …… Stavanger, …….. Date/year

Universitetet i Stavanger

ConocoPhillips

Master's Thesis

Evaluation of WAG injection at Ekofisk

by

Ole Andreas Knappskog

June 15th, 2012

University of Stavanger

Faculty of Science and Technology

Petroleum Engineering, Reservoir Technology

Abstract

In the North Sea many fields are water flooded. Subsequent to water flooding large amounts of water flood residual oil will be left in reservoirs. The challenge is how to improve the oil recovery. On the Ekofisk field such a challenge is to be addressed. The entire reservoir on the Ekofisk field is currently water flooded. The current plan is to continue water injection until the end of license in 2028. To improve oil recovery, EOR mechanisms have been proposed. The EOR mechanism hydrocarbon water-alternating gas has shown good potential and will be studied in this thesis.

The main purpose of this thesis is to evaluate WAG injection at Ekofisk. A number of factors may affect WAG performance, in this study the importance of some of these will be evaluated through simulation work. Miscibility evaluation is performed using a slim-tube simulation model. Mechanistic models are further used to evaluate other key parameters such as trapped gas saturation, hysteresis effect, fracture-matrix system and SORM. Finally a sector model is used to optimize WAG ratios and WAG slug sizes, and to make a comparison of WAG scenarios to a water flood case.

The slim-tube simulation work resulted in the conclusion to use immiscible WAG injection by dry hydrocarbon gas, because of high minimum miscibility pressure and minimum miscibility enrichment.

Mechanistic simulations indicated that trapped gas and SORM should be included in WAG-modeling to avoid over prediction of recoveries for a WAG applications.

Sector simulations showed incremental oil potential to the water flood case for all WAG scenarios. WAG ratio of 1 to 2 gave the largest increase with 8.4 million BOE. Increasing WAG ratio showed decreasing potential. Similar, the WAG slug size of 0.4 pore volumes was best with 4.4 million BOE incremental to the base case. WAG slug sizes showed decreasing potential with decreasing slug sizes.

The results from the sector model indicated the need of optimization of the total volume of gas injected for the WAG application, which is recommended for further studies, together with introducing local grid refinement to avoid numerical dispersion and instability problems.

Table of contents

Acknowledgements

First of all I would like to thank ConocoPhillips for providing me with an interesting and challenging master thesis and for giving me access to all their information and studies. I genuinely appreciate the opportunity to work at ConocoPhillips with some of the best people in this field.

I would especially like to extend my sincere and gratitude to my external supervisor at ConocoPhillips, Robert W. Moe, who has provided me with great guidance and support throughout the process of writing this thesis. He has patiently answered all questions and given me theoretical insight in the difficult parts of my study. I am also grateful for the valuable assistance from the Field Management group, from WAG specialist Arvid Østhus, and from Murali Muralidharan and Russ Bone in ConocoPhillips USA.

Further I would like to give thanks to my internal supervisor at the University of Stavanger, Professor Hans Kleppe for his guidance.

During my time at ConocoPhillips I have enjoyed meeting the other graduates for lunch and coffee breaks. The socialization with you guys has lighted up my workday.

Finally, I thank my family, especially Marija, whose daily support and encouragement I could not do without.

Regards,

Ole Andreas Knappskog,

Stavanger, 15.juni 2012

List of figures

Chapter 2

Chapter 3

Chapter 4

Chapter 5

Chapter 6

Chapter 7

List of tables

Chapter 3

Chapter 4

Chapter 5

Chapter 6

Chapter 7

1 Introduction

Subject and problem statement

In the North Sea many fields are water flooded. Subsequent to water flooding large amounts of water flood residual oil will be left in reservoirs. The challenge is how to improve the oil recovery. It has been recognized that there is large potentials for enhanced oil recovery (EOR). One of the EOR-mechanisms is hydrocarbon water-alternating-gas (HC-WAG) injection.

On the Ekofisk field such a challenge is to be addressed. The entire reservoir on the Ekofisk field is currently water flooded, both vertically and laterally. The current plan is to continue water injection until the end of license in 2028. Since large amounts of water flood residual oil is expected in the reservoir following water flooding, several EOR-mechanisms have been considered to further improve oil recovery on the Ekofisk field. Of the mechanisms, HC-WAG has shown good potential and is the EOR-mechanism which is studied in this thesis.

To model the impact and accurately evaluate the potential oil recovery from a tertiary HC-WAG injection, understanding of parameters and concepts on microscopic scale is essential. Of the important parameters and concepts for WAG-displacement, trapped gas saturation, relative permeability hysteresis effect and miscible flood residual oil saturation (SORM) are evaluated on a pore-scale perspective in this study. During WAG-displacement both two-phase flow and three-phase flow are encountered in different regions of the reservoir. Hence, it is important to understand and model related concepts such as relative permeability and capillary pressure properly based on the number of mobile phases.

The displacement efficiency of WAG-processes is strongly dependent on whether the injected gases are miscible or immiscible with the reservoir oil. To evaluate the condition of gas injection, miscible or immiscible, tests are performed on minimum miscibility pressure (MMP) and minimum miscibility enrichment (MME) of the injected gas and reservoir oil system. Since the Ekofisk field is a fractured chalk reservoir, understanding the matrix – fracture mechanisms will also be important to successfully model a WAG injection.

Evaluation of problem statement

In this thesis evaluation of miscibility is performed using a slim-tube simulation model. Evaluation of miscibility is determined based on the minimum miscibility pressure and the minimum gas enrichment. Based on the results from the miscibility evaluation a decision will be taken to proceed with miscible or immiscible displacement for the further studies.

Important reservoir parameters and the understanding of reservoir mechanisms in a WAG-displacement are then modeled mechanisticly. A homogenous matrix model is used to perform sensitivity runs to evaluate trapped gas saturation and relative permeability hysteresis effect in WAG injection. Further, different matrix-fracture models are developed to identify the impact of different matrix-fracture systems and the residual oil saturation for each system is used as basis for evaluation on SORM. Finally, a sector model, initialized with some of the main parameters from results for the mechanistic models, is used to evaluate the impact of different WAG-ratios and slug sizes, and for comparison with a water flood scenario.

Structure of thesis

The thesis is initiated with a chapter describing the Ekofisk field history and the background for this thesis. Next a literature study on WAG-displacement is given, with presentations of WAG projects worldwide, in the North Sea, and previous WAG-studies on the Ekofisk field that are of interest to this thesis.

The next chapter is a theory chapter. The chapter is initiated with presentation of general reservoir and fluid parameters for reservoir simulations which also are interesting regarding the main parameters of this study. Definitions and explanations of the main parameters and concepts in this thesis as well as important recovery mechanisms for a WAG-process and evaluation of miscibility are then presented. The last part of the theory chapter is an introduction to the full field numerical simulation tool, PSim, which is used for modeling.

The next chapters include descriptions of the three different types of simulation models utilized in this thesis, slim-tube model, mechanistic models and sector model, followed by results and discussion of simulations in these models. In the last chapter main conclusions from the study and recommendations for further research and simulation work is given.

2 Ekofisk field history and background

The Ekofisk field is a giant oil producing field located in block 2/4, in the southern part of the Norwegian Sector of the North Sea, about 300 kilometers southwest of Stavanger. The Ekofisk field is part of the Greater Ekofisk Area, shown in figure 2.1, which makes up totally eight fields. Four of these fields, Ekofisk, Eldfisk, Embla and Tor, are still producing (ConocoPhillips Company (1)) and are part of the production license PL018, which is operated by ConocoPhillips, former Phillips, on behalf of the license co-ventures. Operator ConocoPhillips currently own 35.11 % of the PL018, with the partners Total 39.9 %, Eni Norge AS 12.39 %, Statoil Petroleum AS 7.6 % and Petoro AS 5 % (ConocoPhillips Company (2)).

Figure 2.1: Location of the Greater Ekofisk Area, where the Ekofisk field is one of four producing fields

Discovery of the Ekofisk Field

The petroleum industry first got their eyes on the oil and gas potential in the North Sea in 1959 with the discovery of the giant Groningen onshore gas field in the Netherlands. In 1963 the Phillips Norway Group started seismic surveys in the Norwegian Sector of the North Sea. Two years later, in the 1965, the Norwegian government awarded 22 production licenses, thereby three to the Phillips Norway Group. Phillips started their exploration drilling in 1967, which in 1968 led to the first discovery of petroleum in the Norwegian sector with the Cod gas-condensate sandstone reservoir. Further drilling indicated though that the Cod discovery was not large enough for profitable production, and the field was later abandoned (Dangerfield, et al., 1987), (Norsk Teknisk Museum).

By the fall of 1969 exploration efforts in the North Sea were declining. Over 200 exploration wells had been drilled, thereby 32 Phillips wells, and none had found commercial oil (Sulak, 1990), (Dangerfield, et al., 1987). However, a major turning point in exploration for petroleum in the North Sea was about to occur. On October 25th 1969, a Phillips exploration well drilled from the rig Ocean Viking penetrated an oil-bearing chalk reservoir. Violent autumn storms postponed further drilling and made it difficult to carry out production tests to confirm the discovery. However, early December the process could continue and by little Christmas Eve many knew that a gigantic oil discovery at Ekofisk was made. The oil discovery at Ekofisk was though not public known before June 1970.

The Ekofisk field is the first commercial oil field in the Norwegian North Sea. The discovery at Ekofisk field is seen as the major turning point for petroleum exploration in Western Europe, and rejuvenated the search for oil in the North Sea. Over the next years, five additional fields were discovered in what is now known as the Greater Ekofisk Area (Bark, et al., 1979).

Ekofisk field development

Test production from the Ekofisk field was started in 1971 from the discovery well and three other subsea appraisal wells. Successful test production led to the decision already in 1972 to develop the Ekofisk field with permanent structures. Permanent production facilities

with a design capacity of 54 wells and 300 000 standard oil barrels per day (STB/D) became operational in May 1974 (Sulak, 1990).

The produced oil was initially stored in a one million barrel concrete storage tank and sold via tankers, until October 1975 when a 400 kilometer oil pipeline and stabilizing facilities at Teesside, England were commissioned. Produced gas was initially flared or re-injected into the reservoir via injection wells, until a 500 kilometer gas pipeline to the gas plant in Emden, West Germany was put into service in September 1977. After the installation of the gas pipeline, only gas in excess of contract quantities was re-injected into the reservoir. The oil production at Ekofisk peaked in October 1976 with a production of 350 000 STB/D (Sylte, et al., 1999), (Takla, et al., 1989), (Sulak, 1990).

Oil recovery due to primary depletion, with additional re-injection of gas in excess of contract quantities, was estimated to be 18 % of original oil in place (OOIP). Because of this low oil recovery improved recovery studies were initiated soon after the start of production in 1971 (Christian, et al., 1993).

Water injection

A lot of effort was performed to evaluate how to improve the oil recovery. Water flood laboratory experiments on core plugs initiated in 1977 showed that the Tor formation exhibited excellent spontaneous imbibition characteristics, but that the Ekofisk formation had poor imbibition characteristics. In 1981 a water-flood pilot was initiated in the Tor formation to evaluate water flood performance. The water flood pilot was successful and confirmed the laboratory results. These factors were used as justification for the decision to water flood the northern Tor formation. A 30 wells water-injection platform (2/4 K) with an injection capacity of 375,000 barrels of water per day (BWPD) was approved and water injection commenced in November 1987 (Sylte, et al., 1988, 1999), (Sulak, 1990).

Despite the poor imbibition experimental results for the Ekofisk formation a water flood pilot was initiated to the Lower Ekofisk formation in 1984. The pilot was successful and indicated that water injection of the Ekofisk formation could be effective. The success of this pilot combined with earlier positive results from the water flooding of the northern Tor formation led to the decision to expand water injection. This expansion included injection of

water into the Lower Ekofisk formation as well as expansion of the Tor formation water flood to include the remaining part of the formation. The expanded water flood project was approved in 1989 and increased water injection capacity to 820 000 BWPD (Sylte, et al., 1988, 1999). Following a major field study in 1992, undertaken to determine future operating strategy for the Ekofisk field, the conclusion was drawn to start water flooding of the Upper Ekofisk formation as well (Christian, et al., 1993).

Currently the entire reservoir on the Ekofisk field is being water flooded, both vertically and laterally. The plan is to continue water injection until the end of license in 2028. The estimated recovery factor subsequent to water flooding is expected around 50 percent.

Geological overview

The Ekofisk field is located in the Central Graben in the southern part of the Norwegian Sector of the North Sea. The Central Graben area is a complicated rift system which was created through several phases of extension in the Jurassic period. In the Late Jurassic period thick accumulations of marine shales were deposited in the Central Graben basin. These were very rich in organic content and made up the main source rock in this area. The influx of shale initiated movements in the form of salt swells which eventually created the important hydrocarbon traps in the Ekofisk area. By Maastrichtian time in Late Cretaceous, chalk deposition was widespread in the North Sea with deposition-centers located in the Ekofisk area. Over 3 000 feet of chalk had accumulated in this area by the end of Danian time in Early Paleocene. In the following Tertiary and Quaternary periods more than 10 000 feet of clastic sediments were deposited in the Ekofisk area, which now comprise the Ekofisk overburden. The great layer thickness and following weight of these overburden layers have induced natural fracturing of the chalk (Bark, et al., 1979). Figure 2.2 illustrates the main geological events for the Ekofisk field and the geological timing of these events.

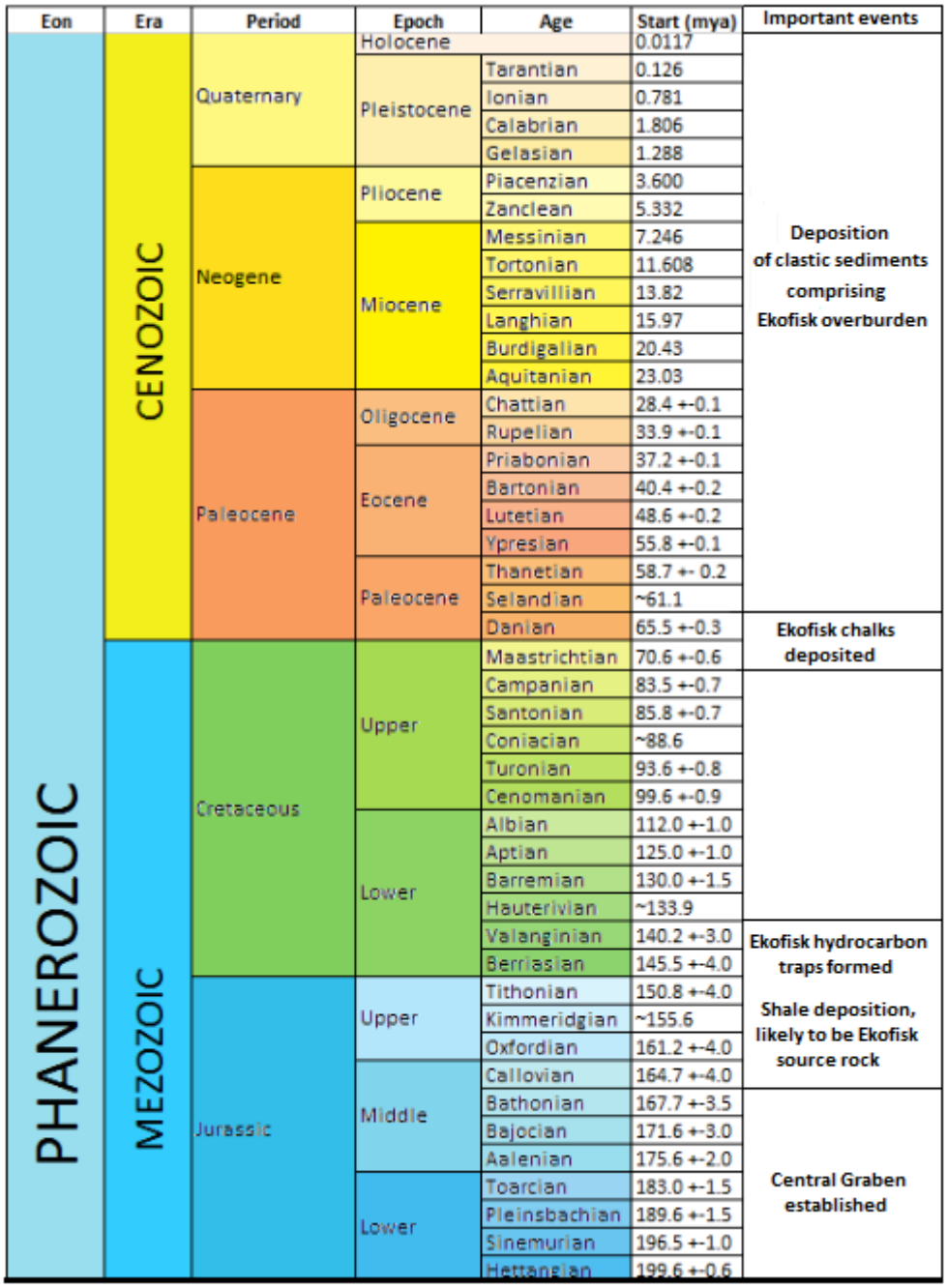

Eon	Era	Period	Epoch	Age	Start (mya)	Important events
PHANEROZOIC	CENOZOIC	Quaternary	Holocene		0.0117	Deposition of clastic sediments comprising Ekofisk overburden
			Pleistocene	Tarantian	0.126	
				Ionian	0.781	
				Calabrian	1.806	
				Gelasian	1.288	
		Neogene	Pliocene	Piacenzian	3.600	
				Zanclean	5.332	
			Miocene	Messinian	7.246	
				Tortonian	11.608	
				Serravillian	13.82	
				Langhian	15.97	
				Burdigalian	20.43	
				Aquitanian	23.03	
		Paleocene	Oligocene	Chattian	28.4 +-0.1	
				Rupelian	33.9 +-0.1	
			Eocene	Priabonian	37.2 +-0.1	
				Bartonian	40.4 +-0.2	
				Lutetian	48.6 +-0.2	
				Ypresian	55.8 +-0.1	
			Paleocene	Thanetian	58.7 +- 0.2	
				Selandian	~61.1	
				Danian	65.5 +-0.3	Ekofisk chalks deposited
	MEZOZOIC	Cretaceous	Upper	Maastrichtian	70.6 +-0.6	
				Campanian	83.5 +-0.7	
				Santonian	85.8 +-0.7	
				Coniacian	~88.6	
				Turonian	93.6 +-0.8	
				Cenomanian	99.6 +-0.9	
			Lower	Albian	112.0 +-1.0	
				Aptian	125.0 +-1.0	
				Barremian	130.0 +-1.5	
				Hauterivian	~133.9	
				Valanginian	140.2 +-3.0	Ekofisk hydrocarbon traps formed
				Berriasian	145.5 +-4.0	
		Jurassic	Upper	Tithonian	150.8 +-4.0	Shale deposition, likely to be Ekofisk source rock
				Kimmeridgian	~155.6	
				Oxfordian	161.2 +-4.0	
			Middle	Callovian	164.7 +-4.0	
				Bathonian	167.7 +-3.5	
				Bajocian	171.6 +-3.0	
				Aalenian	175.6 +-2.0	
			Lower	Toarcian	183.0 +-1.5	Central Graben established
				Pleinsbachian	189.6 +-1.5	
				Sinemurian	196.5 +-1.0	
				Hettangian	199.6 +-0.6	

Figure 2.2: Geological time scale of important geological events for the Ekofisk field

The Ekofisk field structure is an elongated anticline, 10 km long and 5 km wide, with the major axis oriented north-south (Jakobsson & Christian, 1994). The chalk making up the reservoir rock is soft, fine textured, highly porous and is composed almost entirely of skeletal carbonate, particulary from coccolithophorid algaes (Dangerfield, et al., 1987). The fairly similar patterns of chalk sedimentation within the producing part of the Ekofisk field constitute a rather continuous background of chalk deposition interrupted in places by

masses of chalk material deposited elsewhere and introduced in form of turbidities, slumps and debris flows. The producing formations of the Ekofisk field are composed almost exclusively of chalk with similar compositional and mechanical characteristics (Johnson, et al., 1989).

Formations of the Ekofisk field

The Ekofisk reservoir consists of chalk from the Masstrichtian through Upper Danian Age, Late Cretaceous to Early Paleocene epoch. The producing horizons of the Ekofisk field are the Ekofisk and the Tor formations (Johnson, et al., 1989). The Ekofisk field is situated at a sea depth of approximately 200 feet, and the top of the Ekofisk reservoir located at a depth of about 9600 feet.

The Ekofisk formation is divided into three main geological layers. The Upper Ekofisk layer is EA, followed by the middle layer, EM, and the Lower Ekofisk layer, EL. A tight non-producible impermeable zone, represented by the layer EE, separates the Ekofisk and the Tor formations. The underlying Tor formation is subdivided into three geological layers, the upper layer, TA, the middle layer, TB, and the lower layer TC. The uppermost layer, TA, forms the best quality reservoir and also contains the bulk of the reserves in the Tor formation. The Lower Ekofisk layer, EL, is mainly composed of reworked chalk and makes up a good reservoir rock. The upper Ekofisk is more heterogeneous with a higher degree of impurities, mainly silica (Takla, et al., 1989), (Jakobsson, et al., 1994), (Agarwal, et al., 1997).

The full field simulation model of the Ekofisk field is divided into 22 layers. The upper eleven layers comprise the Ekofisk formation, the underlying three layers make up the tight zone, and the remaining buttom eight comprise the Tor formation.

The chalk of the Ekofisk formation has a thickness ranging from 350 to 550 feet with matrix porosities ranging from 25 to 48 %, illustrated in figure 2.3, and a low matrix permeability of 1 to 4 millidarcies (mD). The Tor formation is slightly thinner than the Ekofisk formation, with thickness of 350 to 500 feet with porosities ranging from 25 to 40 % and matrix permeability similar to the Ekofisk formation. The impermeable tight zone separating the producing part of the two formations has a thickness of 50 to 90 feet. Vertical

effective permeability is between 0.001 and 0.1 times that of horizontal effective permeability and depends strongly on the presence of vertical barriers (Jakobsson, et al., 1994). The overburden consists of approximately 9300 feet of clays and shale, which is over pressured below approximately 4500 feet.

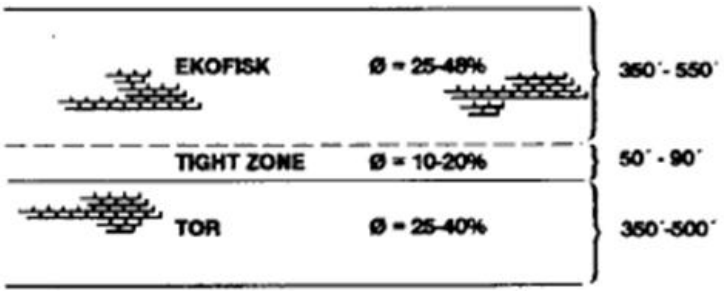

Figure 2.3: Formations of the Ekofisk field (Sulak, 1990)

A chalk reservoir at the depth of the Ekofisk reservoir should normally have porosities less than 10 %. It is therefore important to understand why diagenesis of the Ekofisk and Tor formations has retained porosities ranging from 30 % to over 40 %. There are several possible mechanisms for retaining porosity. At this time, it is appropriate to state that anomalously high porosity in Ekofisk field is probably due to a combination of over pressuring of the reservoir, magnesium-rich pore fluids and early introduction of hydrocarbons into the reservoir (Bark, et al., 1979).

Ekofisk reservoir oil

The original Ekofisk reservoir fluid was an under-saturated, moderately volatile crude oil at initial reservoir absolute pressure of 7103 pounds per square inches (psia) and initial reservoir temperature of 268°Fahrenheit (F) at datum depth of 10 400 ft. The initial oil had an average density of about 850 kg/m^3 and a field wide solution gas to oil ratio (GOR) around 1530 standard cubic feet gas per standard oil barrel (SCF/STB). In 1976 the reservoir oil went through the oil saturation pressure, which initially was 5560 psia at datum depth 10 400 ft, resulting in gas bubbles boiling out of the reservoir oil. The field-wide GOR being constant to this date increased to about 9000 SCF/STB by 1986 (Sulak, 1990). Water flooding of the formations has resulted in the reservoir pressure again increasing above the oil saturation pressure, making the oil under saturated. The current field-wide

GOR is approximately 1100 SCF/STB. The observed field-wide GOR history on the Ekofisk field is illustrated in figure 2.4.

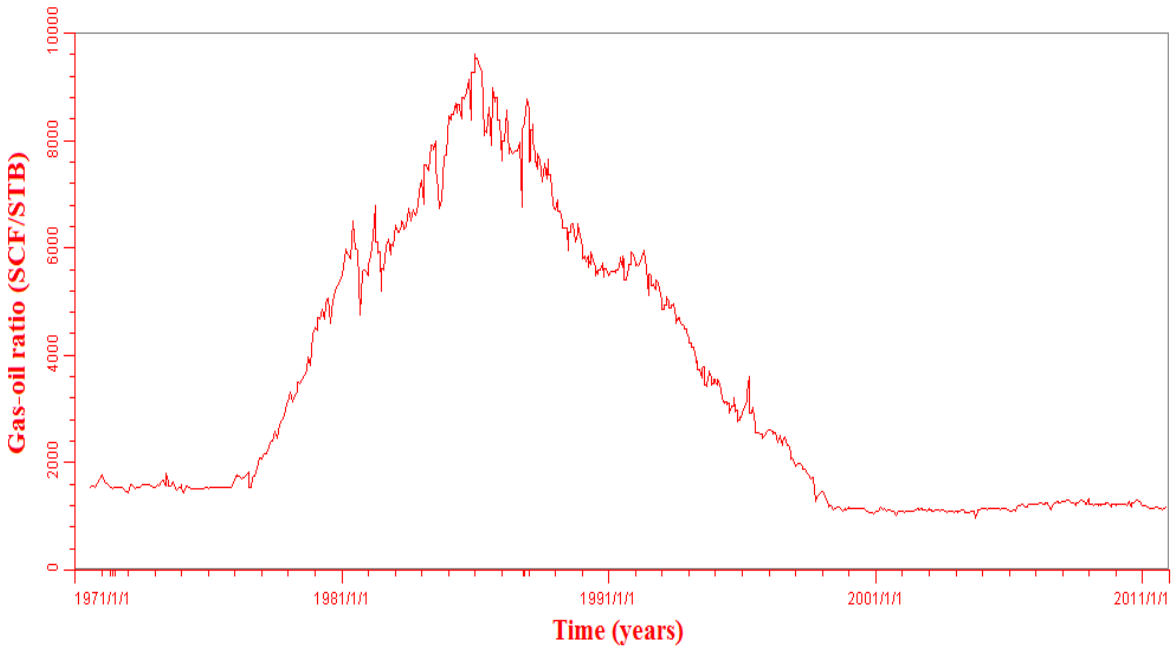

Figure 2.4: Ekofisk field-wide GOR history

Subsidence of the seafloor

The potential of compaction for high porosity chalk was recognized before the development of the Ekofisk field. However, at that time rock mechanics and structural analysis, coupled with case studies, led to development of certain criteria for transfer of reservoir compaction into surface subsidence. These criteria indicated that reservoir compaction at Ekofisk should not lead to significant subsidence (Sulak, et al., 1989). However, in November 1984 subsidence of the seafloor in the vicinity of the Ekofisk complex was discovered, demonstrating that the initial criterias of subsidence were incorrect. The seabed under the Ekofisk complex had subsided about 10 feet by 1984, illustrated in figure 2.5.

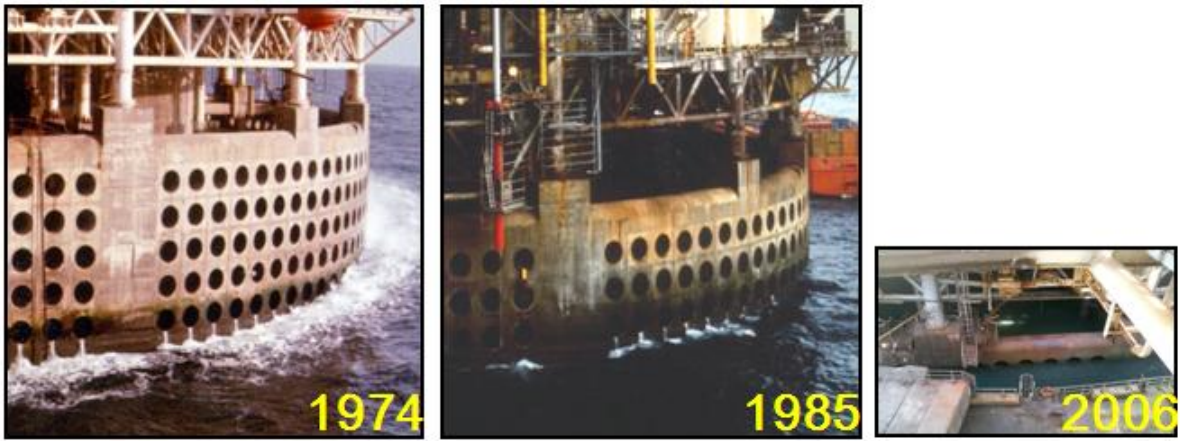

Figure 2.5: Subsidence of Ekofisk seafloor (ConocoPhillips Company(3),2012)

The subsidence is caused by compaction of the reservoir formations being transmitted to the surface through the overburden. Reservoir compaction is caused by deformation of the chalk matrix due increase in effective stress on the rock. The effective stress, the difference between the overburden load on the rock and the pore pressure within the rock, increased due to pressure depletion (Dangerfield, et al., 1987). Under initial conditions, the pore pressure in the reservoir was about 7000 psia. The weight of 3 km thick overburden exerts a pressure of 9000 psia, giving a net effective stress of 2000 psia. With the pore pressure decreasing due to production, the effective stress increases resulting in compaction of the reservoir chalk and following subsidence of the seabed (Jewhurst, et al., 1987).

The main concerns related to the subsidence were protection of the steel platforms and the concrete storage tank. In order to buy time to come up with a solution, produced gas was re-injected and not sold for a period. In 1986 it was decided to elevate the steel platforms and build a concrete protective barrier around the storage tank. All platforms were elevated within 1987 and construction of a protective barrier around the storage tank began in May 1988.

The stepwise increase of water injection in Ekofisk for the purpose of pressure maintenance and improved oil recovery was expected to slow down or eventually stop the subsidence rate. Despite slightly increasing reservoir pressure, subsidence continued just about 40 cm/year to 1998 (Sylte, et al., 1999). After that subsidence rates sharply declined to approximately 10 cm/year, which have continued to present time. Figure 2.6 shows the subsidence rate for the two platforms, Alpha and Bravo, and for the hotel complex.

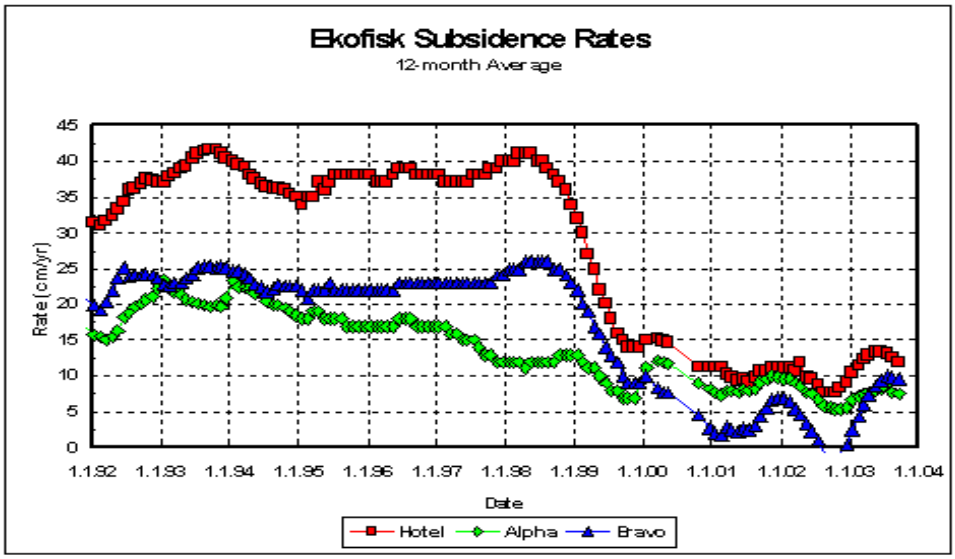

Figure 2.6: Subsidence rate history at Ekofisk (ConocoPhillips Company(3),2012)

Fracture-matrix mechanism

The Ekofisk field has a fracture-matrix mechanism which is crucial for the reservoir being producible. The permeability of the chalk matrix is between 1 and 4 mD. However, the natural fractures can enhance the effective permeability a factor of 50 times the matrix permeability in areas. The effective permeability has been calculated from well tests to be up to 100 to 150 mD. It has been estimated that the reservoir volume represented by fractures is less than 0.5% (Sulak, 1990).

The fractures in the Ekofisk field are of various origins and can generally be classified as stylolite, tectonic, irregular and healed fractures. Stylolite and tectonic fractures, shown in figure 2.7, provide enhanced permeability and are therefore of primary interest. The Ekofisk formation is dominated by tectonic fractures, and stylolite fractures are rare. The Tor formation is dominated by stylolite fractures, but also areas of tectonic fractures (Thomas, et al., 1987). The tectonic fractures in the Ekofisk formation have developed parallel and conjugate sets of fractures. The intensity of fracturing varies both vertically and areally. Highly fractured zone have spacings as small as 5 to 15 centimeters, while zones of lower fracture intensity have spacing of 15 to 100 centimeters. The dip of the tectonic fractures are mainly sub-vertical with a dip varying from 60 to 80 degrees (Hallenbeck, et al., 1989). The stylolites in the Tor formation are parallel to the beding plan and are usually only a few feet

apart. These fractures form permeable zones which can extend laterally for large distances (Dangerfield, et al., 1987).

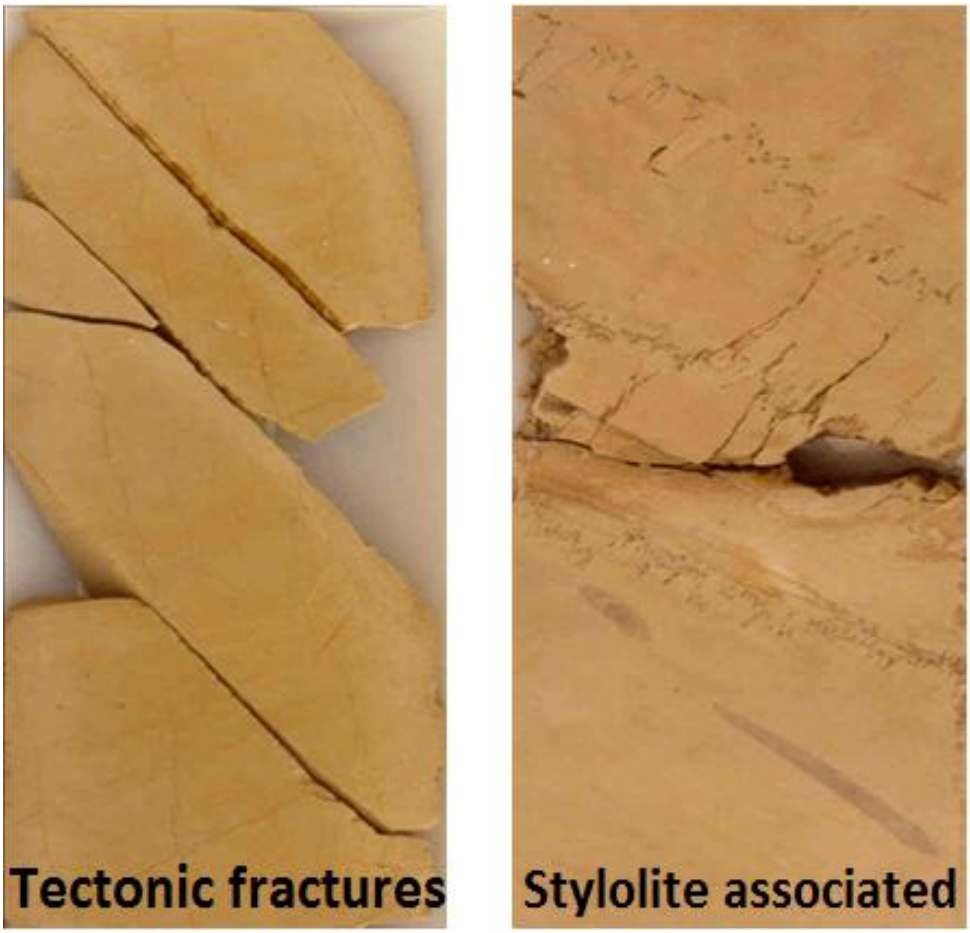

Figure 2.7: Tectonic and stylolite associated fractures (ConocoPhillips Company(3),2012)

Ekofisk drive mechanisms for oil displacement

Solution gas drive and compaction drive have been the dominant natural production mechanisms on the Ekofisk field. Initially, solution gas drive was thought to be the dominating drive mechanism. However, the discovery of subsidence in 1984 led to the conclusion that compaction drive also was a dominant recovery mechanism. Water influx into the Tor formation and oil expansion contributed to oil production the first years. Primary depletion was also augmented by gas injection.

After concluding that water flooding was successful, it was found that the dominating processes responsible for this was spontaneous imbibition of water into the chalk. As the

Ekofisk field is intensively natural fractured, the surface area subjected to imbibition is large, contributing to water injection being effective. When production of formation water was observed it indicated that viscous displacement was a contributing drive mechanism for oil recovery.

Future plans

As earlier mentioned, the current plan is to continue water flooding until the production license expires by the end of 2028. However, a wide range of EOR-mechanisms are considered for improving the oil recovery beyond the Ekofisk water flood scenario.

Hydrocarbon WAG, carbon dioxide WAG, water chemistry and chemical flooding are among the EOR processes assessed. Extensive laboratory experiments, reservoir simulations and even a WAG-pilot, discussed in more detail in chapter 3, have been executed to evaluate the incremental recovery potential. None of the EOR scenarios have yet proven to be economically accepted to be implemented on full-field scale.

3 Literature review

WAG processes have been applied for more than 50 years with good success in most field cases (Christensen, et al., 2001). The first reported WAG application took place in a sandstone reservoir in Alberta, Canada in 1957 with a hydrocarbon miscible WAG-process. Since that WAG applications have been applied extensively worldwide with a gradually increase in projects, see figure 3.1. The majority of WAG injections are in onshore fields located in Canada and United States. However, there are also several fields located in former USSR and in the North Sea.

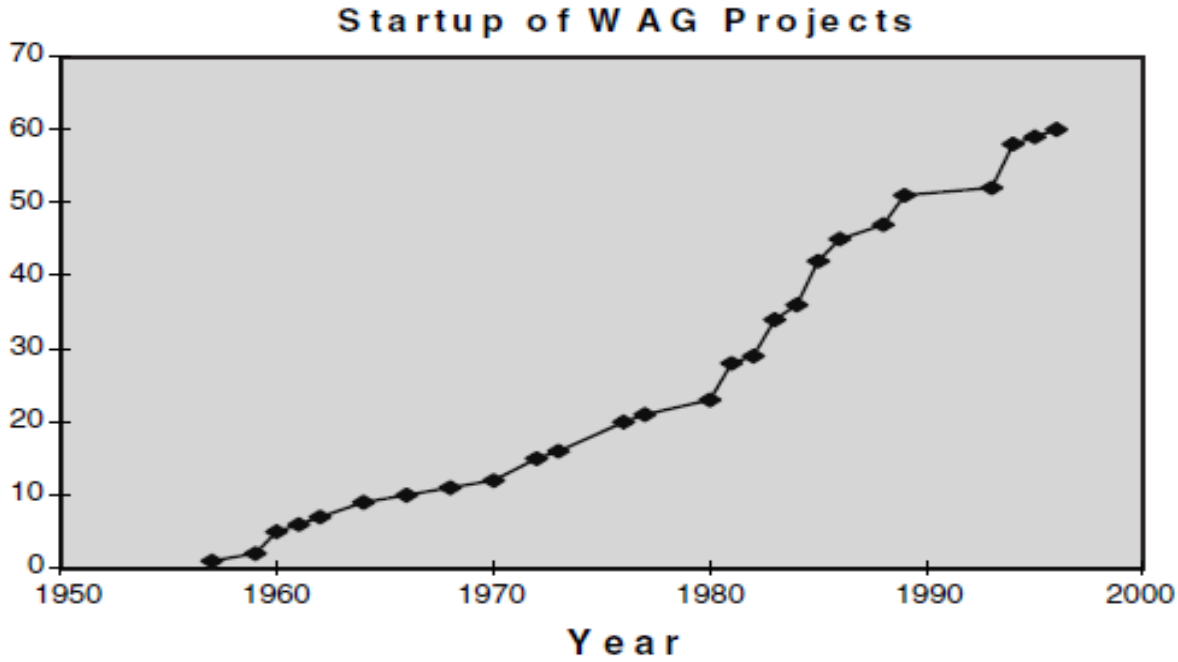

Figure 3.1: Cumulative number of worldwide WAG applications from the first project in 1957 to 1996 (Christensen, et al., 2001)

Purpose of WAG injection

The purpose of WAG injection is to improve oil recovery, by both increasing the macroscopic and microscopic sweep efficiency and for pressure maintenance. The microscopic sweep efficiency is defined by how much oil is recovered in areas contacted by the displacing fluids. The macroscopic sweep efficiency is defined by how effective the displacing fluids contact the reservoir in volumetric sense. In other words, how well the displacing fluids sweep the reservoir, both vertically and areally. The main purpose of the

water slugs is to increase the macroscopic sweep efficiency by a more favorable displacement mobility ratio. By a reduction of the mobility ratio larger parts of the reservoir will be contacted and the displacing front will be more stable resulting in reduced viscous fingering and postponed gas breakthrough to production wells. The purpose of the gas slugs is to increase the microscopic sweep efficiency, and also contact attic oil in areas not contacted by water injection. In high permeable sandstone reservoirs gravity segregation is common. Gas will tend to migrate to the top of the reservoir and the more dense water will tend to migrate to the bottom of the reservoir, hence attic oil in the upper parts of the reservoir may be contacted by the injected gas. Usually residual oil to WAG is less than to water or gas ($S_{orWAG} < S_{orw};S_{org}$). Thus, a combination of the improved microscopic displacement efficiency by gas injected with the improved macroscopic displacement efficiency by water injection improved oil recovery can be achieved (Christensen, et al., 2001), (Kleppe, et al., 2006).

WAG projects worldwide

Christensen et al. (2001) did a review of 59 fields where WAG injection were applied. The review included both miscible and immiscible WAG using different types of displacing gases, both hydrocarbon and non-hydrocarbon gases, such as carbon dioxide and nitrogen. A common trend for the success of the reviewed fields were increased oil recovery in the range of 5 to 10 % of the original oil in place, but increased oil recovery up to 20 % were also reported in several fields. The average improved recovery was calculated to be 9.7% for miscible WAG injection and as expected lower for the immiscible WAG injection at 6.4%. A positive observation from the review related to this study was that the highest improved recovery was obtained in a carbonate formation, however it was not in offshore environments like the Ekofisk field.

Of the 59 fields repored only six were applied in carbonate, and only six reported as WAG injection in offshore environments. All of the six reported offshore fields were located in the North Sea and made use of hydrocarbon gases. A typical trend for all fields were inital WAG-ratio of 1, however some fields varied up to WAG-ratio of 4. WAG-ratio is the ratio between volume of water and volume of gas in a WAG-cycle. The gas slug sizes reported were generally in the range of 0.1 to 3 pore volumes, with use of low volume slug sizes most common (Christensen, et al., 2001).

WAG projects in North-Sea

Kleppe et al. (2006) did a survey summerizing North Sea EOR projects in the period from 1975 to 2005. It was published that WAG injection is the most commom and successful EOR technology for the North Sea. WAG injection have been applied in the North Sea since 1980 and is considered a mature EOR-technology. Of the 19 reviewed EOR projects in the survery, which included both pilots and field-scale applications, nine are WAG-applications. Of these nine WAG-applications, six are classified as immiscible-WAG, Brage and Statfjord being field-scale WAG injections, while Ekofisk, Gullfaks, Thistle and Oseberg Øst are WAG-pilots. Of the three miscible WAG applications only Magnus is field-scale, while the other two at Snorre A and Brae South are WAG-pilots. In all cases hydrocarbon gases has been used, mainly because of the availability directly from production resulting in relativly low costs.

WAG injection in offshore environments such as in the North Sea is quite different from onshore WAG applications. Regular injection patterns are commonly used onshore, with five-spot injection pattern being the most common, however such patterns is typically not used offshore. The reason for this is the high costs of drilling new wells and for data acquisition offshore. Offshore wells are more likely to be placed based on geological considerations (Christensen, et al., 2001), (Kleppe, et al., 2006).

CO_2-WAG has also proven to be a successful EOR technology worldwide. In many cases the method has lower minimum miscibility pressure than hydrocarbon gases which makes it attractive. However, the high costs of CO_2 capture and sequestration have so far been to challenging for the technology to be attractive in the North Sea (Kleppe, 2006).

Previous WAG-studies at the Ekofisk field

Immiscible WAG studies for the Ekofisk field were initiated in the fall of 1993 (ConocoPhillips, January 1994). The plan was to cover a set of phases including experimental laboratory work and reservoir modeling, which eventually could lead to the design of a WAG-pilot and possibly further expansion to full field WAG injection (Østhus, 1998). Laboratory work performed included evaluation of incremental oil recovery, compared to a water flood case, and evaluation of oil recovery mechanisms for gas injection, following complete water imbibition into chalk samples, similar to those in the

Ekofisk field (Reservoir Laboratories AS, 1995). The laboratory studies substantiated WAG potential with incremental oil recovery in the range of 20-25 %. A full field WAG screening (ConocoPhillips, January 1994), based on optimistic assumptions, also gave good results with the potential for WAG injection to be economically feasible. These positive results led to the decision to proceed to pilot planning.

Ekofisk WAG-pilot

The injection well 2/4 W-06 was chosen as the WAG-injection well for the pilot. This well was chosen due to low costs, good water injectivity being a former water injection well, several surrounding production wells and perforations in both the Ekofisk and Tor formations making it representative for the entire field. (Jensen, 2001), (Østhus, 1998). The main objectives of this multiwell pilot was to get information on reservoir performance data including injectivity of gas and water, sweep efficiency of injected gas in the presence of high water saturations, timing of gas breakthrough and production response of oil, gas and water in surronding production wells.

Gas injection in the WAG-pilot well was performed intermittenly in the period between June 1996 and September 1996. Gas was accomodated from the nearby Charlie 2/4 production platform. The WAG-pilot was unsuccesful because substantial gas injection rates were not achieved.

Ekofisk WAG-pilot failure and suggested solutions to hydrate formation problem

Post analysis revealed that hydrate formation in the reservoir was the reason for gas injectivity loss. Gas hydrate formation was caused by the temperature around the former water injection well being around 60˚F.

Labarotory experiments performed at Rogaland Research Institute (Lekvam, et al., 1997) and at the Phillips Research Center in Barlesville (Wegener, et al., 1997) were reported addressing and discussing several options to prevent hydrate formation, given in table 3.1, for WAG injection in the Ekofisk Field.

Table 3.1: Summarize of suggested solutions to prevent the hydrate formation problem for WAG injection at the Ekofisk field (Lekvam, et al., 1997)

Suggestions to avoid hydrate formation
1) Chemical heating of the near wellbore area prior to gas injection
2) Heating of the injection water to rise near wellbore temperature prior to gas injection
3) Sidetrack the injectors outside cooled zones prior to gas injection
4) Co-injection of water and gas
5) Chemical inhibition to prevent and/or retard the onset of hydrate formation

The reports (Wegener, et al., 1996), (Lekvam, et al., 1997) concluded that co-injection of water and gas would not be a solution in itself, but would be required to achieve necessary bottom-hole pressure (BHP), above the reservoir pressures. Further the reports concluded that chemical inhibition would not be capable of avoiding the hydrate formation. Increasing the near wellbore temperature, by chemical heating or by injecting heated water prior to gas injection was neither found to be solutions. A model showed that the injected gas would move much faster than the heating water front and eventually move ahead of the heating front, leading to hydrate formation. Similarly chemical heating might raise temperature near the wellbore. However, the cold zone is pushed ahead into the reservoir and will be reached when injecting gas. The only remaining option was to sidetrack the injection wells outside the cool temperature regions. Sidetracking the injection wells outside the cooled region still means that the injected water temperature needs to be above hydrate formation temperature, and a sufficiently high BHP is needed to overcome the high reservoir pressure. Some unsuccessful attempts were performed to prevent hydrate formation, and the WAG well was eventually changed back to a water injection well (Østhus, 1998).

Ekofisk WAG-studies in the posterity of the WAG-pilot

Full field WAG simulations indicated incremental oil recovery potential up to 6 %, above a Ekofisk water flood case from 1997 (Østhus, 1998). The potential oil production for a full field WAG-simulation, with field gas injection rates of 600 million standard cubic feet per day (SCF/D), was compared to a long term water flood production forecast, from 1997 until end of license in 2028, and is shown in figure 3.2.

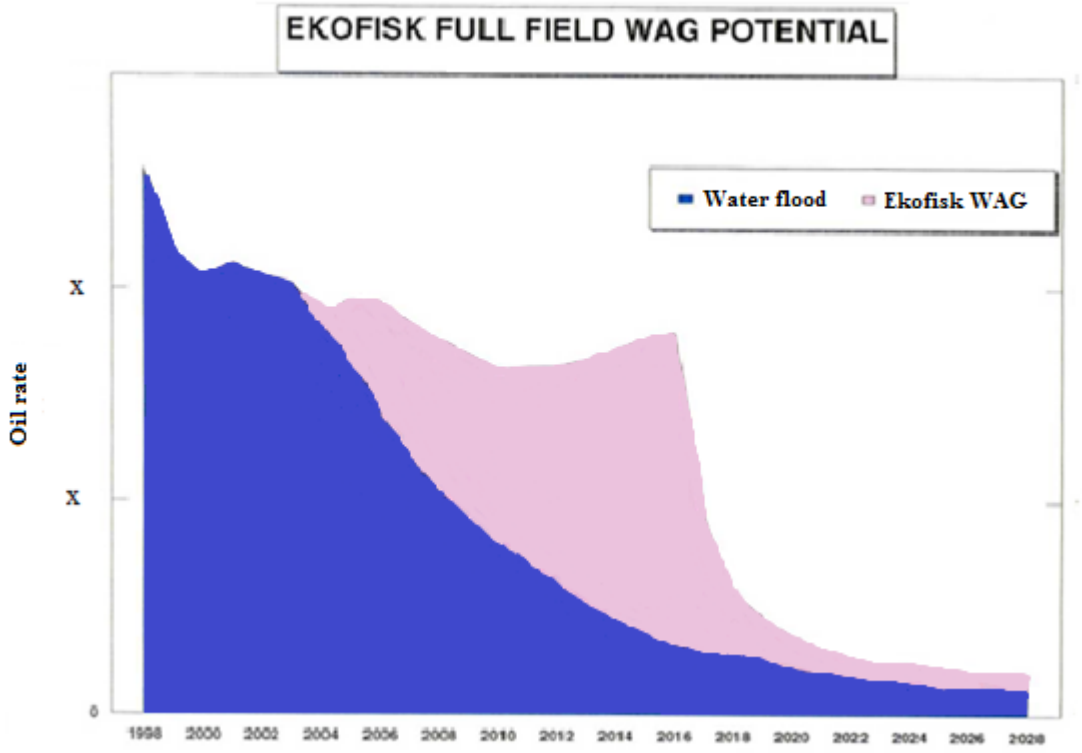

Figure 3.2: Full field WAG-simulation versus long term water flood production forecast (Østhus, 1998)

Some of the assumptions made in the full field simulation model were good gas injectivity, no relative permeability hysteresis effect and low trapped gas saturation. Further assumptions were that injected gas would contact residual oil in the matrix block, either by forced displacement and/or by diffusion mechanisms, and eventually vaporize parts of the residual oil after the water flooding (Østhus, 1998). The displacement process was assumed immiscible, with the injected gas composition used given in table 3.2.

Table 3.2: Composition of injected gas used in previous Ekofisk WAG-simulations (Østhus, 1998)

Component	Mole (%)
Nitrogen, N2	0.4
Methane, C1	85.4
Carbon dioxide, CO2	2.1
Ethane, C2	8.1
Propane, C3	2.8
2-Metylpropan, i-C4	0.3
n-Butane, n-C4	0.9

A major EOR screening study (Harpole, et al., 2000) was performed in 1998-1999 where HC-WAG was reported among the top two processes to be carried forward in further studies. The screening study recommended to update full field WAG development forecasts, with progression towards a new pilot if full field economics were sufficient.

Further WAG studies re-evaluating full field WAG potential were performed in 2000-2001 (Jensen, 2001). A premise for the study was that any unresolved technical or logistical issues had to be successfully addressed or solved prior to further process implementation. Based on the premise the study concluded with WAG not being technically or economically viable at this point.

4 Theory

This chapter is initiated with description of general reservoir and fluid parameters which affect reservoir simulations and the main parameters and concepts of this study. Next, presentation of definitions, correlations and models regarding the main parameters and concepts of this thesis, such as trapped gas saturation, relative permeability hysteresis and SORM are given.

Oil recovery mechanisms for WAG-displacement, divided into oil displacement by gas and oil displacement by water are then presented. The subsequent section presents difference between miscible and immiscible WAG-injection, and how to evaluate miscibility through tests on minimum miscibility pressure and minimum miscibility enrichment. The last part of the chapter is an introduction to the full field numerical simulation tool, PSim, which is used for reservoir modeling in this thesis.

4.1 Rock properties

4.1.1 Porosity

Porosity (φ) of a porous rock is the fraction of the total rock volume that is occupied by void space. The porosity describes the fluid storage capacity of the rock.

4.1.2 Absolute permeability

Permeability (k) of a rock is associated with the rock's capacity to transport fluids through systems of interconnected pores. Permeability is a measure of the fluid conductivity of a particular rock, in terms of Darcy (Ursin, et al., 1997).

Absolute permeability of a porous medium refers to the permeability when saturated with a single fluid. The rock property, absolute permeability, is constant for a particular porous medium and is independent of the fluid type flowing in the rock.

4.1.3 Effective permeability

In cases of multi-phase flow, when several fluids or phases are flowing locally and simultaneously in a system, each fluid phase will counteract the free flow of the other phases and a reduced phase permeability of each phase is measured, called the effective permeability (Ursin, et al., 1997). Effective permeability (k_e) is a measure of the fluid conductance of one particular fluid, when that fluid fills a fraction of the pore space of a porous medium.

4.2 Relative permeability

Relative permeability (k_r) is a property used to describe flow in a multi-phase system. The property is a fluid-rock property and is defined as the ratio of the effective permeability of a particular fluid at a particular saturation to a base permeability of the porous medium, as given in equation 4.1. The base permeability is usually referred to the absolute permeability of the porous medium.

$$k_r = \frac{k_e}{k} \qquad \textit{Equation 4.1}$$

Relative permeability is dimensionless and has values between 0 and 1. If a single fluid is present in a rock, the effective permeability will be equal to the absolute permeability; hence the relative permeability will be equal to one. If the relative permeability of a fluid is zero, the fluid will be immobile.

Relative permeability is mainly a function of fluid saturations and saturation history. Dependence on saturation history is described as relative permeability hysteresis effect. Water relative permeability depends most strongly on its own phase-saturation and typically shows little hysteresis effect. The non-wetting phase relative permeability though depends strongly on both the saturation of its own phase and on the saturation history. This results in a complex saturation pattern which demands special relative permeability description, illustrated in figure 4.1. Relative permeability hysteresis is important in WAG-processes because the alteration between water and gas injection results in changes of saturation, between imbibition and drainage processes, which can result gas getting trapped and consequently change in relative permeability curves. Drainage is referred to as a process

where the wetting-phase saturation decreases and contrary imbibition to a process where the wetting-phase saturation increases. A more detailed discussion on trapped gas and hysteresis effected relative permeability curves will be given in chapter 4.6.

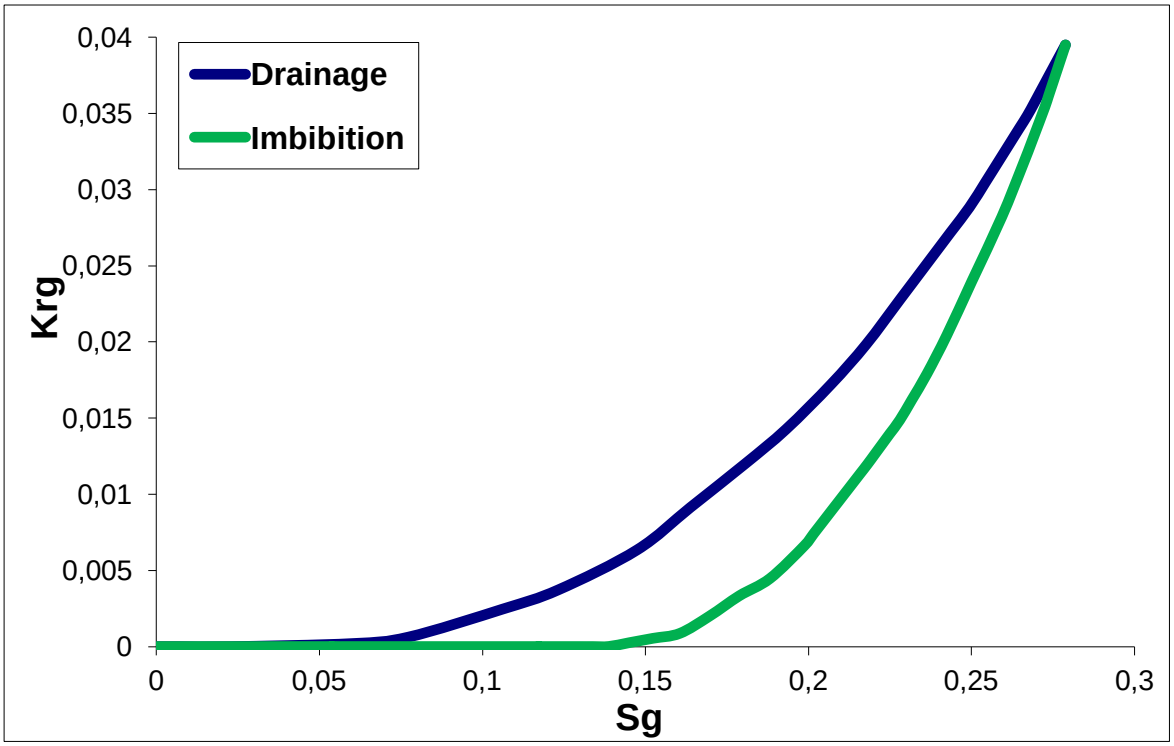

Figure 4.1: Example of hysteresis affected gas relative permeability imbibition curve

4.2.1 Two-phase relative permeability

Two-phase flow refers to a process where only two fluids or phases are flowing locally and simultaneously in a system. Relative permeability of water (k_{rw}) and oil (k_{row}) in a water-oil system are plotted in relative permeability curves as a function of the water saturation. Similarly, the relative permeability of gas (k_{rg}) and oil (k_{rog}) in a gas-oil system are plotted in relative permeability curves as a function of the gas saturation. Figure 4.2 (a) and (b) illustrates typical shape of two-phase relative permeability curves for water-oil and gas-oil systems respectively.

Relative permeability curves allow comparison of fluid flow at different fluid saturation and estimation of residual oil and gas saturations based on endpoint saturations. Endpoint saturations are reflected by the largest saturation of a phase for which the relative

permeability of the respective phase in the respective system is zero. Endpoint saturations in a water-oil system are defined S_{orw} for oil and S_{wr} for water, figure 4.2 (a). Similarly, for a gas-oil system the endpoint saturations are defined as S_{org} for oil and S_{gr} for gas, figure 4.2 (b). If the saturation of a coexisting phase becomes less than the endpoint saturation, the relative permeability will be zero and the phase immobile. Endpoint saturations are also of great importance for estimation of initial fluid distribution and ultimate recovery of systems.

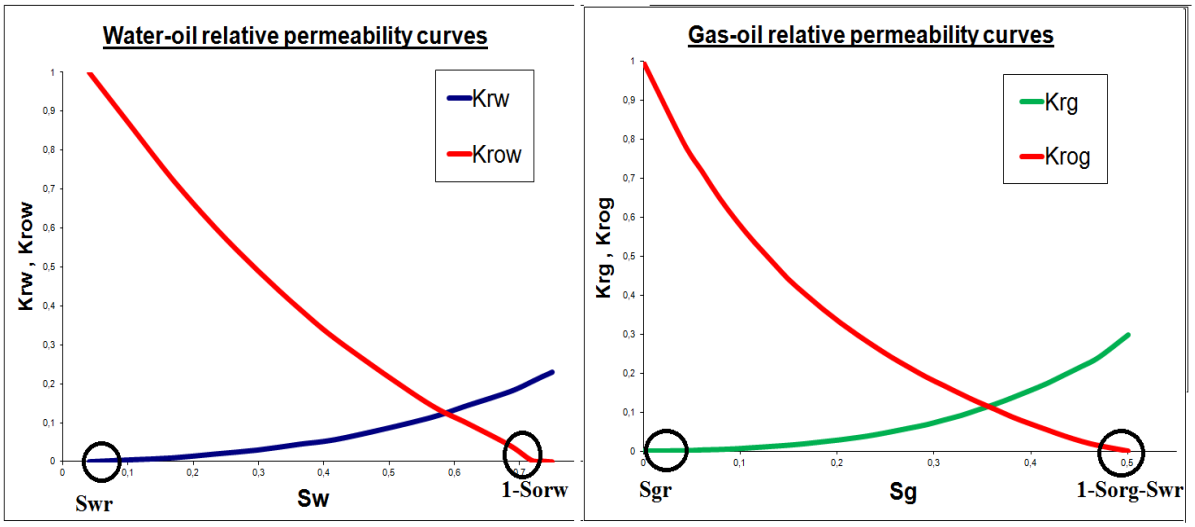

(a) **(b)**

Figure 4.2: Illustration of the shape of (a) water-oil relative permeability curves, and corresponding end-point saturations (b) gas-oil relative permeability curves, and corresponding end-point saturations

Even though there have been attempts to calculate relative permeability on theoretical backgrounds, most work is done experimentally. The experimental work on relative permeability is mostly performed on the two-phase systems water-oil and gas-oil.

Relative permeability data can be obtained experimentally by centrifuge techniques or by core flooding tests under steady-state or unsteady-state conditions. In unsteady-state relative permeability tests, cores with in-situ fluid are flooded with an immiscible fluid, gas or water, at constant rate. Values for relative permeability are determined using a Buckley and Leverett developed equation based on observations of the fractional flow of the displacing fluid phase, which are related to saturation. In steady-state tests two fluids are injected simultaneous in a core at constant rate until the produced fluid ratio comes in equilibrium with the injected fluid ratio. Phase saturations are measured and the corresponding relative permeability is obtained by applying Darcy's law. Relative permeability for different

saturations can be obtained by changing the fluid ratio of the injected fluids (Ibrahim, et al., 2001). In centrifuge tests a liquid saturated sample is placed in an air-filled core holder and subsequently rotated with constant speed in a centrifuge. Relative permeability values are obtained by monitoring the liquid production as a function of time at a given rotational speed (Spronsen, 1982) (Firoozabadi, et al., 1986).

The centrifuge method is relative fast; however it has been limited to determination of wetting-phase relative permeability only (App, et al., 2002). Unsteady-state tests have shown to yield faster results than steady-state tests. Steady-state tests have though been preferred for reservoir with more-scale heterogeneity and with mixed wettability (Ursin, et al., 1997), (Ibrahim, et al., 2001).

In lack of reliable two-phase relative permeability data, simplified models based on experimental data can be used to construct two-phase data. An example of such a model is the Corey-type approximations which uses a power law function to calculate relative permeability based on endpoint saturations and empirical parameters.

4.2.2 Three-phase relative permeability

Locally in reservoirs three phases can flow simultaneously. To describe such three-phase flow, three-phase relative permeability data is required. For WAG-displacement, local three-phase flow is common, and is especially evident close to injectors, see figure 4.3. In a three-phase system there will be an intermediate wetting-phase in addition to the phases present in two-phase systems. In a water-wet system, oil will be the intermediate wetting-phase and act as a non-wetting phase with respect to water and as a wetting-phase with respect to gas.

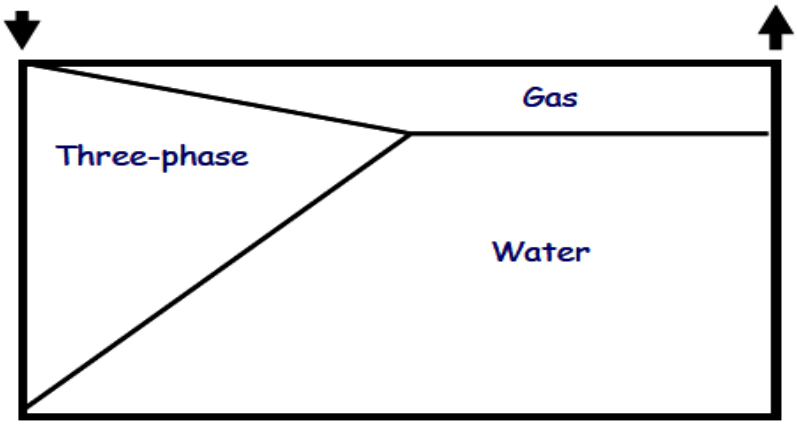

Figure 4.3: Three-phase flow in a WAG-system (Skauge, et al., 2007)

Estimates of three-phase relative permeability are needed to understand three-phase flow. As most experimental data on relative permeability are on two-phase systems, a number of correlations and models to calculate three-phase permeability have been developed. However, there is little experimental data to validate most models (ConocoPhillips Technical Manual, 2010). The most accepted and commonly used three-phase relative permeability models in the petroleum industry are the two proposed by Stone.

4.2.2.1 Stone's models

Stone's models (Stone 1970, 1973) are probability-based models which assume the relative permeability of the wetting and non-wetting phases depend only on the saturation of the wetting and non-wetting phases respectively, while the intermediate wetting-phase relative permeability varies in a more complex manner. For a water-wet system, water will be the wetting phase, gas the non-wetting phase and oil the intermediate wetting-phase.

Stone's models use more easily measured two-phase data, water-oil and gas-oil relative permeability curves, to predict the relative permeability of the intermediate-wetting phase in a three-phase system.

In many reservoirs that involve three-phase flow only gas and oil are mobile in the upper parts, and only water and oil are mobile in the lower parts, as illustrated in figure 4.3. Stone's models therefore predict that the oil relative permeability, k_{ro}, is obtained as function of oil relative permeability from the water-oil system (k_{row}) in presence of water only, and as a function of oil relative permeability from the gas-oil system (k_{rog}) in presence of gas and irreducible water.

In areas of three mobile phases the technique used to obtain three-phase relative permeability for the intermediate wetting-phase is to interpolate between the two sets of two-phase relative permeability data, using k_{rw}, k_{row}, k_{rg} and k_{rog}, k_{rw} and k_{row} are obtained from the water-oil data as function of water saturation. Similarly, k_{rg} and k_{rog} are obtained from the gas-oil data as a function of gas saturation holding the water saturation constant and immobile. Hence, the two-phase relative permeability curves for water-oil and gas-oil are sufficient for use of Stone's models.

Both Stone's models have the desirable property in that they yield the correct two-phase data when only two phases are flowing, and yet provide interpolated data for three-phase

flow that are consistent and continuous functions of the phase saturations. To allow for hysteresis effect, the water and gas saturations should be changing in the same direction in the two sets of two-phase data, as desired in the three-phase system.

4.3 Surface and interfacial tension

Whenever immiscible phases coexist in a porous medium, surface energy related to the fluid interfaces influences the saturations, distributions and displacement of the phases (Green, et al., 1998). The surface force between two fluids is quantified in terms of surface/interfacial tension, σ, which is given as the force acting in the plane of the surface, per unit length of the surface.

Surface tension is usually reserved to the case when the interface is between a liquid and its vapor or air. If the interface is between two different fluids or between a liquid and a solid, the term "interfacial tension" (IFT) is used.

4.4 Rock wettability

Wettability can be defined as the tendency of one fluid to spread or to adhere to a solid surface in the presence of a second fluid. (Ursin, et al., 1997) When two immiscible phases are placed in contact with a solid surface, one phase usually is attracted to the solid more strongly than the other phase. The more strongly attracted phase is called the wetting phase (Green, et al., 1998).

Quantitative evaluation of wettability can be done by examining the interfacial forces that exist when two immiscible fluid phases are in contact with a solid. In figure 4.4, forces between the solid, water and oil are balanced and given by:

$$\sigma_{os} - \sigma_{ws} = \sigma_{ow} \cdot \cos\theta \qquad \textit{Equation 4.2}$$

Where σ_{os}, σ_{ws} and σ_{ow} are interfacial tensions between solid and oil, water and solid and water and oil respectively, and θ is the contact angle measured through the water.

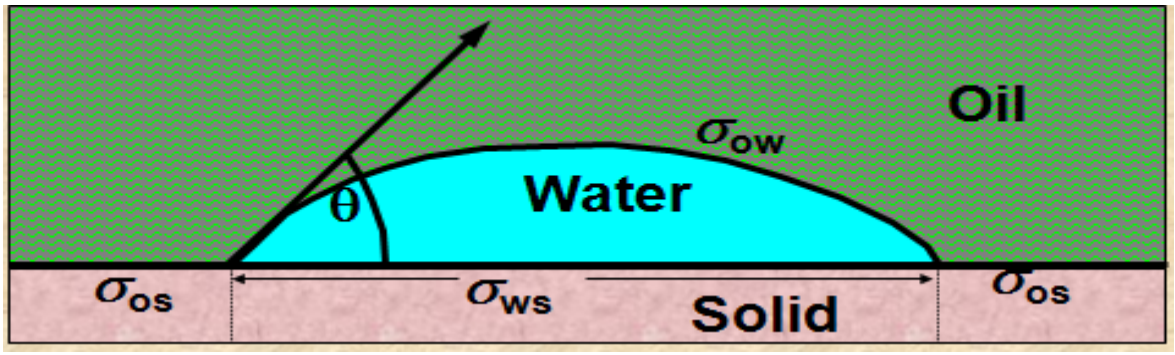

Figure 4.4: Interfacial forces when water and oil are in contact with a solid rock in a water-wet-system

Experimental methods have not been developed to measure σ_{os}, σ_{ws}. Therefore, the wettability preference of a rock is estimated by measuring the contact angle, θ. Contact angles are measured through the water phase, from the solid surface to the fluid-fluid interface. A rock is water-wet if $\theta < 90$ and oil-wet if $\theta > 90$. A contact angle approaching 0 indicates a strongly water-wet system, while contact angle approaching 180 indicates a strongly oil-wet rock. Contact angle close to 90 refers to as intermediate or neutral wet rock (Green, et al., 1998). The wettability preference of a rock based on a rule of thumb for oil-water systems is summarized in table 4.1 and in figure 4.5.

Table 4.1: Wettability preference expressed by contact angle (Ursin, et al., 1997)

Contact angle values	Wettability preference
0 – 30	Strongly water wet
30 – 90	Preferentially water wet
90	Neutral wettability
90 – 150	Preferentially oil wet
150 – 180	Strongly oil wet

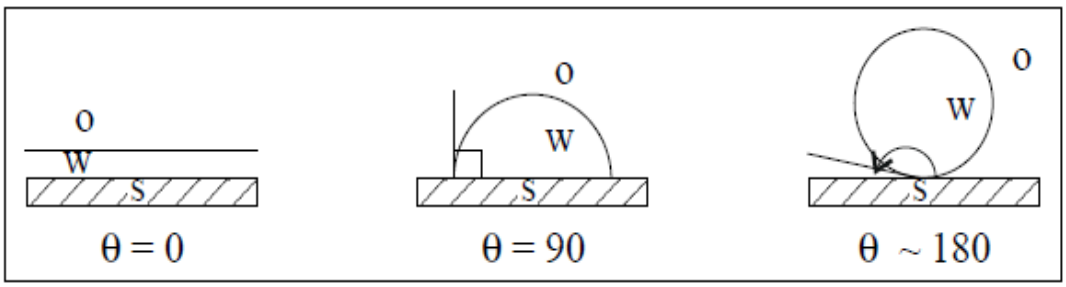

Figure 4.5: Rocks wetting preferences based on contact angle (Ursin, et al., 1997)

The state of rock wettability will affect the distribution of fluids within a reservoir system, see figure 4.6.

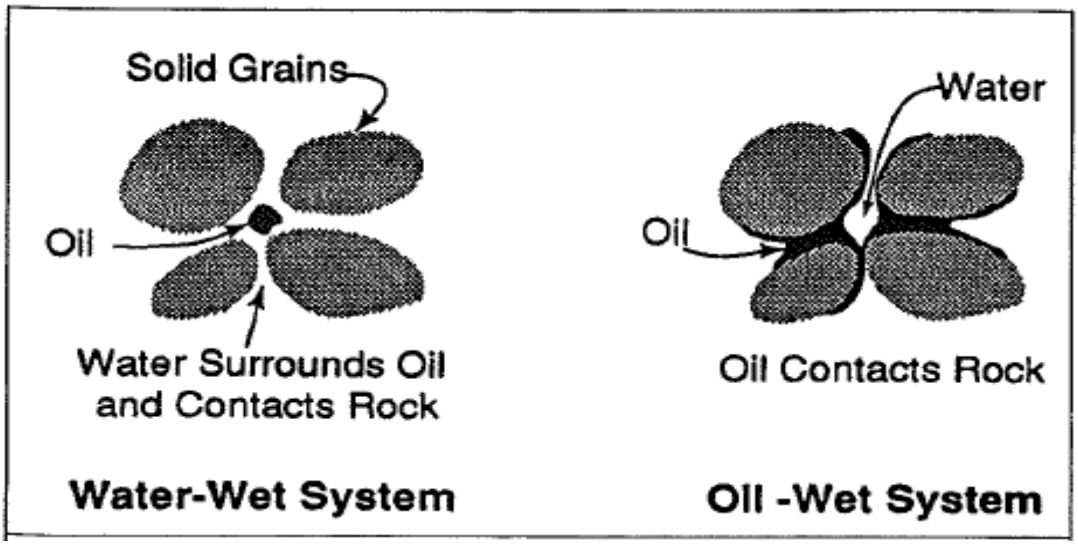

Figure 4.6 Fluid distributions within water-wet and oil-wet systems (Green, et al., 1998)

Rock wettability will also affect relative permeability-, illustrated in figure 4.7, and capillary pressure characteristics of a fluid-rock system, which is likely to result result in differences in residual oil saturations (Green, et al., 1998), (Donaldson, et al., 1969).

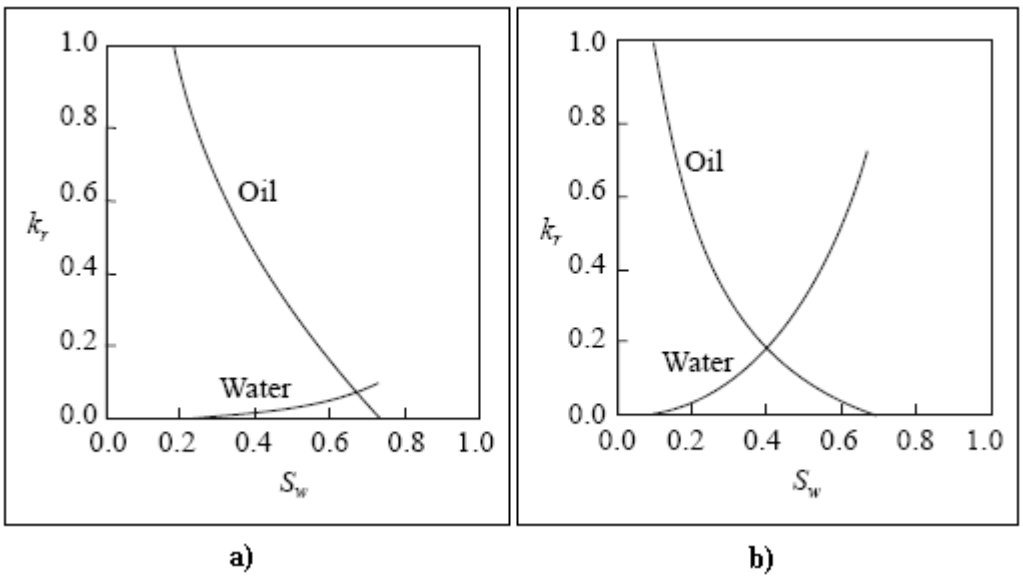

Figure 4.7: Wettability effect on relative permeability curves for (a) water-wet systems and (b) oil-wet systems (Ursin, et al., 1997)

In water-oil systems, oil will be more mobile, and lower water flood residual oil saturations will be exhibit than in an oil-wet system. Likewise, water will flow better in oil-wet systems and higher water flood residual oil saturation will be left in the reservoir.

Strongly water-wet system will spontaneously imbibe more water into the matrix blocks than a preferentially water-wet system. Spontaneous imbibition of water into matrix blocks is important for oil recovery and is described in more detail in chapter 4.9.1.2.

4.5 Capillary pressure

A pressure difference called capillary pressure will exists across the interface between immiscible fluids caused by interfacial tensions. Capillary pressure, P_c, is defined as the pressure difference between the non-wetting phase, P_{nw}, and the wetting-phase, P_w, given by equation 4.3 (Ursin, et al., 1997):

$$P_c = P_{nw} - P_w \qquad \textit{Equation 4.3}$$

Young-Laplace presented a relationship between the capillary pressure and the interfacial tension between two immiscible fluids on a curved surface, given in equation 4.4, with examples of radius of curvature shown in figure 4.8:

$$P_c = \sigma\left(\frac{1}{R_1} - \frac{1}{R_2}\right) \qquad \textit{Equation 4.4}$$

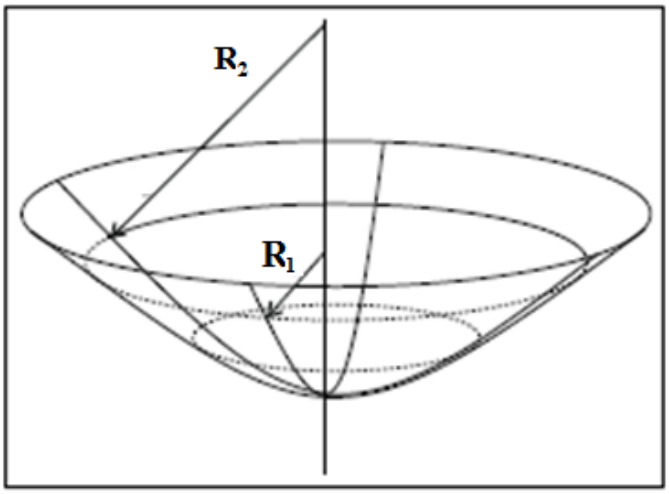

Figure 4.8: Radius of curvature on a curved surface (Ursin, et al., 1997)

If the curvature of the interface is approximately spherical the radius of curvature equal, $R_1=R_2=R$, and easy trigonometry, illustrated in figure 4.9, induces that the radius of the medium r_c can be defined as:

$$r_c = R \cdot \cos\theta \qquad \textit{Equation 4.5}$$

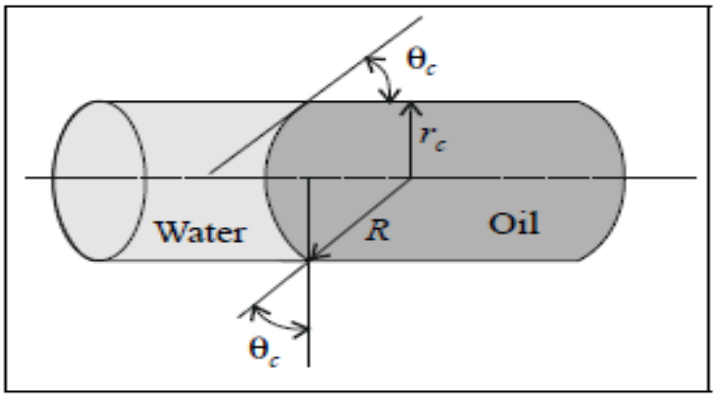

Figure 4.9: Two immiscible fluids forming an idealized spherical curvature (Ursin, et al., 1997)

Combining Young-Laplace equation 4.4 with the above equation 4.5, deduces an equation to calculate the capillary pressure between two immiscible fluids as a function of the IFT and the wettability of rocks, through the contact angle:

$$P_c = \frac{2\sigma \cdot \cos\theta}{r_c} \qquad \textit{Equation 4.6}$$

Drainage and imbibitions laboratory experiments have shown that capillary pressure is dependent on interfacial tension (σ), contact angle(θ) measured through the water phase, fluid saturations ($J(S_w)$), rock porosity (φ) and permeability (k). (Ursin, et al., 1997) A correlation, equation xx, relating the capillary pressure, P_c, to these parameters was defined by Leverett based on dimension analysis. The correlation is widely used for reservoir simulation tasks.

$$P_c = \frac{\sigma \cdot \cos\theta}{\sqrt{\frac{k}{\varphi}}} \cdot J(S_w) \qquad \textit{Equation 4.7}$$

Capillary pressure curves are important for understanding the saturation distribution in reservoirs. Capillary pressure depend on the direction of saturation, being an imbibition or a drainage process, as well as previous saturation history reflected as capillary pressure

hysteresis effect. Common shape of water-oil capillary pressure curves for drainage and imbibition processes are shown in figure 4.10:

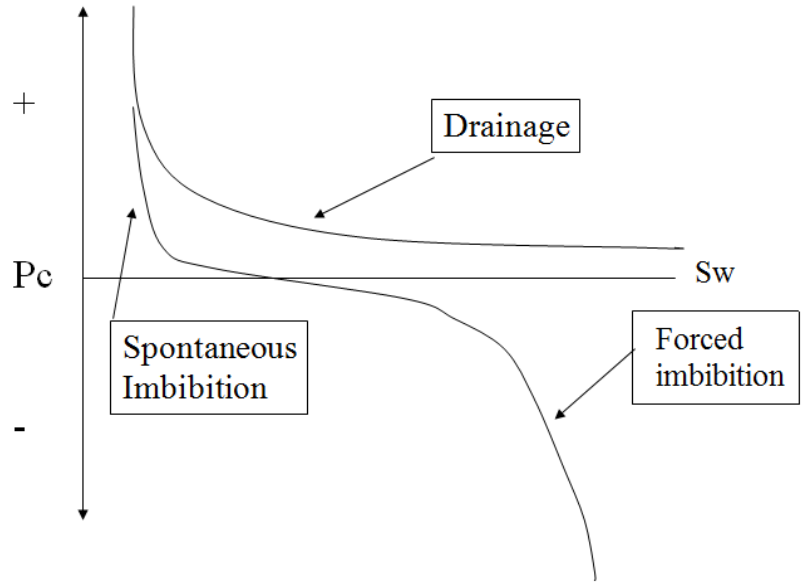

Figure 4.10: Illustration of water-oil capillary pressure curves

The capillary pressure, created as a result of interactions between liquids and solid surface, is responsible for the spontaneous imbibitions of water into the matrix blocks. Water will spontaneous imbibe the matrix block until the capillary pressure equals zero.

In case of three-phase flow, three-phase capillary pressures curves are needed to model the dynamics of gas-oil and oil-water transition zone movements in the reservoir (Helland, et al., 2004). There has been little experimental work done on three-phase capillary pressure (Skauge, et al., 2007). Three-phase capillary pressure curves have traditionally been estimated from experimentally measured two-phase capillary pressure data. However, experimental work on three-phase capillary pressure reported by Bradford and Leij (1995) indicated that this practice may not be valid. Although experimental data is very limited there exist a few correlations to calculate three-phase capillary pressure. Helland and Skjævland (2004) presented a three-phase capillary pressure correlation accounting for direction of saturation change as well as wettability conditions. They validated the correlation with centrifuge measurements from water-wet cores. The correlation have not yet been widely accepted or validated, and capillary pressures are often neglected in three-phase flow processes like WAG-injection.

4.6 Trapped gas saturation and hysteresis effect

4.6.1 Introduction to trapped gas saturation and hysteresis

Phase trapping of gas is a common phenomenon after an imbibition process where a wetting-phase displaces the non-wetting phase gas (Green, et al., 1998). Trapped gas is important in WAG processes, because the WAG cycles lead to oscillation of water and gas with position and time (Skauge, et al., 2007), which induce changes between drainage and imbibition processes.

For water-wet systems gas is always the non-wetting phase, and invades the larger pores and throats (Suicmez, et al., 2006). During the imbibition process the capillary pressure in the larger pores is less than the capillary pressure in the smaller pores. As a consequent, the wetting phase will advance faster in the smaller pores and part of the gas phase will be bypassed by the increasing wetting phase. This disconnection of the former continuous gas clusters will leave a portion of the gas phase immobile and trapped as isolated drops or ganglia. The isolated gas will be held in the larger pores by strong capillary forces which cannot overcome the relative small viscous forces (Green, et al., 1998). As the trapped, immobile part of the gas saturation does not contribute to flow of gas, the gas relative permeability at a given gas saturation will be less for the imbibition process compared to the drainage process. The change of imbibition relative permeability curves compared to drainage curves is called relative permeability hysteresis effect and is mainly caused by the trapped gas. Different models and correlations accounting for hysteresis effect relative permeability curves and for modeling trapped gas saturation will be presented in this section.

Several studies have been performed on determining the parameters that impact the amount of gas getting trapped. Trapped gas saturations have been reported (Suicmez, et al., 2006), (Wegener, et al., 1996) function of on pore geometry and porosity and the saturation history, both current and historical maximum gas saturation. Laboratory experiments on carbonate cores by Keelan and Pugh (1975) indicated that trapped gas is independent of pore geometry and porosity for chalk formation. Further their experiments confirmed that increasing gas saturation is accompanied with increasing trapped gas saturation. Pow et al. (1997) addressed imbibition of water in fractured reservoirs. Field and laboratory information suggested that a large amount of gas was trapped by fast water imbibition through the fractures.

Several correlations have been proposed in the literature to calculate the amount of trapped gas saturation. The most accepted is the one proposed by Carlson S. Land. Land's correlation is the correlation commonly used in hysteresis models to calculate the amount of trapped gas.

4.6.2 Trapped gas saturation correlations and hysteresis models in PSim

4.6.2.1 Land's correlation

Land's trapped gas

Carlson S. Land addressed an empirical correlation (Land, 1968), (Land, 1971) based on available data which relates initial gas saturation at the start of an imbibition process to the trapped gas saturation at complete imbibition:

$$Sgr^* = \frac{Sgi^*}{(1 + C_{Land} \cdot Sgi^*)} \qquad \textit{Equation 4.8}$$

Where:

Sgr^* : Residual (trapped) gas saturation after complete imbibition[1]

Sgi^* : Gas saturation established in the drainage process and the initial gas saturation of the imbibition process

C_{Land} : Trapping characteristic of the porous rock called Lands constant

The trapping characteristic of the porous rock, Lands constant, is determined by:

$$C_{Land} = \left(\frac{1}{Sgr^*_{max}}\right) - 1 \qquad \textit{Equation 4.9}$$

Where:

Sgr^*_{max} : Maximum obtainable residual gas saturation, corresponding to initial gas saturation at one minus critical water saturation.

[1] All saturation marked with stars are effective saturation expressed as fraction of the pore volume excluding the pore volume occupied by the irreducible wetting phase.

Land's relative permeability hysteresis effect

Land further proposed that only the mobile part of the gas-phase should be used to calculate hysteresis affected relative permeability imbibition curves. The total gas saturation, Sg^*, at any point in the imbibition process can be treated as two separate saturations, a mobile fraction of the gas, SgF^*, and the current trapped gas fraction of the gas, $Sgrc^*$:

$$Sg^* = SgF^* + Sgrc^* \qquad \textit{Equation 4.10}$$

If a total saturation, Sg^*, is reduced to a residual trapped gas saturation, Sgr^*, the contribution from the mobile fraction, SgF^*, to residual trapped gas saturation can be found by applying SgF* as an initial saturation in equation 4.8. The gas saturation that gets trapped, contribution of SgF*, during a reduction in gas saturation from Sg* to Sgr*, must equal the residual value Sgr* associated with Sgi*. From this deduction, the current trapped gas saturation can be expressed as:

$$Sgrc^* = Sgr^* - \frac{SgF^*}{(1+C_{Land} \cdot SgF^*)} \qquad \textit{Equation 4.11}$$

Substituting equation 4.10 into equation 4.11 and solving for SgF* deduce the remaining mobile gas saturation when the gas saturation has been reduced from Sgi* to Sg* in an imbibition process:

$$SgF^* = \frac{1}{2} \cdot (Sg^* - Sgr^*) + \frac{1}{2}\sqrt{(Sg^* - Sgr^*)^2 + \frac{4}{C}(Sg^* - Sgr^*)}$$

Equation 4.12

Based on the mobile gas saturation SgF* calculated from equation 4.12, Land proposed that new hysteresis effected gas relative permeability data can be calculated by using equation 4.13:

$$k_{rg} = SgF^{*2}(1 - (1 - SgF^*)^{\epsilon-2} \qquad \textit{Equation 4.13}$$

Where:

ϵ : Empirically determined pore-size distribution factor

4.6.2.2 Coats correlation

Coats proposed a linear correlation relating the initial gas saturation at the start of an imbibition process to trapped gas saturation at complete imbibition (ConocoPhillips Technical Manual, 2010):

$$S_{gr}^{*} = S_{gc} + C \cdot (S_{gmax}^{*} - S_{gc}) \qquad \textit{Equation 4.14}$$

Where:

S_{gc} : Critical gas saturation

C : Trapping characteristic of the porous rock given by:

$$C = \frac{S_{gr}^{*} - S_{gc}}{S_{gmax}^{*} - S_{gc}} \qquad \textit{Equation 4.15}$$

4.6.3 Other relative permeability hysteresis models

A number of hysteresis empirical models have been developed to characterize the hysteresis effect on relative permeability (Spiteri, et al., 2004).The most important parameter determining the significance of hysteresis effect is the trapped non-wetting phase saturation. Relative permeability models that incorporate with hysteresis are usually based on the trapping model proposed by Land in the previous section.

Two-phase hysteresis models have been the standard in most reservoir simulators. The most popular are described by Carlson and Killough (Larsen, et al., 1998). Standard two-phase hysteresis models for non-wetting phase consist of one drainage relative permeability curve and one imbibitions curve connected at the same inflection point. An inflection point is the point where the displacement process shifts from drainage to imbibition (Larsen, et al., 1995). The drainage-imbibition curves form a reversible envelope in which scanning-curves are generated (Skauge, et al., 2007). The standard hysteresis models for the non-wetting phase allows for reduced mobility in the imbibition curve after primary drainage. However, further drainage-imbibition processes are described within the primary drainage-imbibition envelope, where scanning curves are used to represent any subsequent drainage process.

Experimental observations have indicated that the two-phase hysteresis models do not sufficiently describe WAG processes (Skauge, et al., 1994). Experimental observations have shown that the mobility during secondary drainage generally is considerably lower

than during primary drainage. This indicates that the reversibility within two-phase models is inappropriate. Larsen and Skauge therefore developed a three-phase hysteresis model that includes impact further changes in trapped gas saturation have on mobility and following on relative permeability curves.

4.6.3.1 Carlson hysteresis model

Carlson hysteresis model describes hysteresis effect of the relative permeability curves using an experimental primary drainage curve together with an estimated imbibition curve based on Land's trapped gas correlation (Carlson, 1981). Further saturation changes, between drainage and imbibition, are produced by scanning curves parallel to the estimated imbibition curve. The imbibition curve is simply shifted until it intersects with the drainage curve for the relevant saturation for saturation direction change, illustrated in figure 4.11 (Kossack, 2000).

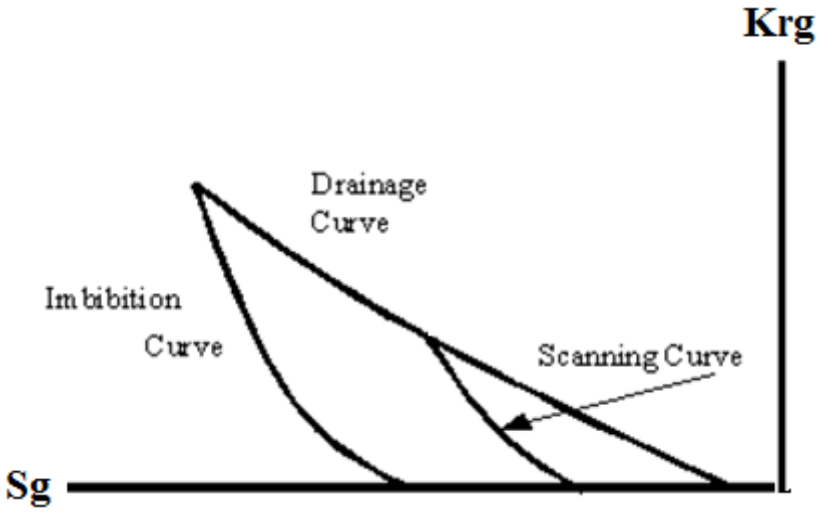

Figure 4.11: Carlson hysteresis affected non-wetting phase relative permeability curves (Kossack, 2000)

The outer lines in figure 4.11 represent a primary drainage curve connected with an imbibition curve, which is estimated based on the largest possible non-wetting phase. These curves make up a relative permeability envelope where scanning-curves are generated (Larsen, et al., 1995). Whenever a drainage process ends, a subsequent imbibition will follow a scanning-curve. After initiating an imbibition process all further processes are assumed reversible; the scanning-curve is followed back to the inflection point and the primary drainage curve is followed to a new historical maximum of gas saturation. If the

drainage process stops on the scanning-curve, imbibition is computed along the same scanning-curve.

4.6.3.2 Killough hysteresis model

Killough hysteresis model is similar to Carlson's model founded on Land's trapped gas correlation (Larsen, et al., 1995) ,(Killough, 1976). The only experimental data needed in this model is the bounding primary drainage curve, and data to estimate the bounding imbibition curve based on Land's correlation. The bounding drainage-imbibition curves make a reversible envelope, where scanning curves are estimated, illustrated in figure 4.12, based on the drainage curve through an interpolation method using a parametric curve or a normalized experimental imbibition relative permeability relation. The hysteresis model predicts the bounding imbibition relative permeability curve by first calculating the amount of non-wetting phase that will be trapped by Land's correlation, and then interpolate between the relative permeability at the historical maximum gas saturation and zero relative permeability at the trapped gas saturation.

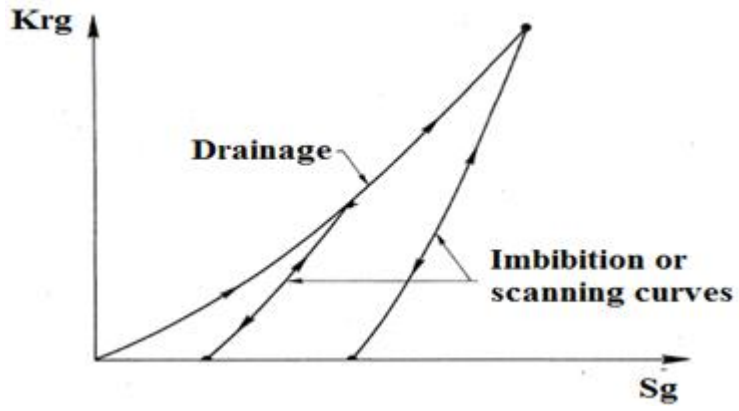

Figure 4.12: Killough hysteresis affected non-wetting phase relative permeability curves (Killough, 1976)

Subsequent to an imbibition process the drainage curve will follow the scanning curve till the maximum historical non-wetting phase has been reached, then continue along the primary drainage curve.

4.6.3.3 Skauge and Larsen three-phase hysteresis model

The hysteresis model of Skauge and Larsen is often referred to as the WAG-hysteresis model and is based on Carlson's hysteresis model and Land's trapped gas correlation (Kossack, 2000). The model contains two Carlson hysteresis envelopes, one for high

mobility and one for low mobility, illustrated in figure 4.13. Each of the envelopes obeys the rules of Carlson model in which scanning curves are produced parallel to the imbibition curves.

Change between the envelopes is activated when gas saturation increases in a drainage process, following the primary drainage-imbibition cycle (Larsen, et al., 1995). In simulation of WAG processes small saturation changes caused by stability problems occur frequently. To prevent these saturation oscillations to change between envelopes, the model was modified by introducing a saturation tolerance limit. This limit must be exceeded before a change between envelopes take place.

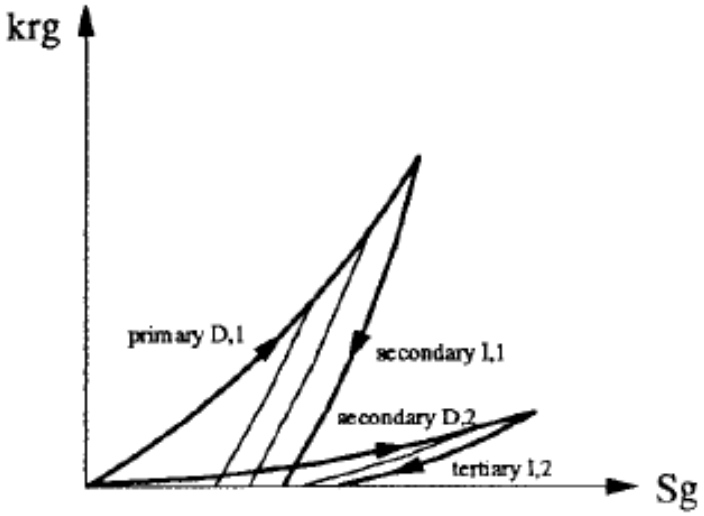

Figure 4.13: Skauge and Larsen hysteresis affected gas relative permeability curves, changing between a high and a low mobility envelope. (Larsen, et al., 1995)

The model can also define different water relative permeability curves within each envelop, illustrated in figure 4.14. Two different water relative permeability curves can be given as input, and a change between the curves occur corresponding to change in gas-phase envelops.

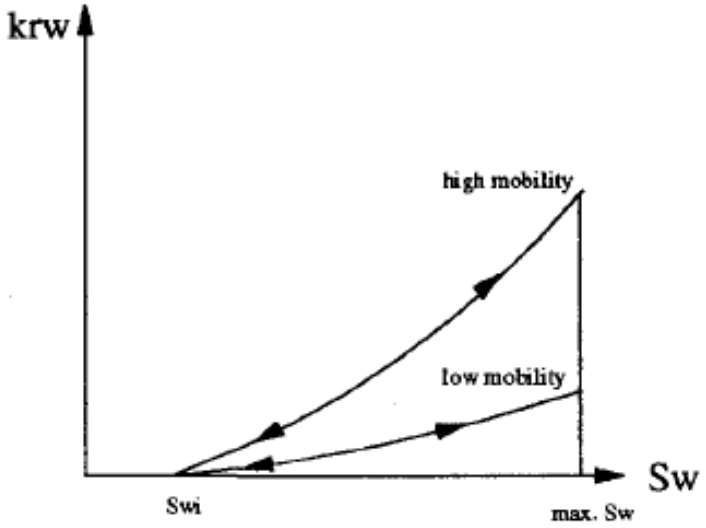

Figure 4.14: Skauge and Larsen water relative permeability curves, changing between a high mobility curve and a low mobility curve in correspondence with the gas-phase envelops in figure 4.13. (Larsen, et al., 1995)

4.7 Miscible flood residual oil saturation (SORM)

The residual oil left behind in the reservoir after a miscible WAG-process, the miscible flood residual oil saturation, is important to include in field-scale reservoir simulations to correctly evaluate the oil recovery. Compositional reservoir simulators may entirely sweep grid blocks in miscible flooding or close to miscible flooding, which will give an optimistic prediction of the oil recovery (ConocoPhillips Technical Manual, 2010). Complete oil sweep is unlikely to be achieved in field-scale even under perfect miscible conditions with first contact miscibility. There are several reasons for this, such as bypassed oil because of heterogeneities as fractures, capillary trapping of oil, viscous fingering and heavy component precipitations as asphaltenes and wax. The assumption of total mixing of all hydrocarbons within grid blocks is the reason for simulation to over predict oil recovery. The equation of state (EOS) in the simulator may allow all oil components to vaporize into the gas phase leading to oil saturations below user-defined Sorg and Sorw.

Various techniques have been proposed to account for SORM. Some of the techniques are:

1) To introduce an artifact heavy component so that, under reservoir conditions, the heavy component will not vaporize into the gas phase. This technique has not been recommended because it may completely miss fluid properties such as the density and viscosity.

2) Treat the miscible residual oil as a part of the rock. A user-defined SORM value can be defined as part of the rock such that oil saturation will not decrease beyond the SORM value. The excluded oil cannot contribute to rock wettability and to solution gas if the pressure falls below the bubble point.

3) Modification of the compositions of oil and gas phases that are flowing into or out of a grid block by an alpha factor method. A drawback of this technique is that there are too many parameters to tune per grid block, and the imposed SORM cannot be exactly honored.

4) The default method implemented in PSim is that a specified volume of the initial oil in place corresponding to SORM will be isolated and considered as a fourth phase in a different medium. A modified three-phase compositional model is used, which includes Sorm as a part of the oil saturation together with the mobile oil saturation, Som.

$$So = Sorm + Som \qquad \textit{Equation 4.16}$$

Various options can be used to account for wettability effect, and mass exchange via vaporization and condensation between the isolated oil and the flowing hydrocarbons.

5) Another technique available in PSim for SORM, is for SORM to only take effect internally for a grid block when the oil saturation in the grid becomes less than or equal to a defined SORM. This way SORM will not impact the flow as long as the oil saturation is larger than the defined SORM in the grid blocks. The check for a triggered SORM is done for each grid block at the end of the time steps (ConocoPhillips Technical Manual, 2010).

4.8 Matrix-fracture mechanisms

In the Ekofisk reservoir most of the fluid is stored in the matrix blocks, however without the fractures the Ekofisk field would likely not be producible. Even though the fractures only comprise about 0.5 % of the total reservoir volume they can enhance the effective permeability from 1 to 4 mD up to 100 to 150 mD, which enables fluid flow towards the production wells.

The primary method for detecting the fractures on the Ekofisk field is through well testing (Dangerfield, et al., 1987). Matrix permeability, k_{mat}, derived from well log porosity and

core permeability correlations are compared with the measured effective permeability from well tests, k_{well}, and a fracture intensity factor, FI, can be deduced:

$$FI = \frac{k_{well}}{k_{matrix}} \qquad \textit{Equation 4.17}$$

Different regions of the Ekofisk fields have different type of fractures, which makes up different kind of fracture-networks. The distribution of fracture types, fracture width, fracture lengths and fracture intensity factors, is not uniform throughout the reservoir. Therefore different matrix-fracture models representing different regions of the reservoir will be designed in this thesis.

The traditional yet efficient and effective approach to model naturally fractured reservoirs has been through dual porosity models (Heeremans, et al., 2006). In dual porosity models the fracture and matrix systems are separated into different continua with its own sets of properties.

When reservoirs with fracture systems are depleted, initially fluid will only be produced from the fractures (Dangerfield, et al., 1987). Because the fractures only comprise about 0.5 % of the reservoir volume, they are quickly depleted. As the fractures are depleted, a pressure difference between matrix blocks and fractures will develop. The pressure difference will lead to matrix blocks starting to feed fluid to the fracture system. Eventually, the production rate will be determined by the fluid influx rate from the matrix into the fractures. The fractures will then only enhance the net flow capabilities of the chalk matrix. The mass transfer between matrix blocks and fractures is in dual porosity models modeled through a transfer function, which is the heart of the dual porosity models as it controls the matrix-fracture interaction and production performance of naturally fractured reservoirs (Heeremans, et al., 2006) (Warren, et al., 1963).

At this time dual porosity models are not available in PSim, instead a single porosity/single permeability model is used to describe matrix-fracture systems in full field simulations where matrix and fractures are modeled within the same grid blocks with a shared set of properties.

4.9 Recovery mechanisms relevant to WAG

The oil left in the reservoir after water flooding comprises both bypassed oil in unswept reservoir zones and residual oil in water swept zones. Bypassed oil is associated with poor macroscopic sweep efficiency, while the residual oil in water swept zones is associated with poor microscopic sweep efficiency. WAG-injection is implemented to improve microscopic sweep efficiency compared to water injection because of gas half-cycles, and to improve macroscopic sweep efficiency compared to gas injection because of water half-cycles.

In this section WAG recovery mechanisms, displacement of oil by gas and by water, will be presented.

4.9.1 Oil recovery mechanisms for water injection

The most important forces acting to recover oil from water injection are viscous forces, gravity forces and capillary forces (Morrow, 1979).

4.9.1.1 Gravitational displacement

Displacement of oil in a fractured system by gravitational forces is the mechanism where water forces into the matrix blocks due to difference in fluid densities.

Gravitational forces might arise because of different water-oil contact in the fracture system and the matrix blocks. Difference in fluid densities give rise to a pressure difference and a gravity potential for water to be forced into the matrix blocks. The gravity potential,ΔP, is a given by:

$$\Delta P = (\rho_w - \rho_o) \cdot (X_{Wf} - X_{Wm}) \cdot g \cdot H \qquad \textit{Equation 4.18}$$

Where:

X_{Wf} : Fractional height of water in the fracture

X_{Wm} : Fractional height of the gas in the matrix

ρ_w : Water density

ρ_o : Oil density

g : Gravitational constant

H : Height of matrix blocks

In the case of the Ekofisk field, matrix blocks heights are estimated in the range of one to three feet, and the gravity potential between water and oil is normally negligible compared to capillary and viscous forces.

4.9.1.2 Capillary displacement - spontaneous imbibition

Spontaneous imbibition is the mechanism where one fluid displaces another from a porous medium as a result of capillary forces only. The matrix is a porous medium with a capillary pressure, and the fractures have approximately zero capillary pressure (Heeremans, et al., 2006). This results in a capillary pressure potential which allows the water to flow into the matrix to release oil.

Spontaneous imbibition has been widely studied because of its importance on oil recovery, with much emphasis on carbonate rocks. In fractured reservoirs, spontaneous imbibition of water due to strong capillary forces is regarded as an important and necessary mechanism to attain high displacement efficiency

The rate of imbibition is primarily dependent on the rock permeability, pore structure, rock wettability, and the interfacial tension between fluids. Oil recovery due to spontaneous imbibition can be determined from the capillary imbibition pressure curve. The higher water saturation value for capillary pressure equals to zero, the better is the spontaneous imbibition. The limit of spontaneous imbibition is determined where the imbibition capillary pressure curve equals to zero. The degree of spontaneous imbibition is a function of wettability as illustrated in figure 4.15. For more water-wet system higher water saturation can be achieved for capillary pressure equals to zero, hence better water imbibition into matrix blocks.

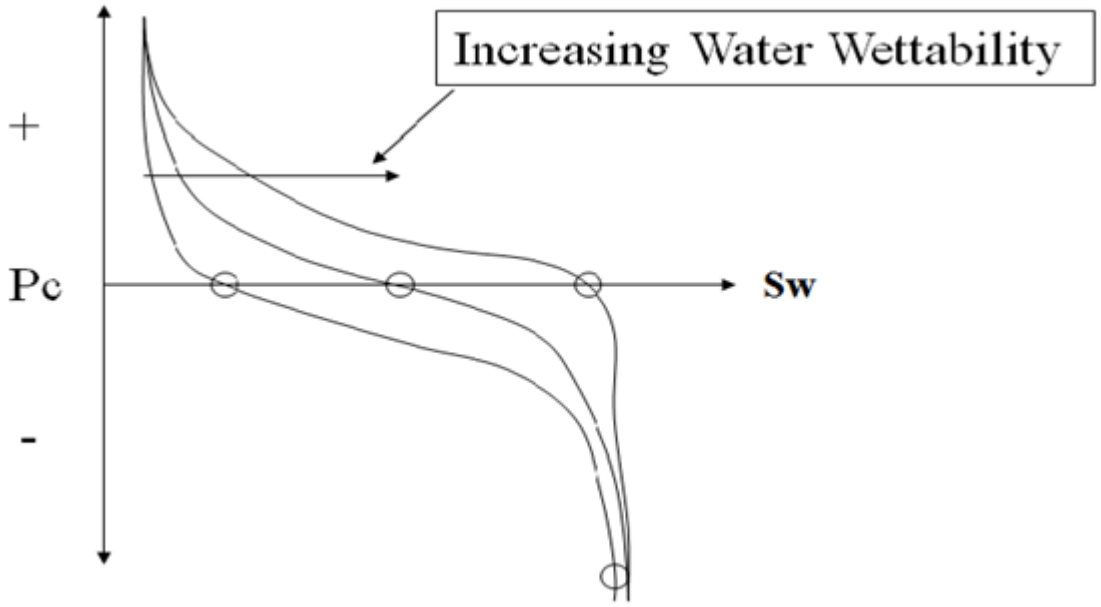

Figure 4.15: Capillary imbibition as a function of wettability

Further forced imbibition of water into matrix blocks at negative capillary pressures requires external forces like viscous or gravitational forces. In fractures reservoir where both spontaneous imbibition and viscous displacement is evident, the residual oil saturation after water flooding will depend more on the shape of the negative part, forced imbibition, of the capillary pressure curve and the magnitude of pressure drop than on the spontaneous imbibition part.

4.9.1.3 Viscous displacement

Viscous displacement is the mechanism where water is forced from the fracture system into matrix blocks due to a pressure gradient over the matrix blocks. Pressure differences in the reservoir results due to production, extracting fluids and decreasing the pressure, and injection, adding fluids and increasing the pressure.

The external pressure drop, over the matrix blocks, will force water into the matrix blocks until a balance between the viscous forces and capillary forces are reached. In the case of the Ekofisk field the pressure drop over matrix blocks is about 1 psi/ft.

4.9.2 Oil recovery mechanisms for gas injection

The most important oil recovery mechanisms for gas injection into a fractured reservoir are condensation of gas into oil, vaporization of oil, gravity drainage, diffusion and viscous displacement (Jakobsson, et al., 1994). Viscous displacement, gravity drainage and diffusion

are mechanisms for gas to enter the matrix blocks, while condensation and vaporization are the mechanisms for oil to expel into the fractures to be produced. The mechanism of viscous displacement for gas is such as described for water and will not be presented.

4.9.2.1 Vaporizing gas drive / oil stripping

Vaporizing gas drive is the mechanism where low molecular-weight hydrocarbons, ethane to heptanes, vaporize from the reservoir oil (Holm, 1987). As injected gas enters the matrix blocks it will not be in equilibrium with the reservoir oil, and a vaporization process will be initiated where lighter oil components will vaporize and transfer to gaseous phase (Jakobsson, et al., 1994). The gas in the matrix block will gradually increase its enrichment; hence the produced gas becomes more enriched than the injected gas. The vaporization process ultimately results in lower residual oil saturation, but will also give a heavier and more viscous residual oil.

Laboratory experiments conducted on Ekofisk chalk in 1994, as part of a WAG research program (Reservoir Laboratories AS, 1995) proved that vaporization of oil is the recovery mechanism for gas injection that produces most oil. The experiments were performed by injecting gas into completely water flooded core plugs, and take fluid samples to identify the physical mechanisms which acts to produce oil.

4.9.2.2 Condensation gas-drive / oil swelling

Condensing gas-drive is the mechanism of oil displacement by condensation of intermediate hydrocarbons components, ethane to pentane, from injected gas going in solution with the reservoir oil (Holm, 1987) (Wu, et al., 1990). Mass transfer of intermediate components from the injected gas into water flood residual oil makes the oil swell and become less viscous. The higher mobility results in oil being expelled from the matrix blocks into the fracture system to be produced.

The laboratory WAG research program (Reservoir Laboratories AS, 1995) indicated that oil swelling only produces water, and is not considered an important oil recovery mechanism. Following water flooding, the matrix blocks are highly water saturated and the relative permeability of water is high, while the relative permeability of oil is low. When gas enters oil in the matrix and swells into the oil it will expand in the pores. Even though the oil viscosity will decrease, the low oil relative permeability will unable oil to flow into the

fractures; however the high mobility water flow more easily into the fractures and be produced.

4.9.2.3 Gravity drainage

Gravity drainage is the mechanism where gas is forced into matrix blocks due to gravitational forces. Gravitational forces are caused by differences in fluid densities between injected gas and reservoir oil. As gas is injected into a fractured chalk reservoir, the gas will surround the matrix and create a gravity-potential between the matrix blocks and the fractures (Jakobsson, et al., 1994). If the gravitational forces overcome the capillary forces, gas will enter the matrix block where oil will be driven to the bottom of the block before the oil will drain to the fracture. The matrix will continue to drain out oil until the capillary forces, working against the gravity to keep the oil in the matrix pore system, are equal to the gravitational forces. The pressure difference,ΔP, due to gravity is given by (Heeremans, et al., 2006):

$$\Delta P = (\rho_o - \rho_g) \cdot (X_G - X_g) \cdot g \cdot H \qquad \textit{Equation 4.19}$$

Where:

X_G : Fractional height of gas in the fracture

X_g : Fractional height of the gas in the matrix

H : Height of matrix block

ρ_o : Oil density

ρ_g : Gas density

The amount of oil produced to the fracture is dependent on the balance between gas-oil capillary forces and gravitational forces caused by difference in oil and gas densities. The effectiveness of gravity drainage is directly related to the matrix block size, because liquid height is directly related to capillary forces (Reservoir Laboratories AS, 1995). The smaller the block size the less efficient is the gravity drainage.

4.9.2.4 Molecular diffusion

The diffusion process is of molecular nature and results from random motion of molecules in a solution. Molecular diffusion is present in all systems in which miscible fluids are brought into physical contact, and is an important phenomenon for dispersion of fluids

(Green, et al., 1998). The diffusion process may be described quantitatively using Fick's first law. Fick's first law relates the diffusion of a fluid into another fluid as proportional to the concentration gradient between the fluids.

In a fractured reservoir, significant component mass transfer between matrix and fracture may occur by molecular diffusion. In a matrix block filled with under saturated oil, transport of injected gas from the fracture into the matrix block occurs primarily by molecular diffusion (Reservoir Laboratories AS, 1995). The oil along the edge of the matrix block becomes saturated, which creates a concentration gradient within the matrix blocks. The concentration gradient will induce molecular diffusion. After some time, the innermost part of the matrix block will also become saturated with the injection gas, and equilibrium gas will be expelled from the matrix blocks. This process will continue until thermodynamic equilibrium is reached (Jakobsson, et al., 1994).

4.9.2.5 Combination of vaporizing and condensing mechanisms

If most of the mass transfer is from the oil to the gas, then the mechanism is termed as vaporizing drive. If the bulk of the mass transfer is from the gas to the oil, the mechanism is termed condensing drive. However in most cases, the mass transfer is actually a mixture of both these cases, and the displacement is a condensing-vaporizing drive (Al-Wahaibi, et al., 2007).

Zick (1986) was the first to present a detailed description of this mechanism. Zick stated the explanation that as enriched gas comes into contact with oil, the light intermediate components will condense from the gas into the oil, making it lighter. At the same time middle intermediate components in the oil are vaporized into the gas. Thus, the oil at the upstream location tends to become saturated with light intermediate components, but depleted of middle intermediate components. Such mechanism can result in low residual oil saturations and following increased oil recovery (Green, et al., 1998), (Elsharkawy, et al., 1992).

4.9.3 Capillary continuity

Capillary continuity is a mechanism for fractured reservoirs where the effect of gravity and viscous mechanisms are improved because matrix blocks are connected with a permeable contact and acts as one block.

If vertical capillary continuity exists, meaning matrix blocks are contacted on top of each other and acts as one tall block, the gravity potential increases because the height, H, in equation 4.18 and 4.19, will be the total height of all individual contacted blocks in the vertical direction. More water and gas will enter the connected block system and might increase the oil recovery substantially.

If horizontal capillary continuity exists; meaning matrix block are connected horizontally and acts as one long horizontal block, the pressure drop will be the sum of each individual block in the horizontal direction. The viscous forces will come in equilibrium with the capillary forces at a higher capillary pressure, resulting in higher recovery.

4.10 Miscible and immiscible WAG

The displacement efficiency of WAG-injections is highly dependent on whether the displacing gas is miscible or immiscible with the reservoir oil. Most miscible WAG projects are re-pressurized to create miscibility (Christensen, et al., 2001). However, because of failure to maintain sufficient pressure, real cases may oscillate between miscible and immiscible displacement.

4.10.1 Miscible displacement

Miscibility is defined as the physical condition between two or more fluid that permits them to mix in all proportions without existence of an interface (Holm, 1987). At any mixing ratio a single homogeneous phase is formed. Miscible displacements can be first-contact miscible or multi-contact miscible.

4.10.1.1 First contact miscibility

In a first-contact miscible (FCM) displacement, the injected gas and reservoir oil will mix instantly to create a single phase in all mixing proportions (Al-Wahaibi, et al., 2007). To achieve first-contact miscibility, injection of highly rich gases with hydrocarbons such as ethane, propane, butane, or mixtures of liquefied petroleum gas (LPG) are used (Holm, 1987). For leaner gas system FCM can be achieved by gas injection at very high pressure.

However, it is often not economical to inject a gas that is FCM with the oil. Instead, the injected gas can be design to develop multi-contact miscibility with use of leaner hydrocarbons (Al-Wahaibi, 2009).

4.10.1.2 Multi-contact miscibility

In a multi-contact miscibility (MCM) displacement, mass exchange between the injected gas and the reservoir oil will result in miscibility between the two phases, after a number of contacts, within a mixing zone of the flood front (Al-Wahaibi, et al., 2007).

The injected gas and the reservoir oil are not initially miscible. As more gas is injected, an enriched gas mixture is pushed away from the injection well and forms a new even richer mixture. The process continues and creates a transition zone of contiguously miscible liquid compositions, ranging from injection gas at the wellbore to unaltered oil just ahead of the flood front in the reservoir (Jethwa, et al., 2000).

Multi-contact miscibility can develop through a vaporizing process, a condensing process or a combination of the processes. In the vaporizing process the intermediate molecular weight hydrocarbons from the oil are transferred to the leading edge of the gas front, enabling it to become miscible with the reservoir oil after a number of contacts (Elsharkawy, et al., 1992), (Wu, et al., 1990).

In the condensing process, the injected gas is enriched with light hydrocarbons. The reservoir oil left behind by the gas front is enriched by net transfer of light hydrocarbons from the gas phase into the oil. Enrichment of the reservoir oil proceeds until it becomes miscible with the injected gas (Elsharkawy, et al., 1992), (Wu, et al., 1990).

Miscibility can partly develop through a combination of the vaporizing and the condensing processes. As in the condensing process, the light intermediate components in the injected gas condense into the crude oil, while the middle intermediate components vaporize into the gas phase.

4.10.2 Immiscible displacement

Immiscible displacement is a process where two separate fluid phases form after adding some proportion of one fluid (Al-Wahaibi, et al., 2007). Immiscible gas injections have the possibility of enhancing oil recovery. Even though two separate phases will create when

injecting immiscible gas, some mass exchange between the two phases will occur. Gas vaporization from the oil or condensation of gas into the oil or a combination of the two processes could appear. Dependent on the degree of mass exchange the process could get nearly miscible and result in favorable changes in the fluid viscosity and fluid density (Dong, et al., 2005), (Christensen, et al., 2001).

For WAG processes, immiscible displacement has been applied to improve macroscopic sweep efficiency by improving the frontal stability and by contacting un-swept regions (Christensen, et al., 2001), and also improve the microscopic sweep efficiency by some mass exchange between oil and gas. Microscopic sweep efficiency for immiscible WAG displacement is usually determined by gas residual oil saturation, S_{org}, in gas invaded zones and by water flood residual oil saturation, S_{orw}, in water dominated zones (Skauge, et al., 1994).

4.10.3 Evaluation of miscibility

The displacement efficiency of a WAG process, as presented in the previous section, is highly dependent on whether the injected fluid will be miscible or immiscible with the reservoir oil. It is therefore important to be able to evaluate if injected gases will create miscibility or be immiscible with the reservoir oil. Such evaluation can be done by studying two parameters, the minimum miscibility pressure (MMP) and the minimum miscibility enrichment (MME).

4.10.3.1 Minimum miscibility pressure (MMP)

The displacement efficiency of reservoir oil by gas injection is highly pressure dependent and miscible displacement is only achieved at pressures greater than a certain minimum pressure, termed the minimum miscibility pressure. Minimum miscibility pressure is defined as the lowest pressure for which a given injected gas composition can develop miscibility through a multi-contact process with a given reservoir oil at reservoir temperature (Green, et al., 1998). The reservoir to which the process is applied must be operated at or above the MMP to develop miscibility. Reservoir pressures below the MMP result in immiscible displacements and consequently lower oil recoveries (Elsharkawy, et al., 1992). The minimum miscibility pressure has been reported a strong function of the reservoir oil, the composition of the injected gas and the reservoir temperature (Ahmed,

2000). Temperature dependence of MMP has mostly been investigated for CO_2-gases. Elsharkawy et.al (1992) reported that MMP for three different oils with CO_2 increased in the range of 1250 to 1500 psia when temperature was increased from 100 to 200˚F. Other reports on CO_2 have agreed with the observation, except at very high temperatures above 300˚F, where MMP has showed a decreasing trend with increased temperatures. However, the very little data reported on temperature dependence of MMP for hydrocarbon gases has not shown any clear trends. Firoozabadi and Aziz (1986) reported that for 100 % methane injected the MMP decreased with temperature. Lee and Reitzel (1982) reported though that no trend on MMP with temperature could be seen from a dry hydrocarbon gas with a content of 85 % methane.

4.10.3.2 Minimum miscibility enrichment (MME)

Minimum miscibility enrichment is defined as the lowest gas enrichment at which the injected gas can develop miscibility through a multi-contact process with a given reservoir oil at reservoir temperature and a given constant pressure (Green, et al., 1998). The injected gas composition must be enriched to or above the MME to develop miscibility with the reservoir oil. The minimum miscibility enrichment is a function of composition of reservoir oil, reservoir pressure and reservoir temperature.

4.10.3.3 Evaluation of MMP and MME

The challenge is to determine MMP and MME for a given reservoir oil at existing reservoir conditions. There exist both laboratory methods, empirical correlations based on experimental data and phase-behavior calculations based on an EOS and computer modeling to determine MMP and MME.

The empirical correlations are based on experimental results and are relative simple to apply. However, the predicted values can be significantly in error so empirical correlations are typically only used to obtain first pass estimates and as a screening tool for evaluation of miscibility (Green, et al., 1998).

Most phase-behavior correlations are design to evaluate miscibility for CO_2-injection. Tarek Ahmed (2000) though presented a methodology to determine MMP also for other displacing gas-types. Ahmed proposed a method combining a modified Peng and Robinson equation of state (PR-EOS) with a miscibility function to get estimates of the MMP. The

miscibility function is a mathematical expression used to describe miscibility conditions in terms of injection pressure and overall composition. Such phase-behavior methods can be used to obtain reliable results (Green, et al., 1998). However, the approach requires availability of a significant amount of compositional data for the reservoir fluids. Such data are often not available and tedious laboratory analyses are needed to obtain them. Further, an appropriate modified PR-EOS and a miscibility function is needed, together with a powerful computer to solve a complex solution algorithm. Because of the complexness and the lack of necessary data, such models will not be discussed in more detail in this thesis.

The more common way to evaluate miscibility of a system is through laboratory measurements (Elsharkawy, et al., 1992), (Randall, et al., 1988). Primarily two laboratory methods are used to measure MMP and MME, namely the slim-tube method, and the rising-bubble method. Slim-tube displacement tests have been widely used since early 1950s and are often referred to as the "industry standard" for evaluating miscibility. The rising-bubble nmethod was developed in the early 1980s, and laboratory experience has indicated that this method is considerably faster than the slim-tube method. In this thesis a ConocoPhillips created slim-tube model for simulations on MMP and MME will be used. A more detailed description of the slim-tube method will therefore be given.

4.10.3.4 Slim-tube tests

Slim-tube tests have become a generally accepted procedure for miscibility evaluation, although slim-tube design, operating procedure and criteria for interpretations have not been standardized by the petroleum industry (Green, et al., 1998). A great variety of specifications for slim-tube apparatus have therefore been reported with different slim-tube lengths, diameters, type of packing and permeability and porosities of packing. A good design of a slim-tube apparatus is to use long tubes to minimize the effect of transition zone length and small tubing diameter to prevent viscous fingering.

The slim-tube apparatus is operated by completely saturating the slim-tube with oil at the start of each displacement test. Gas is then injected to displace oil. Water is absent in slim tube tests. Laboratory one displacement test takes one day, with another day or two for cleaning and re-saturating the slim-tube. Determination of MMP for a gas-oil system with a slim-tube requires from one to two weeks (Elsharkawy, et al., 1992), (Shyeh-Yung, 1991).

To evaluate and interpret the MMP based on slim-tube experiments, oil recovery at gas breakthrough, oil recovery at 1 to 1.2 pore volumes of injected gas, and ultimate recovery can be plotted as a function of operating pressure. One criteria of determining MMP is the break-over pressure of the recovery curves. If the break-over is not sharp, the MMP can be chosen as the pressure for in which incremental oil recovery per incremental pressure increase is less than some arbitrary value. MMP could also be defined as the pressure when the oil recovery is 90 to 95 percent (Elsharkawy, et al., 1992).

To evaluate the MME, oil recovery from several slim-tube tests with increasing levels of enrichment at constant pressure are compared. To interpret MME oil recovery at gas breakthrough, oil recovery at 1 to 1.2 pore volumes of injected gas, the enrichment at 90 to 95 percent oil recovery, and ultimate recovery can be plotted as a function of enrichment level (Elsharkawy, et al., 1992).

Slim-tube laboratory experiments to determine MMP or MME for Ekofisk crude oil are not available. Slim-tube simulations will be performed to investigate potential MMP for the produced dry hydrocarbon gas; to evaluate what reservoir pressures are needed to achieve miscibility, and to study MME to evaluate what gas enrichments are needed at different pressures to achieve miscibility.

The temperature around water injection wells are lower compared to production wells because of cooling of the formation due to 20-30 years of cold water injection. Since both MMP and MME have been reported to be functions of temperature, sensitivity studies of MMP and MME to temperature will be included as part of the slim-tube simulation study.

4.11 Introduction to the numerical reservoir simulation tool (PSim)

PSim is a ConocoPhillips developed full field numerical reservoir simulation tool, specialized for the Ekofisk field. The tool has special formulations treating reservoir compacting and behavior of chalk as in the Ekofisk field case. The tool is generalized for simulation of black oil and compositional problems in single-porosity reservoirs. The model has been tested against SPE Comparative Solution Project problems and has been used in numerous field studies (ConocoPhillips Technical Manual, 2010).

Discrete mass balance equations for each grid blocks are linearized in PSim by either IMPES or implicit formulations. In IMPES formulations, pressures are treated implicitly and saturations are treated explicitly. In implicit formulation all unknowns are implicitly solved simultaneously using Newton-Raphson method. IMPES is the default formulation in PSim and usually requires less CPU time than the implicit formulation. However, IMPES method is conditionally stable and sufficiently fine grid and small time step lengths are needed to avoid instability. The implicit formulation is always stable (Kleppe, 2011). The linear equations can then be solved in PSim by the three linear solvers; bandwidth direct (D-4 ordering), Orthomin preconditioned by Nested Factorization and Orthomin preconditioned by ILU (ConocoPhillips Technical Manual, 2010).

For compositional problems Peng-Robinson or Soave-Redlich-Kwong equation of state can be used to compute fluid properties for any number of components. For each component molecular weight, critical temperature and pressure, critical z-factor, shift factor, acentric factor and cubic EOS constants have to be specified.

Two- phase water-oil and gas-oil relative permeability and capillary pressure tables can be entered for multiple rock types, i.e. for the fracture system and for the matrix blocks, which are normalized before use in the simulations. For three-phase permeability Stone's first model is default, but also Stone's second model and Baker's saturation-weighted linear interpolation method is available. Correlations for trapped gas saturation with associated relative permeability hysteresis effect are also available, with Coats as default and also the choice of Land's non-linear and linear method. In PSim any number of pressure-volume-temperature (PVT) tables, black oil or compositional, can be entered, and each grid block must be assign to a set of PVT-tables. All compositional PVT tables must use the same number and names of components (ConocoPhillips Technical Manual, 2010).

The tool provides a variety of outputs for analysis; including rates, cumulative production and injection, which all can be specified how frequently printed and from which regions of the reservoir/model. The output data is analyzed in the ConocoPhillips program CView.

5 Slim-tube modeling

The recovery efficiency of WAG-injection is highly dependent on whether the process is miscible or immiscible. The slim-tube simulation model has been used to evaluate if injected gas will be miscible or immiscible with the Ekofisk crude oil. This has been done by evaluating the MMP and MME. In this chapter description of the slim-tube simulation model, methodology to determine MMP and MME, and results and discussion from simulations are presented. Finally a decision has been taken to proceed with miscible or immiscible process for the further studies.

5.1 Description of the slim tube model

The slim-tube simulation model used in this study was initially designed for evaluation of CO_2-gas miscibility with Ekofisk crude oil. However, a revised EOS, tuned against hydrocarbon gas experimental data at ConocoPhillips research center in Bartlesville, has made it applicable for miscibility evaluations for hydrocarbon gases.

The slim-tube model is a one dimensional, compositional, 400 grid-blocks displacement model of oil by gas, illustrated in figure 5.1. Each grid block has the length in x-direction of 2.5 ft, making the total model 1000 ft long. The size of each grid block is 14037.5 ft^3, with grid block sides of 2.5 ft, 561.5 ft and 10 ft, in the x-,y- and z-direction respectively. An injection well is perforated in grid block (1,1,1), and a production well is perforated in grid block (400,1,1). The pressure difference between the injection well and production well is 1000 psia in all simulations, resulting in a pressure gradient of 1 psi/ft. The grid blocks properties in the model are homogeneous with constant porosity and absolute permeability of 10 % and 10D respectively.

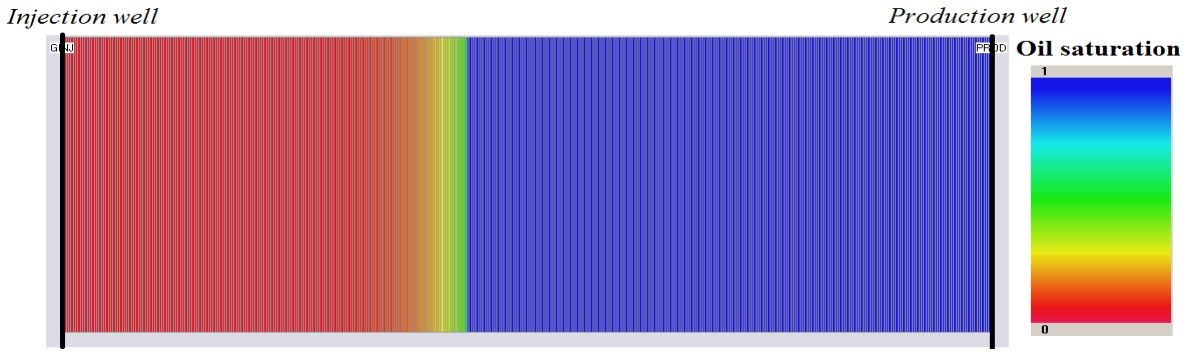

Figure 5.1: Illustration of slim-tube model after some time of gas injection

The slim-tube is always initialized with single phase oil. The input oil composition and corresponding saturation pressure for the slim-tube model has been obtained by running a simulation on the homogeneous mechanistic model, described in the chapter 6. The simulation is performed by running primary depletion and water flooding with initial Ekofisk oil composition and saturation pressure as input, to mimic the Ekofisk history. At the end of the simulation, the output in-situ oil composition and the new saturation pressure are monitored, which are used as input for the slim-tube simulation. This way, the oil composition will be more close to the current Ekofisk oil composition and results are more reliable and in accordance to the timing of a potential WAG-injection. The oil compositions and corresponding saturation pressure are given at a reference depth of 10280 feet.

Two different EOS are used to compute fluid properties for the components at given conditions. One is for use at high temperatures and the other is for use at lower temperatures. Both EOS are 15-components modified Peng-Robinson type EOS designed for the Ekofisk crude oil and tuned against measured phase behavior data of oil vaporization by immiscible hydrocarbon gas at high and low temperatures. A test simulation with the high temperature EOS at 60˚F was compared with a similar run with the low temperature EOS, which showed some difference in oil recovery. Both EOS consist of the same components, shown in table 5.1, and use the same set of PVT data. The only difference between them is their binary coefficients.

Table 5.1: The 15 components used in EOS for slim-tube simulations

Composition	Abbreviation in EOS
Nitrogen	N2
Carbon dioxide	CO2
Methane	C1
Ethane	C2
Propane	C3
Iso-butane	iC4
n-butane	C4
Iso-pentane	iC5
n-pentane	C5
Hexane	C6
Heptane + Octane	C7P1
C9-C13	C7P2
C14-C19	C7P3
C20-C29	C7P4
C30+	C7P5

The last five components of the EOS given in table 5.1 are pseudo-components. A pseudo-component is a lumping of several components into one component comprising a shared set of compositional PVT data.

5.2 Methodology for slim tube model

5.2.1 Methodology minimum miscibility pressure

Miscibility of a gas with reservoir oil in a WAG-process is highly pressure dependent. To determine if a WAG-process will be miscible or immiscible one can evaluate the minimum miscibility pressure of the gas-oil system. The minimum miscibility pressure (MMP) is, as presented in chapter 4.10.3.1, the lowest pressure for which a given injected gas composition can develop miscibility through a multi-contact process with a given reservoir oil at reservoir temperature.

To evaluate MMP, simulations are run in PSim where gas is injected into the slim tube model at different operating pressure between simulations. Following each run, oil recovery as a function of gas volume injected, and mole composition produced and injected are printed. For each simulation gas is injected at constant temperature and pressure, and the oil recovery at 1.2 pore volumes of gas injected is monitored. After a number of simulations with different operating pressures, a graph of oil recovery at 1.2 pore volumes of gas injected can be plotted against operating pressures, all at constant temperature. MMP can then be determined by the criteria of break-over pressure of the curve, presented in section 4.10.3.4. Plotting oil recovery at 1.2 pore volumes of gas injected versus operating pressure and using the criteria of break-over pressure of the curve to determine MMP is the most commonly used practice for slim-tube tests. This is the reason for the selection of such procedure in this study.

In all slim-tube simulations where MMP is evaluated, the injected gas composition used is similar to the composition of dry hydrocarbon gas produced at Ekofisk, shown in terms of mole percent in table 5.2:

Table 5.2: Composition of Ekofisk dry hydrocarbon gas

Components	Mole %
N2	0.28
CO2	2.65
C1	84.02
C2	9.41
C3	2.94
iC4	0.22
C4	0.41
iC5	0.04
C5	0.03

In chapter 4.10.3.1 it was presented that MMP has been reported to be temperature dependent for different injection gas types. Temperatures around injection wells can be as low as 60˚F, because of the cold water injection, and increases towards production wells up to the initial reservoir temperature of 268˚F. Because of the great variety of temperatures within the Ekofisk field, MMP dependence to temperature for dry hydrocarbon gas is included in this study. To do this MMP is evaluated at 60˚F, 100˚F, 150˚F, 200˚F and 268˚F. The high temperature EOS is used for simulations at reservoir temperatures of 200˚F and 268˚F, while the low temperature EOS is used for simulations at reservoir temperatures of 60, 100 and 150˚F. Evaluation of temperature dependence on MMP is performed by repeating the procedure presented above, running several simulations at different operating pressure for each temperature. The output data are then monitored and graphs of oil recovery at 1.2 pore volumes of gas injected versus operating pressures are plotted for the different temperatures and evaluated by the break-over pressure criteria.

5.2.2 Methodology minimum miscibility enrichment

Miscibility of gas with reservoir oil in a WAG-process is strongly dependent on the enrichment level of the injected gas. To determine whether a process will be miscible or immiscible the minimum miscibility enrichment of gas-oil systems can be evaluated. Minimum miscibility enrichment (MME) is, as presented in section 4.10.3.2, the lowest gas enrichment at which injected gas can develop miscibility through a multi-contact process with a given reservoir oil at constant temperature and pressure.

Evaluation of MME is performed in this study by injecting gas, with increasing amounts of natural gas liquid (NGL) added to the dry hydrocarbon gas, into the slim-tube model at constant pressures until miscibility is achieved. The NGL composition is given in table 5.3, and the dry hydrocarbon gas is the one given in table 5.2. The amount of NGL that is required to be added to achieve miscibility at a given reservoir pressure and temperature is defined as the minimum miscibility enrichment.

Table 5.3: Composition of the NGL added to dry gas in MME evaluations

Components	Mole %
CO2	1.16
C1	1.96
C2	18.59
C3	28.68
iC4	6.56
C4	19.32
iC5	6.59
C5	7.35
C6	7.28
C7P1	2.45
C7P2	0.06

The NGL composition used has gone through process facilities and separation from the produced Ekofisk gas, and is usually meant to be transported in pipelines for sale.

In each MME-simulation gas is injected at constant temperature and pressure, and the oil recovery at 1.2 pore volumes of gas injected is monitored. Injected gas composition is then altered for new simulations and the procedure is repeated. Injected gas compositions with 0 %, 2 %, 5 %, 8 %, 10 %, 12 %, 15 % and 20 % NGL added to the dry hydrocarbon gas are simulated, comprised gas compositions are given in appendix A.

When the above procedure is completed for all enrichment levels, a graph of oil recovery at 1.2 pore volumes of gas injected can be plotted against enrichment level (amount NGL added) all at constant temperature and pressure. MME can then be determined by the criteria of 95 % oil recovery, as presented in chapter 4.10.3.4. MME have often been hard to evaluate based on the break-over criteria, which is the reason for the criteria of 95 % oil recovery is chosen to determine MME in this study.

The MME is, as presented in chapter 4.10.3.2, dependent on the reservoir pressure. The current reservoir pressures around injection wells are commonly between 6000-6800 psia, and lower around production well, commonly between 5000-6000 psia. Since the pressures throughout the reservoir vary greatly, study of MME dependence to pressure is necessary. MME is therefore evaluated at operating pressures of 5000 and 6000 psia.

MME has also been reported temperature dependent. As earlier mentioned the reservoir temperature varies within different regions of the reservoir. Study of MME dependence to temperatures is therefore necessary. Evaluation of temperature dependence on MME is therefore performed at 60 ˚F, 150 ˚F and 268 ˚F. The low temperature EOS is used for temperatures of 60 ˚F and 150 ˚F, while the high temperature EOS is used for 268 ˚F. For each temperature constant operating pressure of 6000 psia is used and the procedure presented above is repeated by running simulations with each enrichment level for all temperatures. The output data are monitored and graphs of oil recovery at 1.2 pore volumes of gas injected versus enrichment levels can then be plotted for the different temperatures. Evaluation of MME according to the 95 % oil recovery criteria can then be used to compare MME for the different temperatures.

5.3 Results and discussion of slim-tube simulations

The results from the slim-tube simulations are presented in this section, divided into MMP and MME evaluation.

5.3.1 Minimum miscibility pressure

Slim-tube simulations to evaluate MMP were run in PSim at constant temperature of 268 ˚F and the recovery factor at 1.2 pore volumes of injected gas for different operating pressures were monitored, and is plotted in figure 5.2 and 5.3 based on the data given in appendix A.

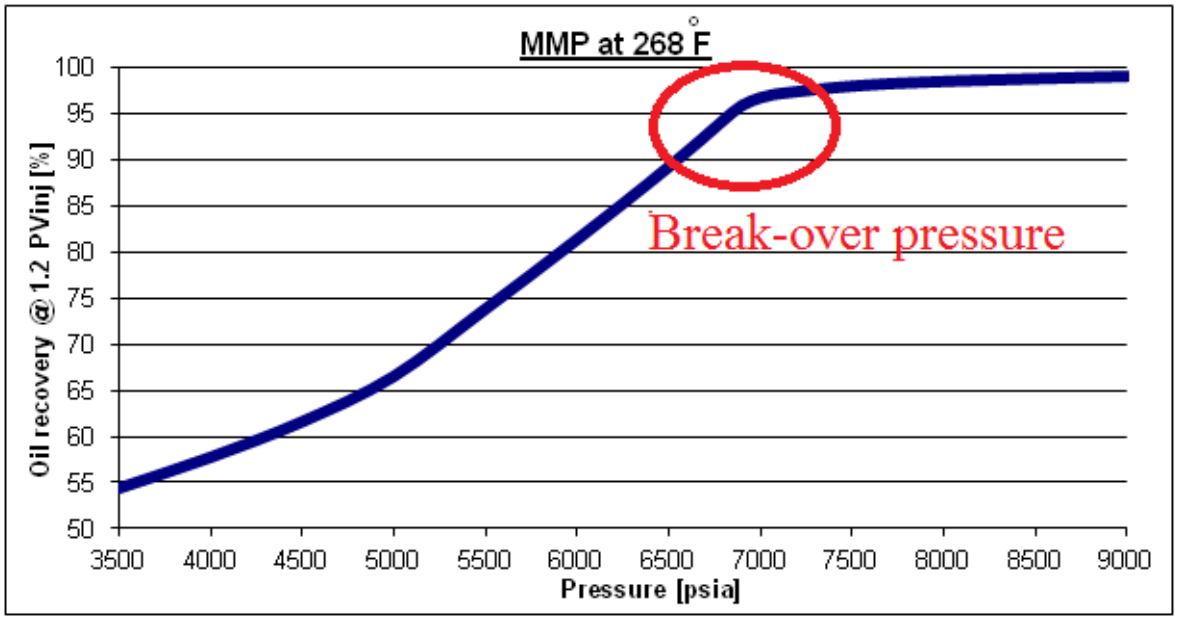

Figure 5.2: MMP evaluation at 268˚F

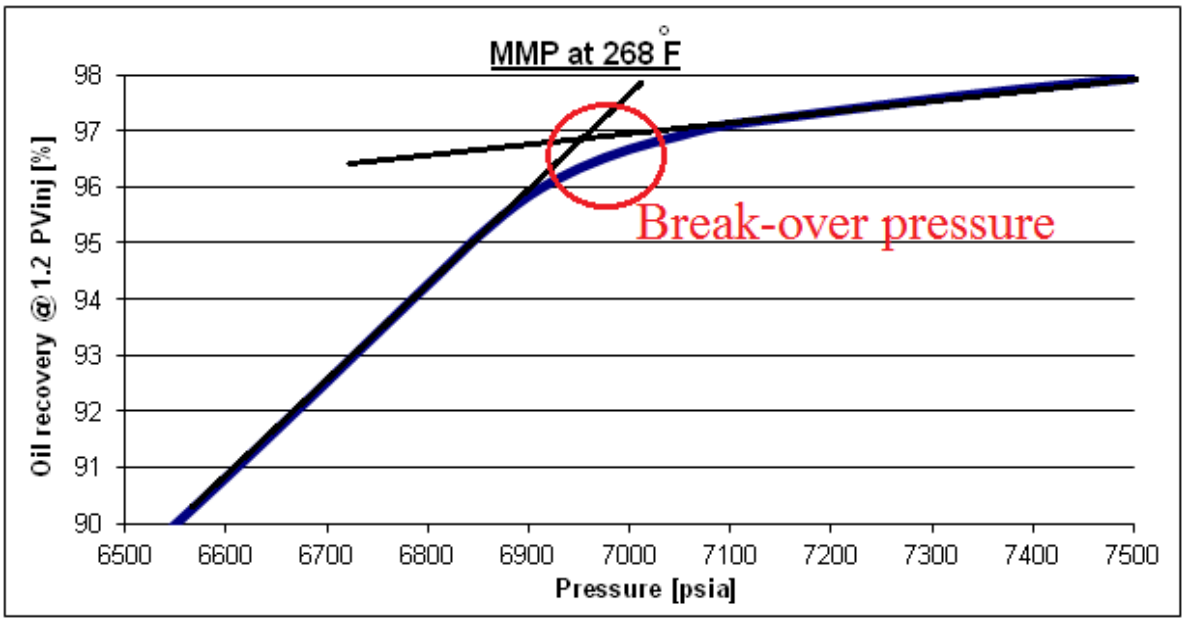

Figure 5.3: MMP evaluation at 268˚F, zoomed to the break-over pressure region

MMP at 268˚ F is determined by the break-over pressure criteria, presented in chapter 4.10.3.4, to be between 6900 and 7000 psia, illustrated in the red circle in figure 5.3.

At low pressures when 1.2 pore volumes of gas is injected, compositional analysis from the output data indicates that large amount of residual oil is left behind as both lean and heavy hydrocarbons components. As the pressure was increased to 6500, near the minimum miscibility pressure, most of the lean components up to C9 were produced, however still a considerable amount of heavier components C10+ remained unproduced. At the MMP, of

6900-7000 psia, nearly all heavy oil components above C10+ were also produced. Further increase of pressure above MMP had little effect on residual oil, which is also seen on the oil recovery curve in figure 5.2, which flattens out for pressures above the MMP.

Simulations were further run in PSim with different temperatures of 60 ˚F, 100 ˚F, 150 ˚F, 200 ˚F and 268 ˚F with varying operating pressures for each temperature. Oil recoveries at 1.2 pore volume of gas injected were monitored as a function of operating pressure for the different simulations, given in appendix A, and plotted in figure 5.4 for different temperatures.

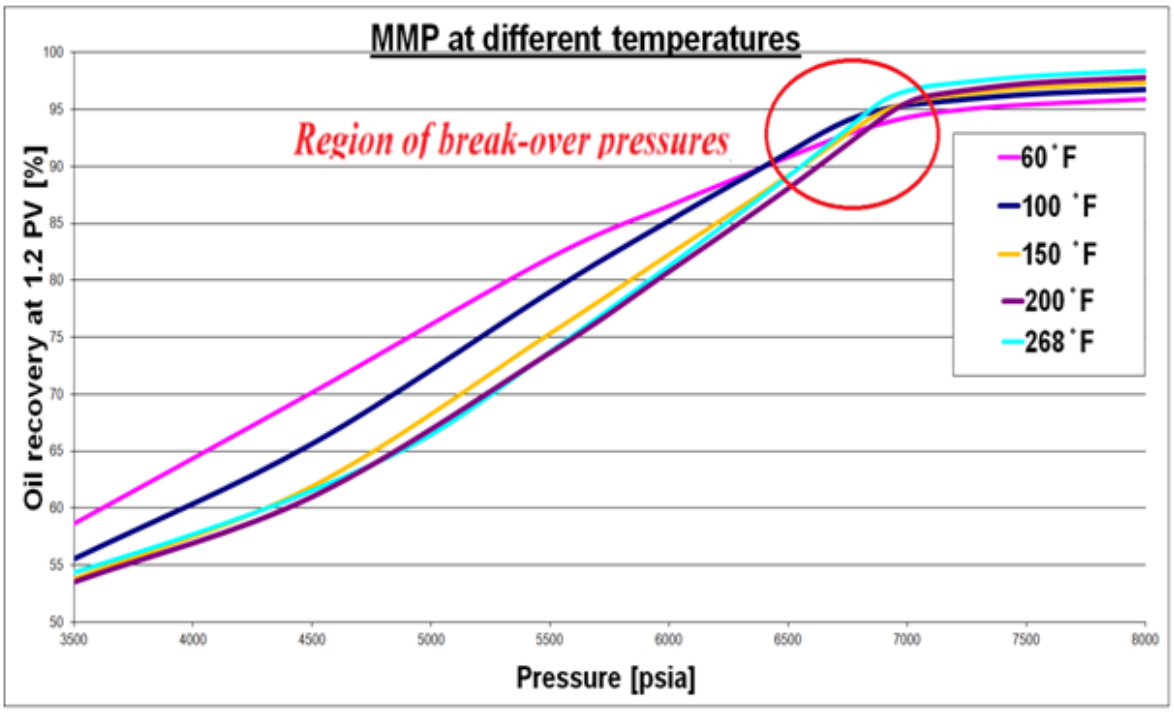

Figure 5.4: MMP evaluation at different temperatures

The break-over pressure criteria was used to determine MMP for the different temperatures and showed to be in the range of 6600 to 7100 psia, within the red circle in figure 5.4.

To determine if any temperature trends for MMP can be observed, the range in which MMP was determined to is plotted against temperature in figure 5.5.

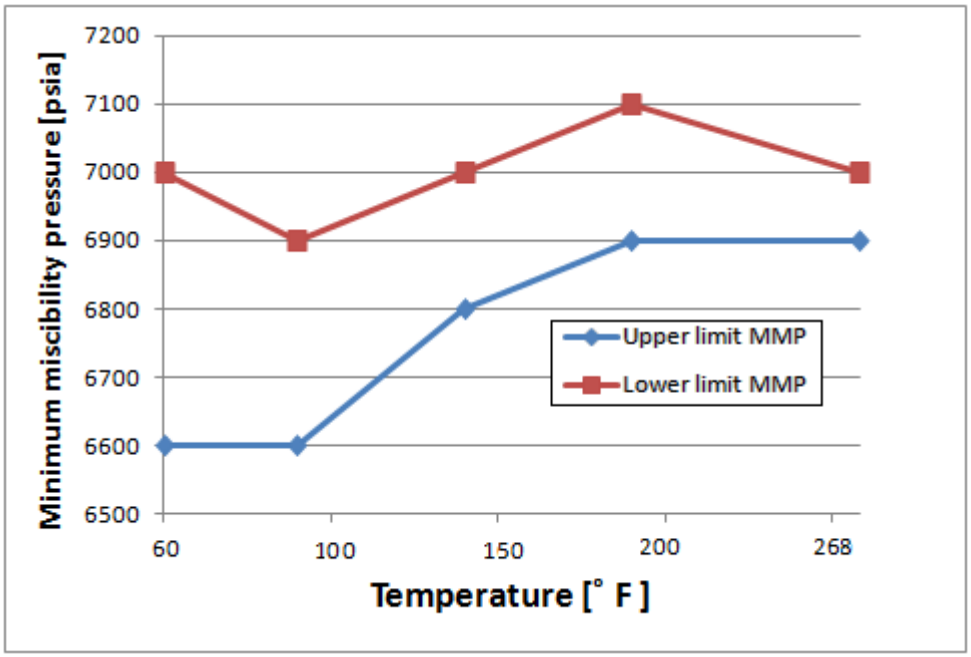

Figure 5.5: The pressure range which MMP was determined in for different temperatures

The results of temperature dependence of MMP show no clear trends, analogous to what was reported by Lee and Reitzel (1982) with a hydrocarbon gas with methane content of 85 %. The injected gas used in this study had a methane content of 84 %. Because the MMP for different temperatures is determined to be within a small pressure range, it is concluded that dry hydrocarbon gas with the Ekofisk crude oil do not significantly affect the MMP at different temperatures.

MMP conclusion

Based on the current reservoir pressures at Ekofisk, which in most regions are below the determined MMPs, WAG injection will most likely by immiscible when injecting dry hydrocarbon gas. Close to injection wells pressures can be up to 6800 psia and miscible or close to miscible processes can be achieved. As gas is injected the enrichment of the injected fluid front will increase because of mass exchange with the oil, however as the injection front moves further into the reservoir the pressures are much lower and the process will most likely be immiscible.

To achieve miscibility one can start the WAG injection at a later stage, when continued water injection has increased reservoir pressures above the MMP. Another alternative to achieve miscibility is to enrich the injection gas above the MME. The latter alternative will be presented in the next section.

5.3.2 Minimum miscibility enrichment

To evaluate the MME, slim-tube simulations were run in PSim at 268˚F with different enrichment levels of the injected gas shown in appendix A. Output oil recoveries at 1.2 pore volumes of gas injected were monitored as a function of the amount NGL added at reservoir pressures of 5000 and 6000 psia plotted in figure 5.6 based on the data in appendix A.

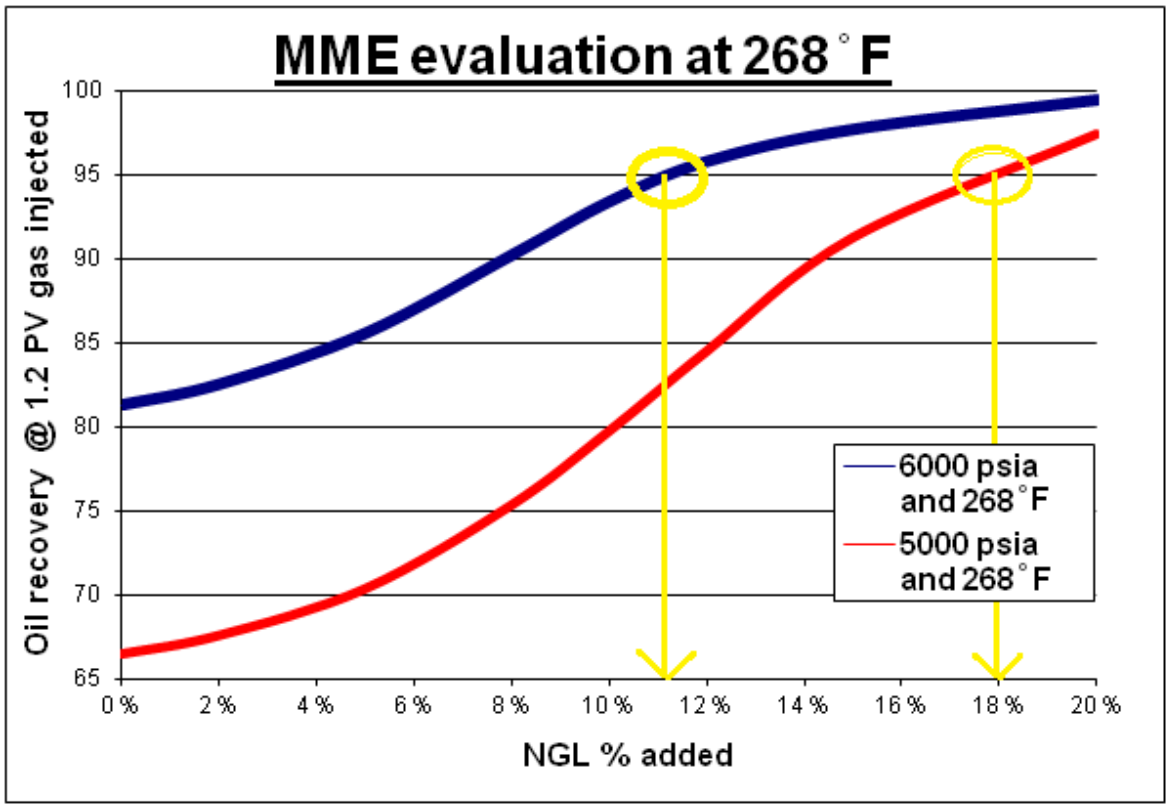

Figure 5.6: MME evaluation at operating pressures of 5000 psia and 6000 psia and constant temperature of 268˚F

Based on the criteria of 95 % oil recovery, MME is determined as 11 % enrichment of NGL at pressure of 6000 psia and 18 % enrichment of NGL at pressure of 5000 psia.

The results on MME to pressure agree with the theory stating that higher pressures are needed to achieve miscibility for leaner gases than for more enriched gases.

Based on the gradient of the two curves in figure 5.6 it is observed that for lower pressures increased enrichment will have greater effects on the oil recovery than for equal increase in enrichment for higher pressures. To achieve miscibility a more enriched gas is required for low pressures. The incremental oil recovery for low pressure is however larger than for

high pressure, so when increasing the enrichment level equally for the two cases the curves converges as enrichment level is increased.

Figure 5.6 illustrates that the largest gradient of the two curves are from 6 to 11 % enrichment level for the 6000 psia case and from 7 to 14 % for the 5000 psia case. This observation indicates that miscibility is not necessarily to be achieved to increase oil recovery substantially. Actually the largest increase in oil recovery for increasing enrichment levels is in the immiscible, close to miscible, region. Above the MME increased enrichment level will have less effect on oil recovery and the curves will eventually flatten out.

Simulations were further run in PSim with different temperatures of 60˚F, 150˚F and 268˚F with the different enrichment levels for each temperature, all at constant pressure of 6000 psia. Oil recoveries at 1.2 pore volume of gas injected as a function of enrichment levels were monitored for the different simulations, and is given in appendix A and plotted in figure 5.7 at different temperatures.

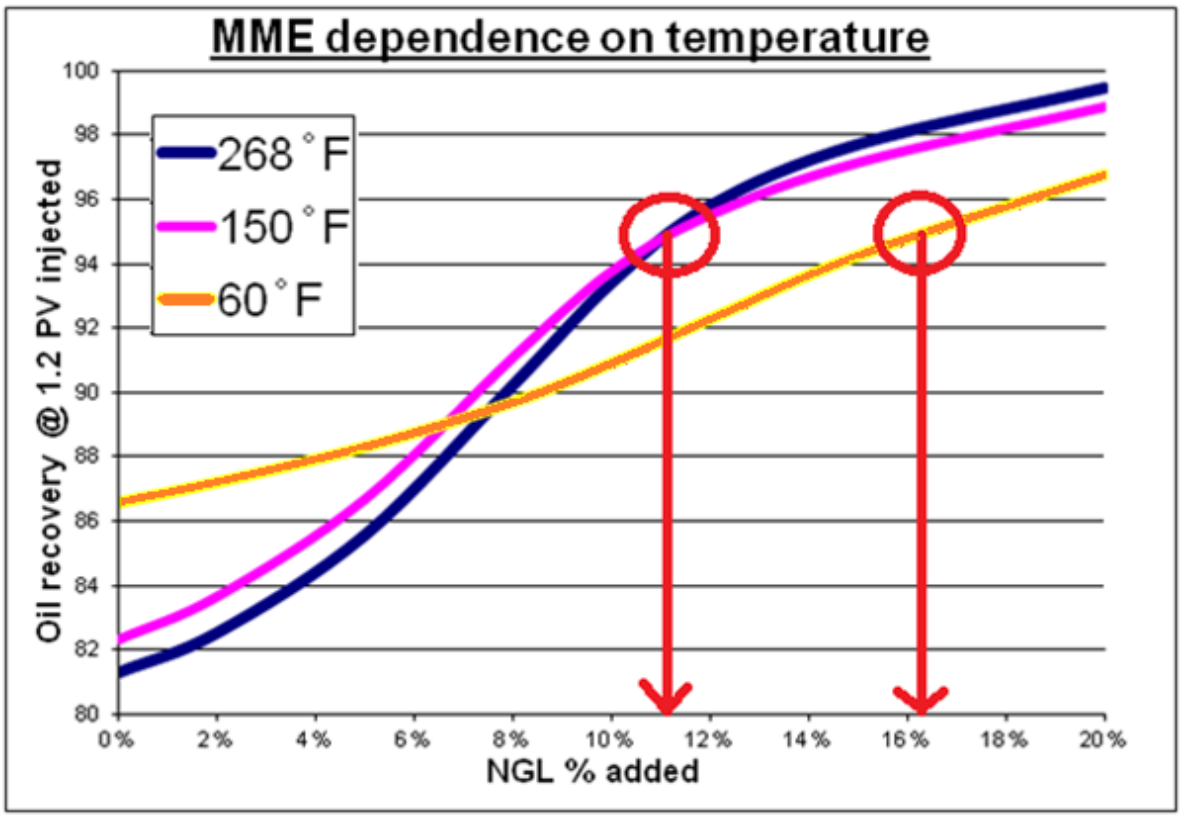

Figure 5.7: MME evaluation at temperatures of 60, 150 and 268˚F and constant operating pressure of 6000 psia.

Based on the criteria of 95 % oil recovery, MME at pressure of 6000 psia is determined to 11 % enrichment of NGL at both 268˚F and 150˚F, and to 16.5 % enrichment of NGL at 60 ˚F.

MME conclusion

To achieve miscibility through enriching the injected gas, large amounts of NGL is required to be added to the dry gas 11 to 16.5 % NGL at 6000 psia. Assuming that totally around 0.3 to 1 pore volume of gas is injected in the WAG-process; the total volume NGL delegated from sale to injection to achieve miscibility will be large. Such delegation of NGL from sale to injection involves high economical risks, as current NGL price is high and a significant incremental oil recovery from the WAG-process is needed for a successful process, which yet is highly uncertain. It has therefore been decided to proceed with the much cheaper hydrocarbon dry gas for the further studies.

6 Mechanistic modeling

The mechanistic models are designed to get an understanding of the behavior of important parameters, concepts and oil recovery mechanisms for WAG-displacement. The parameters and concepts studied in this section are trapped gas saturation and the connected relative permeability hysteresis effect, miscible flood residual oil saturation (SORM) and matrix-fracture mechanisms. For the study of trapped gas saturation a homogeneous matrix model is designed. Studies of matrix-fracture mechanisms are performed by introducing different matrix-fracture models to describe different types of fracture networks and fracture intensity factors within different regions of the reservoir. Based on the results from the different matrix-fracture models evaluation of SORM is performed. Finally, obtained results are used as basis for further sector modeling.

6.1 Description of mechanistic models

The mechanistic models in this study are compositional, two-dimensional models in the xz-plane with 1156 grid blocks, 34 in x-direction and 34 in z-direction. A vertical injection well is perforated in the grid block (1,1,1) through (1,1,34) and a vertical production well is perforated in the grid blocks (34,1,1) through (34,1,34). The size of each grid block, both matrix and fracture grid blocks, is 10 ft^3 with grid block sides of 0.1 ft, 1000 ft and 0.1 ft in the x-,y-, and z-direction respectively.

The homogeneous matrix model and the matrix-fracture models make use of the same matrix grid block properties. Fracture properties used are also equal for the fracture grid blocks within the matrix-fracture models.

Matrix properties

The properties of the matrix grid blocks used are based on laboratory and field data from the Ekofisk and are summarized in table 6.1.

Table 6.1: Matrix properties used in the mechanistic models

Parameter	Value
Initial pressure (z = 10280 ft)	7103 psia
Porosity	40 %
Horizontal permeability	2 mD
Vertical permeability	0.2 mD
Initial water saturation	0.04
Initial oil saturation	0.96
Critical gas saturation	0.05

The input two-phase matrix gas-oil and water-oil relative permeability curves are illustrated in figure 6.1 (a), and figure 6.1 (b) respectively.

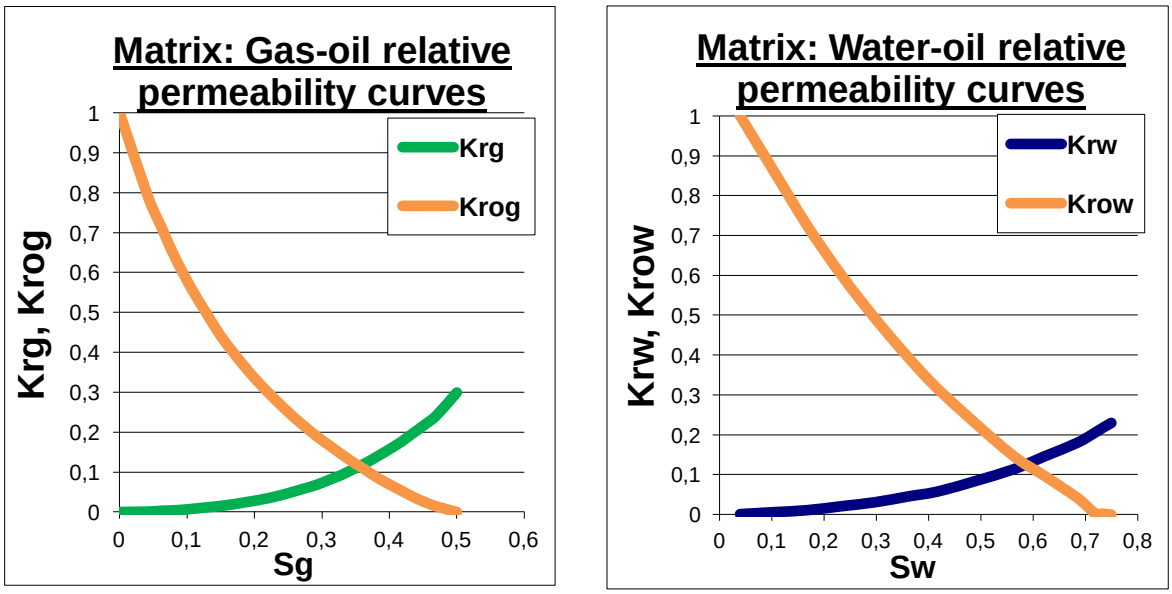

(a) **(b)**

Figure 6.1: Input matrix (a) gas-oil and (b) water-oil relative permeability curves for the mechanistic models

If the assumption of no trapped gas is made, the gas drainage and imbibition curves coincide and will be represented by the green line in figure 6.1(a). However, if trapped gas saturation is included, the imbibition curve will be different. Results from trapped gas studies and presentation of new hysteresis affected relative permeability curves are presented in chapter

6.3.1. Since three-phase flow is encountered in WAG-displacement, Stone's first model is used to calculate three-phase oil relative permeability data. The gas-oil capillary pressures are very small and can therefore be neglected.

The input drainage and imbibition water-oil capillary pressure curves are important for displacement of oil by water, and are shown in figure 6.2.

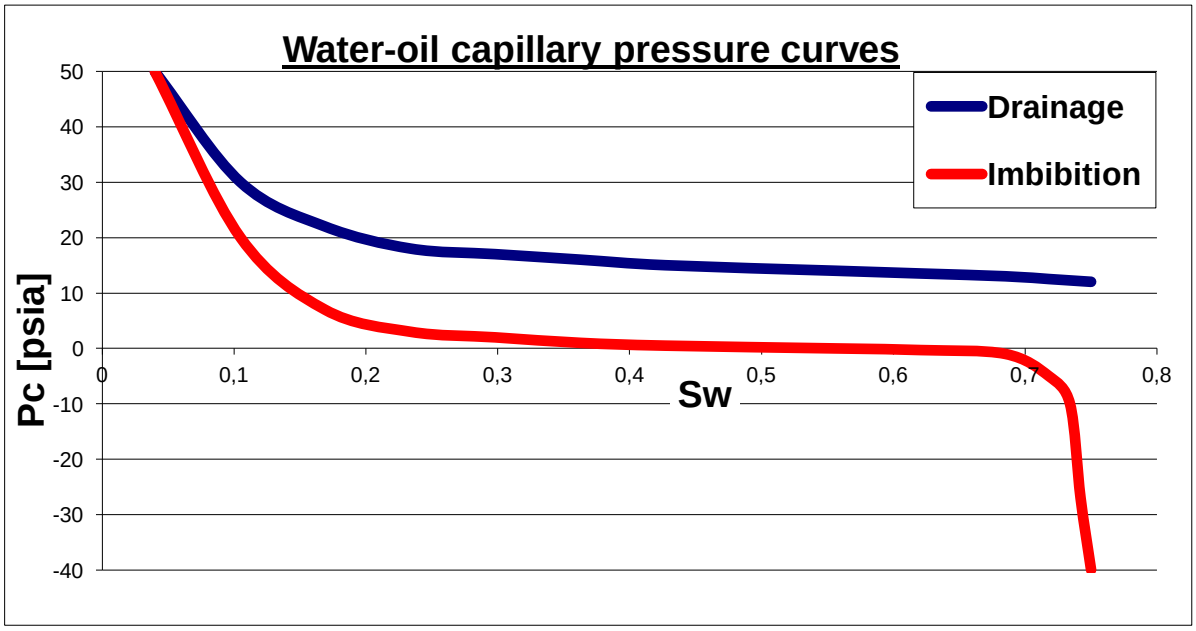

Figure 6.2: Matrix water-oil capillary pressure curves for the mechanistic models

The capillary imbibition curve in figure 6.2 indicates that spontaneous imbibition ends at water saturation of about 0.56, corresponding to zero capillary pressure. The degree of spontaneous imbibition for this system gives the indication of the rock being moderately water-wet, based on the capillary pressure relation to rock wettability presented in section 4.4. Further imbibition of water into the matrix blocks may be achieved by forced imbibition by external forces like viscous or gravitational. Forced imbibition can imbibe water up to possibly water saturations of 0.75, resulting in Sorw of 0.25, as seen in figure 6.2.

Fracture properties

The fracture properties used within each matrix-fracture mechanistic models are constant for all fracture grid blocks and given in table 6.2.

Table 6.2: Fracture properties used in the matrix-fracture mechanistic models

Parameter	Value
Initial pressure (z=10280 ft)	7103 psia
Porosity	100 %
Horizontal permeability	1000 mD
Vertical permeability	1000 mD
Initial water saturation	0.04
Initial oil saturation	0.96

The permeability of the fractures on the Ekofisk has not been fully understood. However, well tests have measured effective permeability up to 100-150 mD. Fracture permeability of 1000 mD is therefore used to give effective permeability for the matrix-fracture model up to this range.

The water-oil and gas-oil relative permeability curves for the fractures are linear and illustrated in figure 6.3 (a) and figure 6.3 (b) respectively. The capillary pressures in the fractures are assumed to be zero.

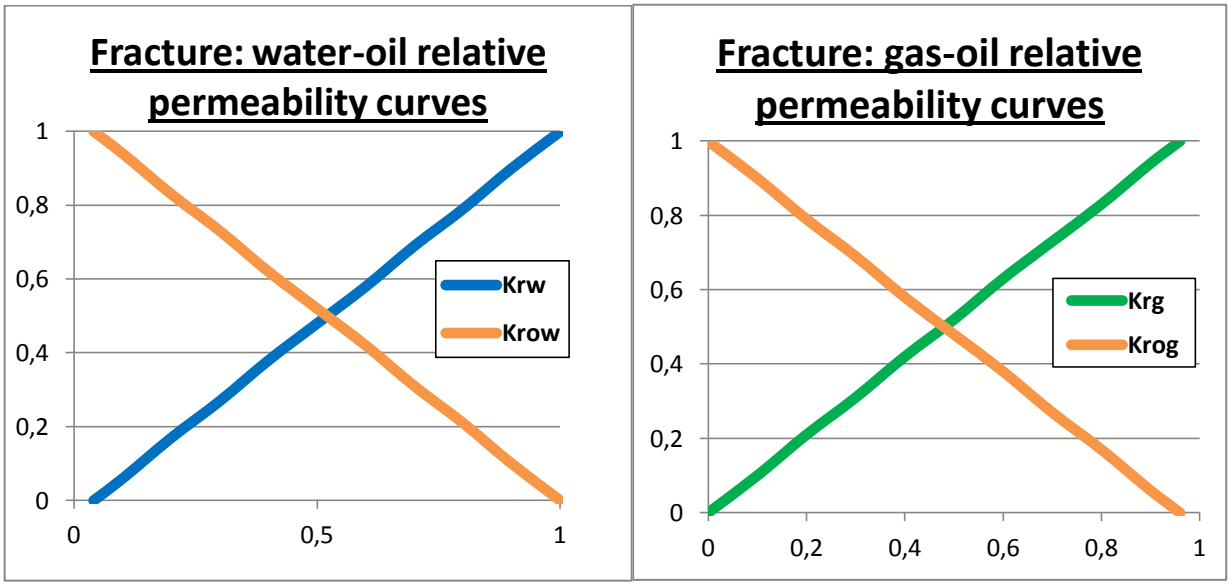

(a) **(b)**

Figure 6.3: Fracture (a) water-oil and (b) gas-oil relative permeability curves for matrix-fracture models

PVT data

In an immiscible displacement process less compositional changes over each time-step is expected compared to miscible displacement. Therefore, an EOS with fewer components may sufficiently describe an immiscible displacement. A simulation test was performed to investigate the difference between a 7-component EOS and the 15-component EOS which was used for slim-tube modeling. The result from the simulation showed that the 7-component EOS gave almost the exact results as the 15-component EOS, seen in appendix B, and the 7-component EOS was therefore chosen for the further studies to reduce central processing unit (CPU) time of simulations.

The 7-component EOS is a Peng-Robinson type EOS tuned to match the same data as the 15-component used for slim-tube simulations. The main difference is that some components with similar properties in the 15-components EOS are lumped into pseudo-components in the 7-components EOS, shown in table 6.3. The lumping of components into pseudo-components results in new set of compositional PVT data and also new set of binary coefficients.

Table 6.3: 7-components EOS

Components	Abbreviation in EOS
Carbon dioxide	CO2
Nitrogen and methane	N2C1
Ethane and propane	C2C3
Butane to hexane	C4C6
C7-C13	C7P1
C14-C30	C7P3
C30+	C7P5

Simulation procedure

A three-stage development is modeled, first primary depletion, followed by water flooding to S_{orw}, to imitate the Ekofisk history and then further prediction studies with WAG-injection. All models are initialized with matrix and fracture grid block properties as presented above. In addition to the matrix and fracture properties presented above, the input SORM option five, presented in chapter 4.8, with SORM value equal to 0.03 is used for all matrix blocks. Input maximum trapped gas equal to 0.2 for all matrix grid blocks is also used is a standard, with trapped gas saturation calculated based on Lands correlations, presented in section 4.6.2.1. The composition of the in-situ reservoir oil is similar to the

initial Ekofisk crude oil. The initial reservoir pressure and temperature in the models are 7103 psia and 268F˚ respectively, at a datum depth of 10280 feet. The initial reservoir pressure is above the oil saturation pressure which is calculated to be 5390 psia at initial conditions, and the oil is following initially under saturated.

The models are simulated by running a primary depletion with BHP-control by stepwise decreasing the BHP at the production well to a pressure of 3500 psia. The oil recovery factor following primary depletion is between 16-20 % for the different models. Water flooding is then performed by introducing the injection well and gradually increasing the BHP at both the injection and production well, retaining a constant pressure difference. The pressure difference between the wells for water injection is set to 750 psia, giving a pressure drop of 220 psi/ft. This high pressure drop is used because the interest is to reach water flood residual oil saturation as fast as possible. Water flooding is performed to water flood residual oil saturation of 0.3-0.35, resulting in oil recovery of approximately 65-70 % for the different models. The reservoir pressure following water flooding is about 6400 psia. WAG-studies are then initiated with BHP-control, with BHP of the injection well at 6500 psia for both gas and water injection and BHP of the production well at 6000 to make sure a pressure drop exist across the matrix blocks. Dry hydrocarbon gas as presented in table 5.2 is used for the gas half-cycles. An illustration of the oil recovery and reservoir pressure for primary depletion and water flooding for the homogeneous case is shown in figure 6.4.

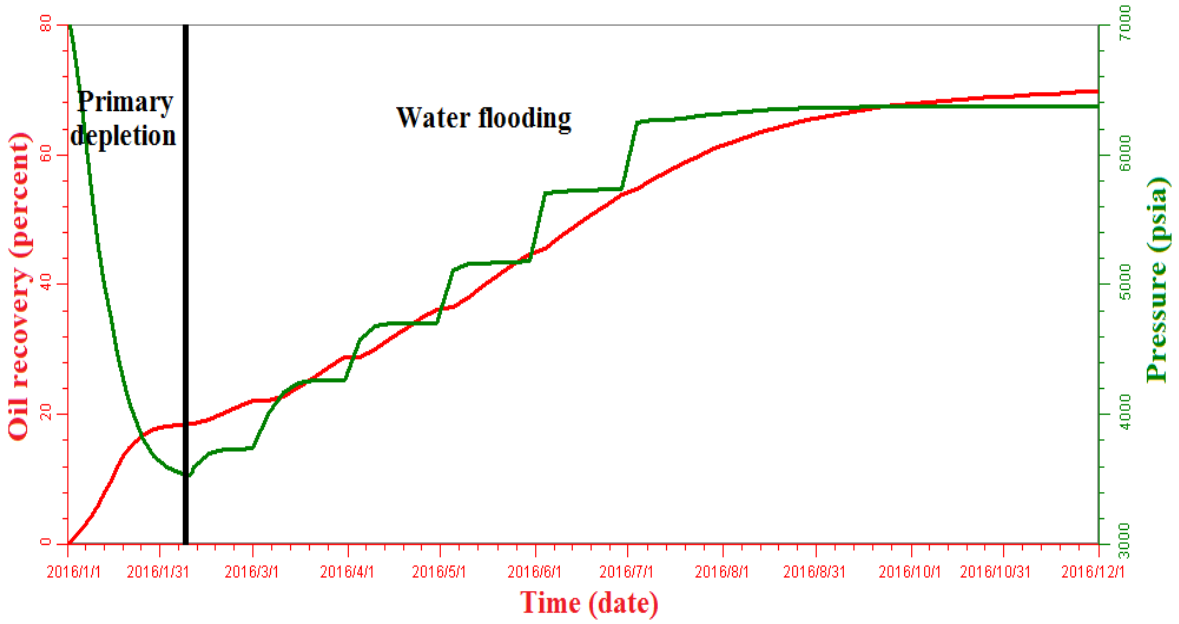

Figure 6.4: Oil recovery and reservoir pressure for the homogeneous matrix model

Two different strategies are used for WAG-injection in the mechanistic models. One is to inject small pore volume slugs to pretend that the mechanistic model represents a region of the reservoir. The other strategy is to inject large pore volumes to pretend that the mechanistic model represents a small part of the reservoir like a core sample. Using the latter method, the entire mechanistic models will eventually be flooded and similar ultimate oil recoveries will be reached for different cases. The choice of strategy will be stated in each section.

6.2 Methodology for mechanistic modeling

Methodologies to evaluate the different main parameters studied in mechanistic models for this thesis, trapped gas saturation and hysteresis effect, matrix-fracture systems and SORM are presented in this section.

6.2.1 Trapped gas saturation and relative permeability hysteresis effect

Phase trapping of gas and corresponding relative permeability hysteresis effect is common after an imbibition process where a wetting-phase displaces the non-wetting phase gas. These phenomenas are typical in WAG processes, because the alternation between water and gas injection induce changes between drainage and imbibition processes. To evaluate trapped gas saturation and relative permeability hysteresis effect in WAG processes, available options in PSim are used and evaluated against laboratory and other reported data for chalk.

The available trapped gas correlations in PSim are those by Coats and Land. Because PSim lacks standard hysteresis options, such as the WAG-hysteresis model or the models by Carlson or Killough presented in chapter 4.6.3, the available options will be investigated. Hysteresis affected relative permeability curves can be calculated in PSim based on the two trapped gas correlations.

The two correlations are compared in the homogeneous model by investigating how trapped gas saturation is calculated as a function of historical maximum gas saturation with Sgr input equal to 0.2. Further the impact on relative permeability curves is considered. The evaluation is performed by choosing a reference cell in the homogeneous model where gas saturation, Sg, current trapped gas saturation, Sgrc, and relative permeability of gas, k_{rg}, is monitored at each time step.

To evaluate the best matching trapped gas correlation and Sgr input value for the Ekofisk chalk, simulations results are compared with reported data on chalks and laboratory results by ConocoPhillips on trapped gas. Sgr input values of 0.2, 0.3 and 0.35 for Lands correlation and Sgr input values of 0.2 and 0.5 for Coats correlation are studied. The evaluation is done by comparing how trapped gas saturation is calculated as a function of historical maximum gas saturation and comparing this with reported and laboratory data. The same reference cell as used earlier is used to obtain data for the evaluation.

Finally an evaluation of the impact trapped gas saturation has on a WAG-process is done by comparing the best matching Sgr-input value with a run where trapped gas is negligible, Sgr=Sgc=0.05. Trapped gas of 0.05 equals a run where trapped gas is neglected, since the critical gas saturation is 0.05. In each sensitivity run all parameters other than Sgr are unchanged and kept equal to the standard, presented in section 6.1. The homogeneous matrix model is assumed to be a larger part of a reservoir and small slugs are therefore injected in this evaluation.

6.2.2 Matrix-fracture systems

In the Ekofisk chalk reservoirs it is the naturally fractures that makes the reservoirs producible. The Ekofisk field has different types of fractures making up different kind of Ffracture-networks within the matrix. The different matrix-fracture systems lead to different flow performance in the reservoir resulting in different oil production from a WAG-process in different regions. Five matrix-fracture models are designed in this thesis to investigate the impact of different matrix-fracture systems within a reservoir and their impact on WAG-displacement. All matrix grid blocks and all fracture grid blocks within the different models have similar properties, as presented in section 6.1. The five different models design for the matrix-fracture evaluation are:

1) Homogeneous matrix model with no fractures.

2) 3-layer fracture model with three horizontal layered fractures introduced within the matrix model, illustrated in figure 6.5.

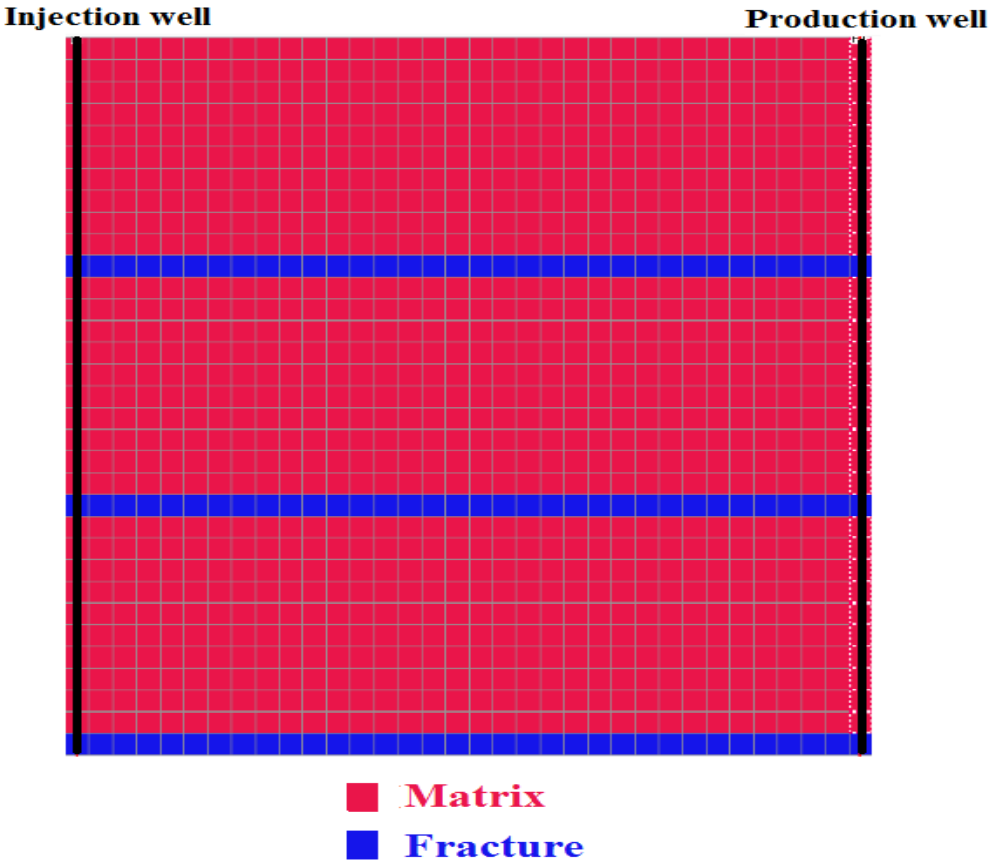

Figure 6.5: 3-layer fracture model in the xz-plane

3) Six-layer fracture model with three additional horizontal layered, totally six, fractures introduced in the homogeneous matrix model, illustrated in figure 6.6. The model is used to evaluate the impact of fracture intensity factor, given by equation 4.17.

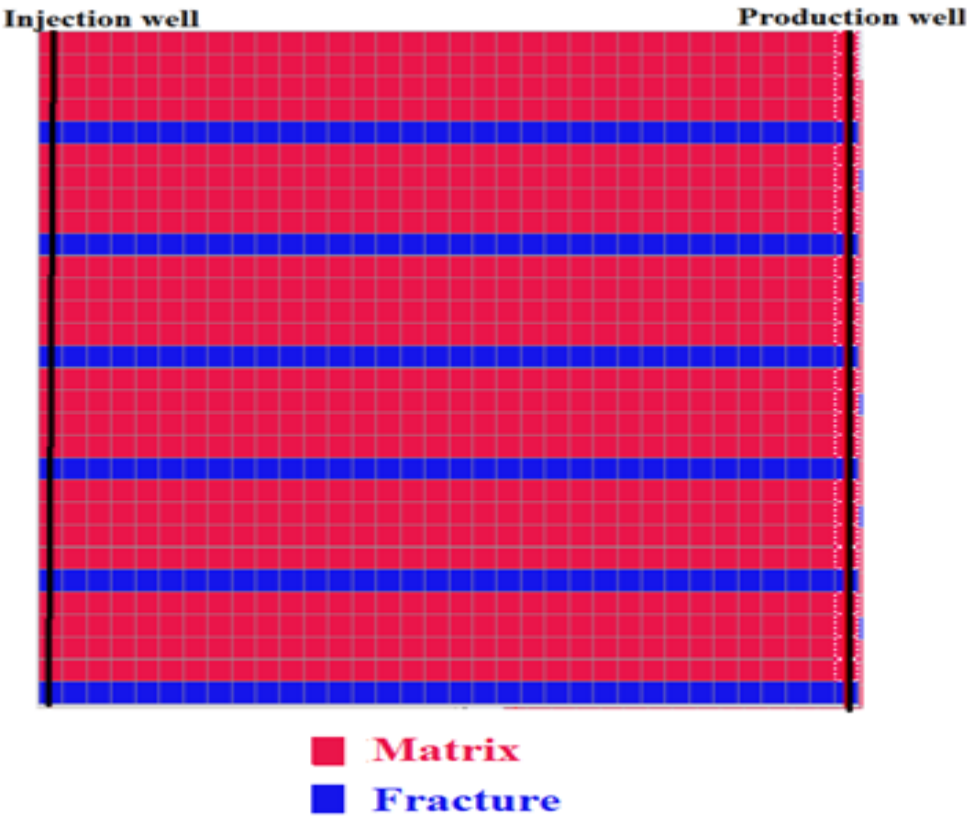

Figure 6.6: Six-layer fracture model shown in the zx-plane

4) Discontinuous fracture model with three discontinuous fractures introduced within the homogeneous matrix model, illustrated in figure 6.7.

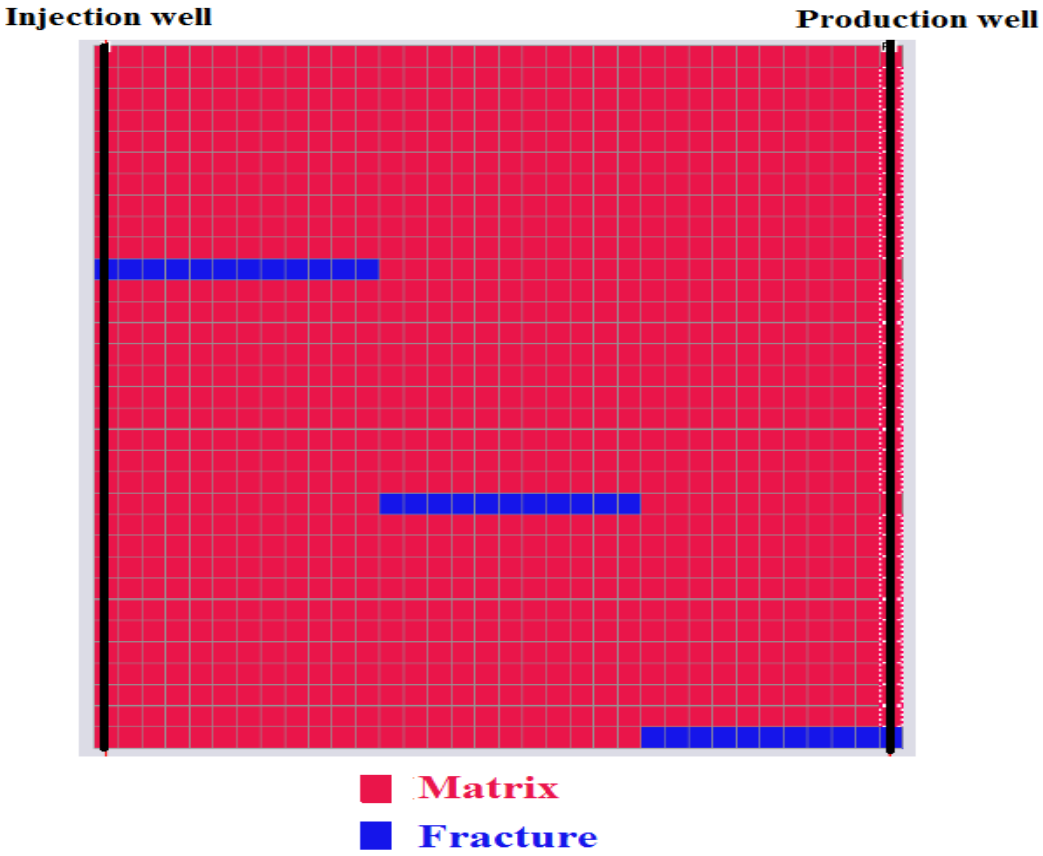

Figure 6.7: Discontinuous fracture model in the xz-plane

5) 9-block model with three horizontal and two vertical continuous fractures within the homogeneous matrix model, illustrated in figure 6.8.

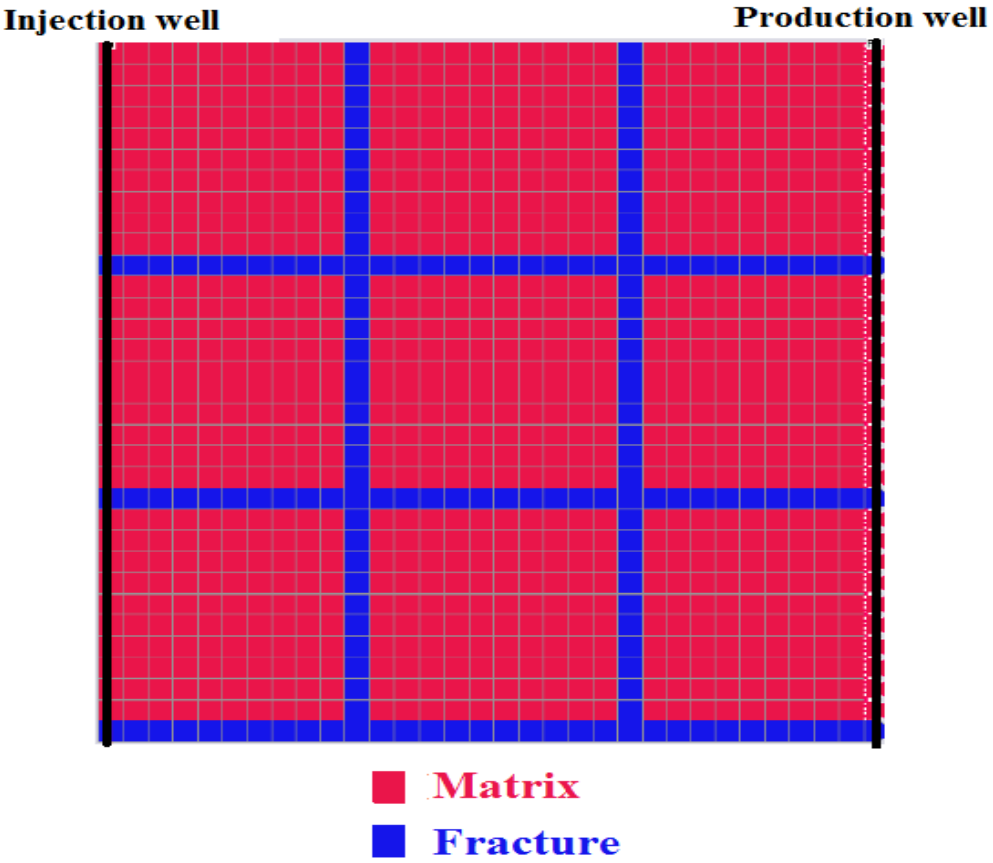

Figure 6.8: 9-block fracture model in the xz-plane

The models are assumed to be core plugs sizes and large slugs of two pore volumes are therefore injected in each model. The impact of WAG-injection in the different models is studied by evaluating incremental oil recovery to water flooding, and the timing of gas breakthrough. The impact of perforating in matrix grid blocks or both matrix and fracture grid blocks is also studied.

Different models with different properties are originally used to represent different areas of the reservoir in a full field model. A presentation of upscaling from mechanistic models to full field model is therefore included following the results.

6.2.3 Miscible flood residual oil saturation

In miscible or close to miscible WAG-processes reservoir simulator may over predict the oil recovery by completely sweeping the grid blocks. This could result in residual oil saturation

(SORM) approaching zero. As presented in chapter 4.7, this is unlikely to occur in field cases for several reasons. To avoid over estimation of oil recovery in full field simulations several methods have been proposed. Two methods, SORM options, are available in PSim to account for the problem, discussed in detail in chapter 4.7.

To evaluate how the different SORM options operate, simulations with input SORM of 0.2 are performed in the homogeneous matrix model for both options. Since the main interest is to capture how the options operate at low oil saturations, the homogeneous matrix model is used and assumed to be core plug size and therefore entirely flodded with two pore volumes slugs.

To account for SORM in full-field reservoir simulations of WAG-processes the incremental recovery from the different matrix-fracture mechanistic models is used as a basis for SORM in the upscaled grid blocks in the sector model.

6.3 Results and discussion of mechanistic simulations

The results from mechanistic simulations are presented in this section, divided into trapped gas saturation and relative permeability hysteresis effect, matrix-fracture systems and miscible flood residual oil saturation.

6.3.1 Trapped gas saturation and relative permeability hysteresis effect

Simulations were run in the homogeneous matrix model with input Sgr equal to 0.2 to evaluate how trapped gas saturation is calculated for the different trapped gas correlations in PSim. The reference cell (18,1,18) was chosen to monitor how trapped gas saturation is calculated as a function of maximum historical gas saturation, plotted in figure 6.9, assuming that a complete imbibition process is initiated at the maximum historical gas saturation.

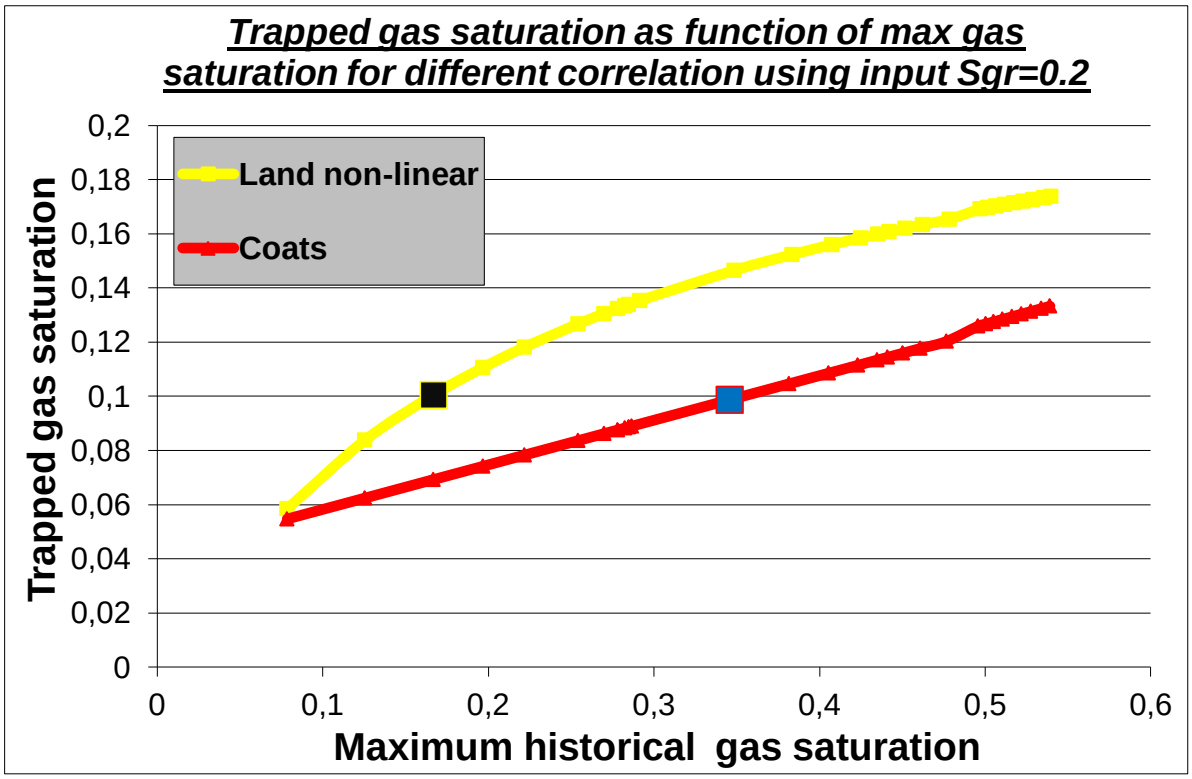

Figure 6.9: Land and Coats trapped gas saturation as function of maximum historical gas saturation for reference grid block (18,1,18)

Land's non-linear correlation relates the amount of gas being trapped to the maximum historical gas saturation by applying equation 4.8, where C_{Land} is calculated by equation 4.9 to be 4, based on the input Sgr value of 0.2. In example the black box on the Land non-linear curve has the gas saturation of 0.1669. Assuming this is the maximum historical gas saturation at the start of a complete imbibition process, the trapped gas saturation is calculated by applying equation 4.8:

$$S_{gr}^{*} = \frac{S_{gi}^{*}}{1+C_{Land} \cdot S_{gi}^{*}} = \frac{0.1669}{1+4 \cdot 0.1669} = 0.1000$$

Coats correlation relates the amount gas being trapped to the maximum historical gas saturations by using the linear correlation given in equation 4.14. The trapping constant C, given by equation 4.15, is 0.1648 corresponding to the slope of Coats curve in figure 6.9. In example the blue box on Coats curve has the gas saturation of 0.3458. The trapped gas saturation, assuming this gas saturation is the maximum historical gas saturation at the start of a complete imbibition process, is calculated by applying equation 4.14:

$$S_{gr}^{*} = S_{gc} + C \cdot \left(S_{gi}^{*} - S_{gc}\right) = 0.05 + 0.1648 \cdot (0.3458 - 0.05) = 0.0987$$

Gas trapping can in both cases only occur if the gas saturation increases above the critical gas saturation at 0.05, because an imbibition process subsequent to a drainage process can only occur when gas is flowing, accordingly above the critical gas saturation.

To find gas relative permeability curves corresponding to the two correlations, the reference cell (18,1,18) was used to monitor gas saturation and gas relative permeability as a function of time. Gas relative permeability as a function of gas saturation in the first WAG gas cycle, drainage process, and first WAG water cycle, imbibition process is plotted in figure 6.10, for the two different correlations.

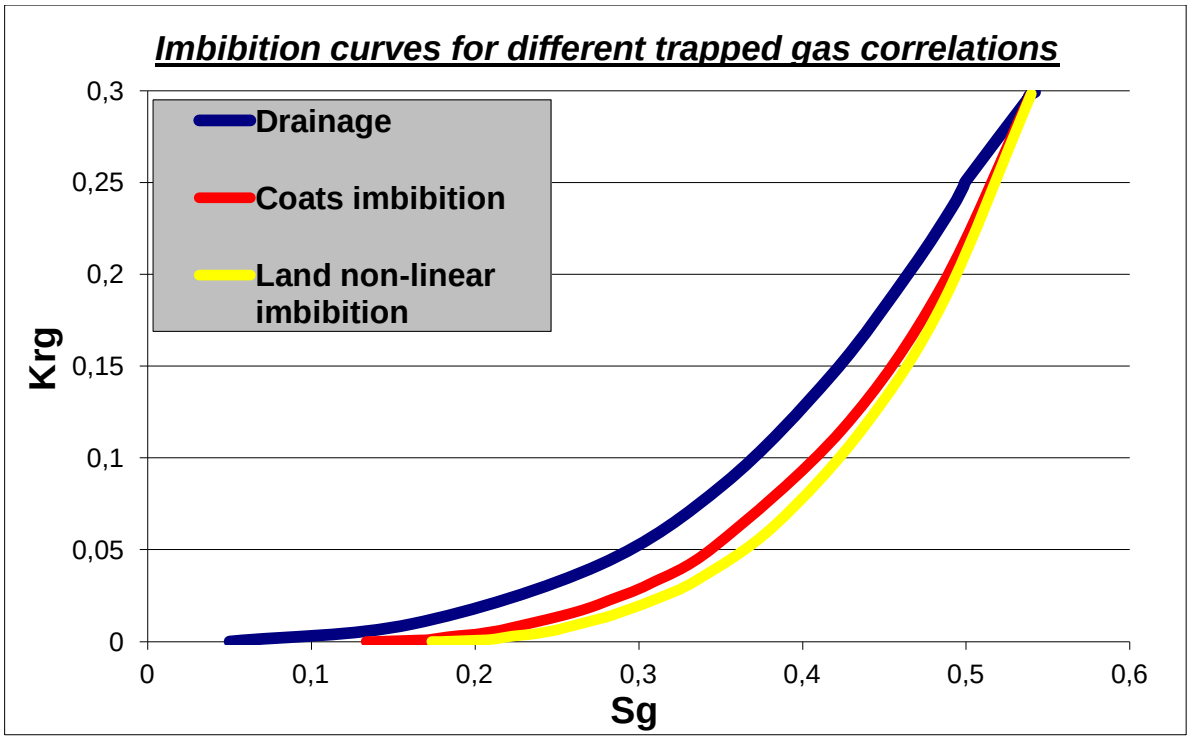

Figure 6.10: Gas relative permeability curves for Coats and Lands correlations with input maximum trapped gas saturation of 0.2 based on data from the reference grid block (18,1,18)

To calculate the hysteresis effected imbibition curve, maximum gas saturation in the start of the imbibition process is used to calculate the amount of trapped gas of a complete imbibition. At any point along the imbibition process relative permeability is calculated based on the mobile part of the total gas saturation, given by equation 4.12. The mobile gas saturation is then used to calculate hysteresis effected relative permeability data in the imbibition process by applying equation 4.13.

The drainage curve for the next WAG gas cycle will follow the imbibition curve, possibly up to the maximum gas saturation achieved during previous drainage process, and then along the input relative permeability curve if gas saturation is further increased.

To evaluate which trapped gas correlation and Sgr input value that matches best with chalk, simulation results for different Sgr input values for both correlations were compared with reported (Keelan, et al., 1975) and laboratory data (Maloney, 2003) on trapped gas (shown in figure 6.11)

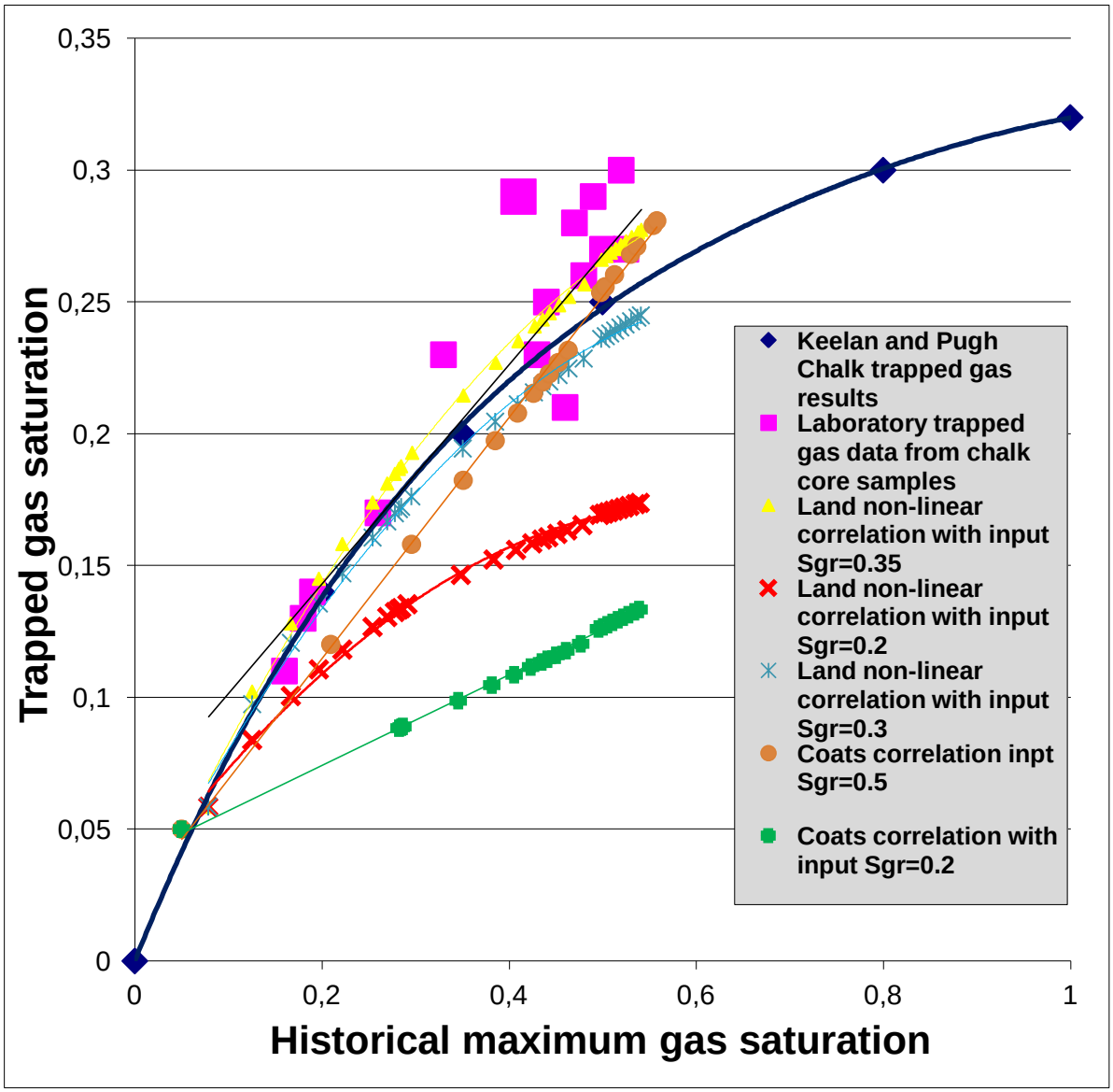

Figure 6.11: Trapped gas correlations and different Sgr-input values compared to reported and laboratory data on trapped gas

Land's correlation with input Sgr of 0.35, the yellow curve in figure 6.11, matches the laboratory data and Keelan and Pughs trapped gas data on chalk the best. Based on this result the homogeneous model with Land's correlation and Sgr-value of 0.35 will be compared to a run with negligible trapped gas. Sgr-value of 0.35 will also be used as basis for sector modeling.

Two sensitivity runs were carried out with Sgr equal to 0.05 and 0.35, and all other parameters kept unchanged from the properties presented in section 6.1. Five WAG-cycles were injected with half-cycle slug sizes of 0.1 pore volumes. In figure 6.12 the oil recovery is plotted as function of time to for the two cases. To get a better understanding what happens in the simulations, gas saturation, oil saturation, oil saturation pressure and reservoir pressure where plotted for the reference grid block (18,1,18) as a function of time for both cases (shown in appendix C).

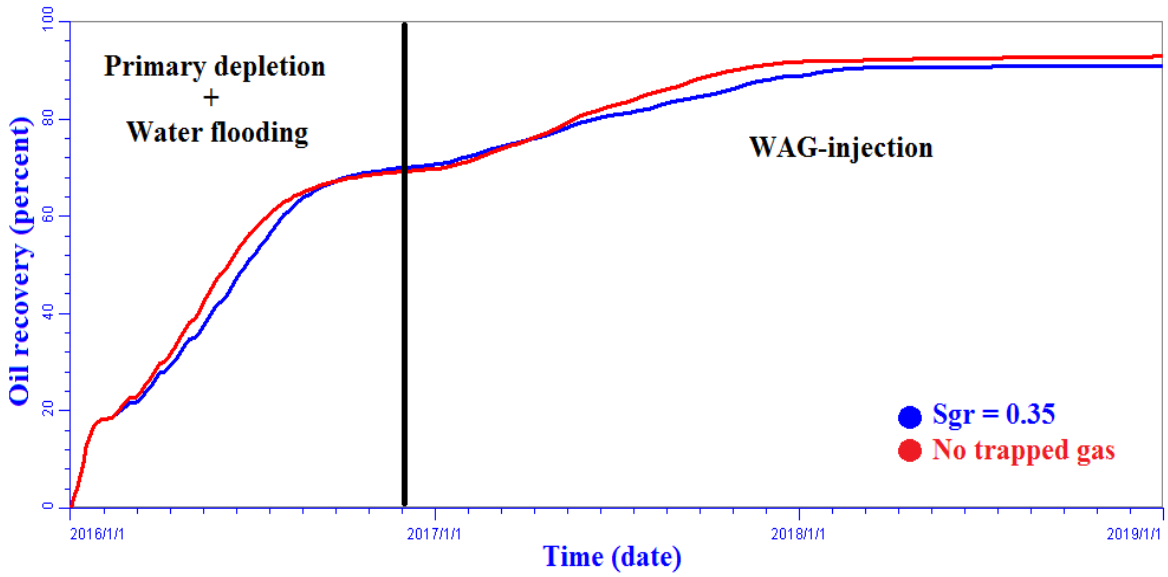

Figure 6.12: Impact of trapped gas on oil recovery for WAG-displacement

No effect of trapped gas is observed during the primary deletion period because this is a drainage process where the gas saturation increases. As water injection is initiated, the gas saturation decreases, hence starts an imbibition process where gas trapping can occur. From the reference cell, the gas saturation obtained after primary depletion is 0.285. Based on the maximum historical gas saturation, Land's correlation calculates the trapped gas, for Sgr input of 0.35, to be 0.188. The gas relative permeability is lower during imbibition than during drainage because gas is gradually being trapped. During water injection gas

eventually becomes immobile at the gas saturation of 0.188. As the pressure increases due to water flooding, the pressure will eventually increases above the oil saturation pressure and gas will go into solution with oil. When gas goes into solution, the oil saturation pressure will increase. Eventually as pressure is further increased all gas will be in solution with the oil and no trapped gas is left in the reservoir. For the case with trapped gas included, more gas will go in solution because more gas is present. Following water flooding the oil recovery from both cases are similar, as illustrated in figure 6.12. The case with negligible trapped gas saturation though has a higher gas recovery, and following a higher oil equivalent recovery than the case where gas.

When gas injection in the WAG-process is initiated the reservoir pressure will be above the oil saturation pressure, and gas will go in solution until the oil saturation pressure exceeds the reservoir pressure. The amount gas going into solution is equal for both runs because no gas is present in the reservoir following water flooding. When gas is injected at reservoir pressure lower than the oil saturation pressure, free gas will start develop in the grid blocks and increase till the end of the drainage process. Gas trapping will occur during the subsequent water injection, and hence imbibition process. The oil recovery following WAG-injection is 2 % higher when trapped gas is neglected compared to the case with input Sgr of 0.35. Similarly the gas recovery following WAG-injection is 35 % higher when trapped gas is neglected. This illustrates that neglecting trapped gas will give an optimistic prediction of both oil and gas recovery.

6.3.2 Matrix-fracture systems

The matrix-fracture models presented in section 6.2.2 were all run using the simulation procedure presented in section 6.1. Two different strategies were investigated, perforating only in matrix grid blocks and perforating in both matrix and fracture grid blocks. Table 6.4 and figure 6.13 show the oil recovery after water flood and after WAG injection for the different models with perforation in matrix grid blocks only.

Table 6.4: Oil recoveries for the matrix-fracture models perforated in matrix only

Model Type	Water flood recovery	WAG recovery	Incremental recovery
Homogeneous matrix model	69.4 %	93.7 %	**24.3 %**
3-layer fracture model	66.5 %	80.9 %	**14.4 %**
6-layer fracture model	65.0 %	76.3 %	**11.3 %**
Discontinuous fracture model	69.4 %	91.5 %	**22.1 %**
9-block fracture model	65.2 %	77.8 %	**12.6 %**

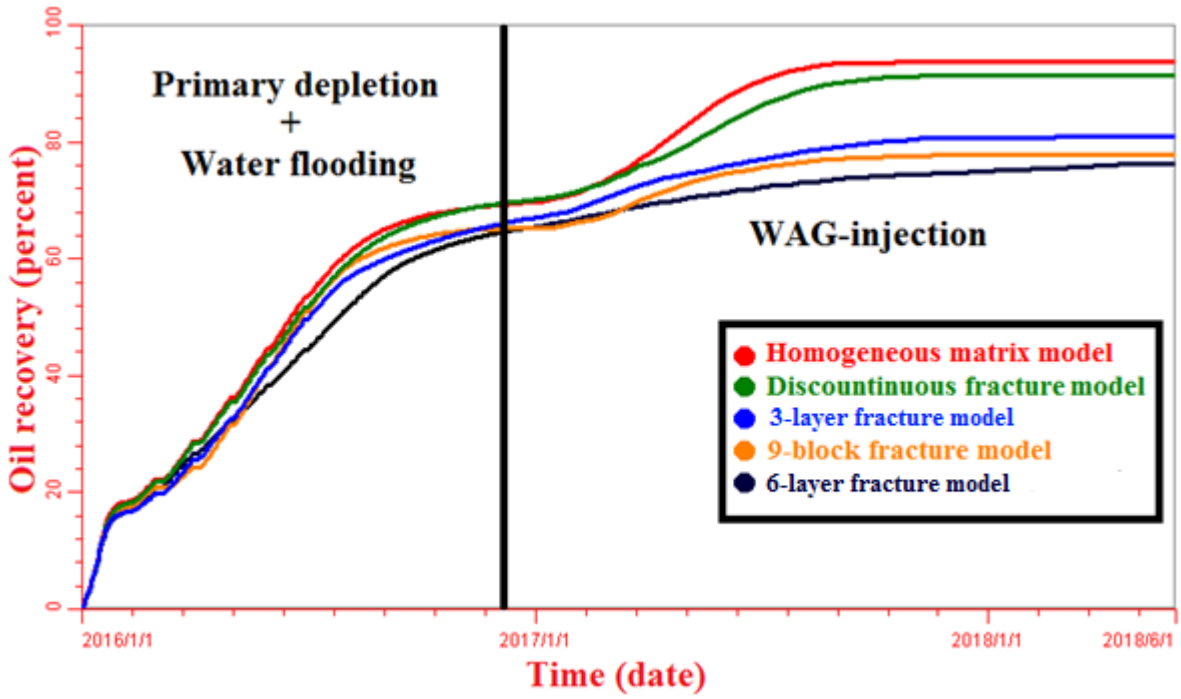

Figure 6.13: Oil recovery for the matrix-fracture models perforated in matrix only

The incremental oil recovery above water flood clearly shows the impact of fractures, ranging from 11 % incremental oil recovery for high fracture intensity factor to 22 % with low fracture intensity factor.

The reason for difference in oil recovery between the matrix system and the matrix-fracture systems is that injected fluid will tend to flow into the high permeable fractures and

displacement of oil in the matrix becomes less efficient. As the number of fractures is increased, the volume injected fluid going into the fractures increases and hence decreased displacement efficiency in the matrix blocks is observed. Gas saturation in the 3-layer and the 6-layer fracture model early in the WAG-process are illustrated in figure 6.14 and 6.15.

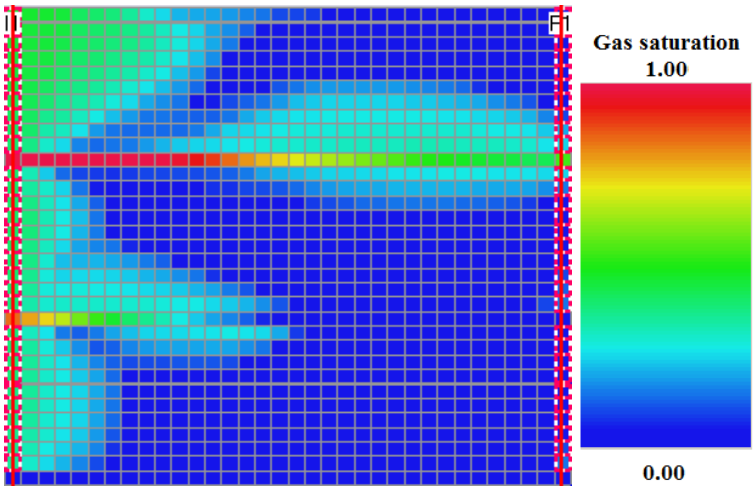

Figure 6.14: Gas saturation in the 3-layer fracture model

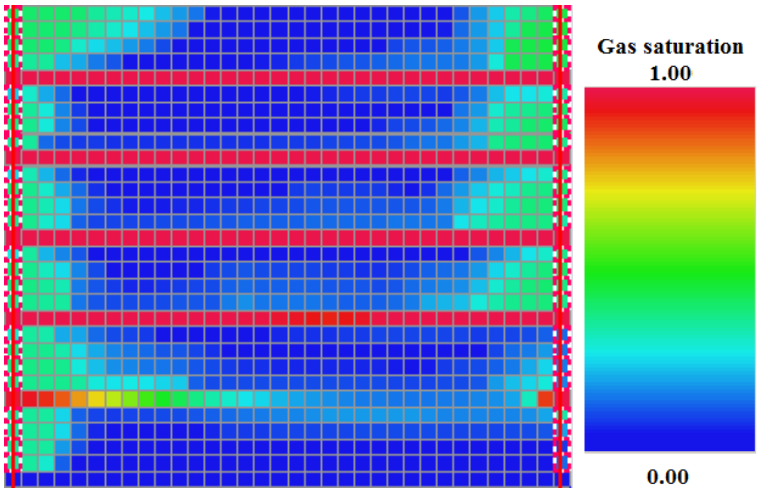

Figure 6.15: Gas saturation in the 6-layer fracture model

For the discontinuous fracture model, gas is forced out of the fractures and into the matrix. This will result in better matrix sweep efficiency compared to the continuous fracture models and hence high recovery, slightly less than what is observed for the homogeneous matrix model.

For the 9-block fracture model, the sweep of injected fluid in the grid blocks close to the injection well is good, however as injected fluid reach the fracture, it follows the fracture all the way to production well which result in poor sweep of the middle matrix blocks, illustrated in figure 6.16. The reason for high gas saturations in the matrix grid blocks close to the production well is that the production well is perforated in the matrix only, and gas has to enter the matrix block by any of the mechanisms described in chapter 4.9.2.1 to be produced.

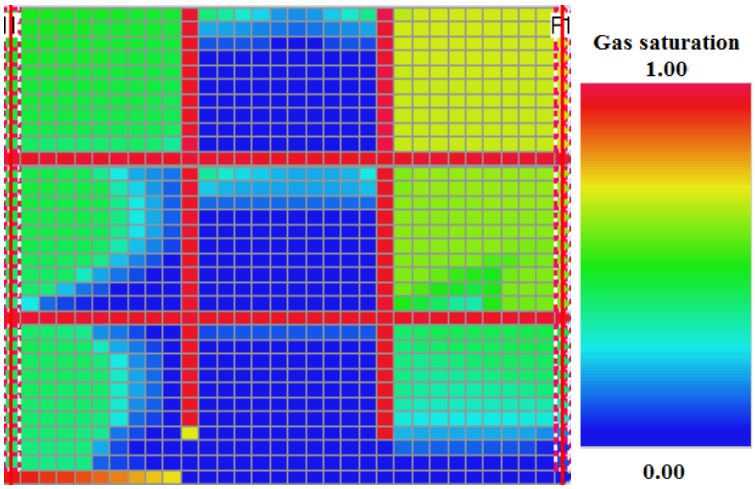

Figure 6.16: Gas saturation in the 9-block fracture model

Table 6.5 and figure 6.17 show the oil recovery after water flood and after WAG injection for the different models with perforation in both matrix and fracture grid blocks only.

Table 6.5: Oil recoveries for the matrix-fracture models perforated in both matrix and fractures

Model Type	Water flood recovery	WAG recovery	Incremental recovery
Homogeneous matrix model	69.4 %	93.7 %	**24.3 %**
3-layer fracture model	66.9 %	78.7 %	**11.8 %**
6-layer fracture model	66.0 %	74.3 %	**8.3 %**
Discontinuous fracture model	69.0 %	89.5 %	**20.5 %**
9-block fracture model	64.3 %	72.3 %	**8.0 %**

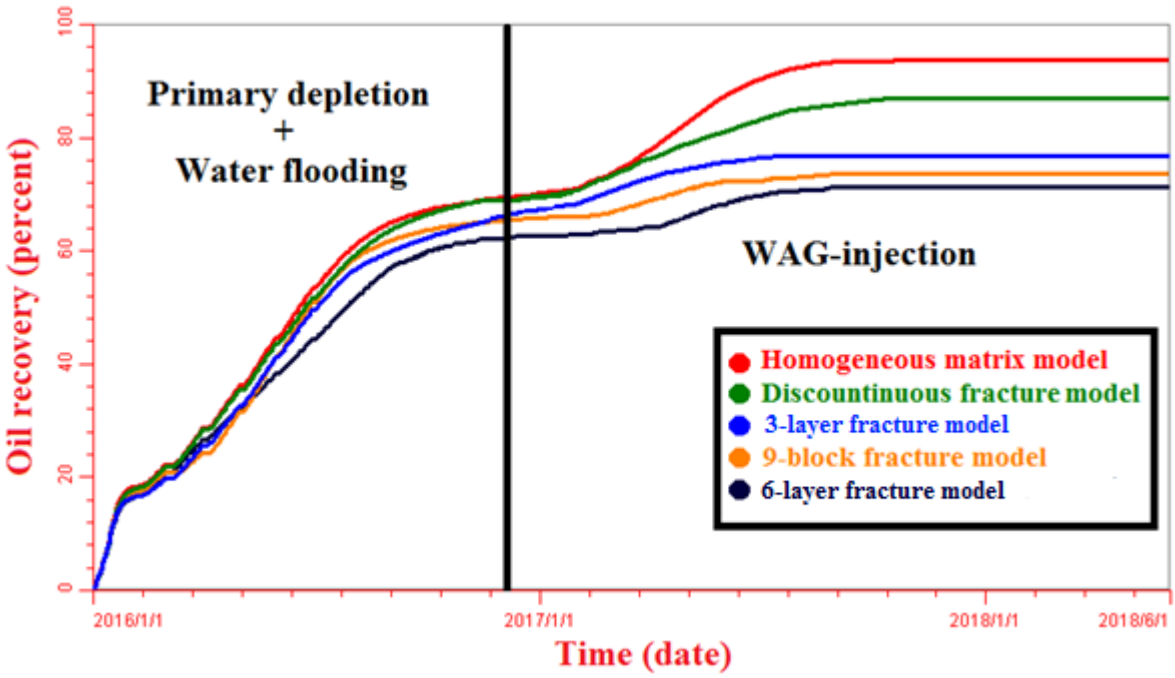

Figure 6.17: Oil recovery for the matrix-fracture models perforated in matrix and fracture grid blocks

When perforating in both matrix and fracture grid blocks lower oil recoveries are observed, compared to perforation only in matrix grid blocks. Incremental oil recoveries to water flood ranges from 8 % in high fractured areas to 20 % in areas with low fracture intensity factor. The difference in incremental oil recoveries between perforations in matrix only and in both matrix and fractures are between 2 to 5 %. The reason for this is that gas is forced into the matrix blocks before it can reach the fractures when perforating in the matrix only, hence giving a better sweep efficiency and better oil recovery.

Because the exact locations of different fractures in the reservoir are not known, the wells are commonly perforated in both matrix and fractures. Based on well test data, indicating high effective permeability, one has an idea of areas with high degree of fractures and perforating wells in these areas can therefore be avoided. Production wells though are always perforated along the entire reservoir region where it is believed to be oil.

Upscaling

The grid blocks used in the mechanistic models are far too fine to be used as grids in full field reservoir models. All grids within a high resolution mechanistic model may be represented by only one or a few grid blocks in a full field model. To close the gap upscaling from mechanistic models are used to make single grid blocks represent the same

behavior as entire mechanistic models. An example is how different matrix-fracture system should be represented by single coarse grid blocks in a low resolution full field model. This means that both matrix and fractures needs to be described within the same grid block and alteration of parameters between the scales is necessary. Input parameters to mechanistic models may be obtained by fluid samples, core samples, laboratory work and well testing. The ultimate goal of upscaling is to construct low resolution models which mimic the recovery characteristics of the higher resolution models. To do this reservoir parameters and reservoir performance in high resolution models are matched in low resolution models. The upscaling technique may involve averaging of reservoir parameters and alteration of relative permeability curves in the low resolution model to match flow behavior and important factors affecting the recovery efficiency in the higher resolution models.

Upscaling techniques have been applied to give properties to the grid block in the Ekofisk full field simulation model. Based on the grid properties, if-functions have been used to assign each grid block to a set of relative permeability curves representing different kind of systems.

In this study a sector model, region of the full field model, is used which already have been upscaled. However, trapped gas saturation and SORM will be altered according to the results obtained in this chapter of the thesis.

6.3.3 Miscible flood residual oil saturation

SORM is introduced to avoid over prediction of oil recovery when the matrix-fracture models are upscaled into the sector model. Since the mechanistic matrix-fracture models gave significant differences in oil recoveries, different SORM-values need to be assigned to different grid blocks in the sector model representing different matrix-fracture models.

The matrix-fracture models have different effective permeability which is used as a basis to upscale SORM to grid blocks in the sector model. This is done by using setting SORM values in grid blocks based on the horizontal permeability. Within different ranges of horizontal permeability different SORM-values are assigned.

The homogeneous matrix model is used to represent areas without fractures. As the matrix permeability is believed to range between 1 to 4 mD, all grid blocks in the sector model with horizontal permeability less than 4 mD are assigned SORM-values of 0.06 which

represents the ultimate oil recovery from the homogeneous model. The discontinuous fracture model is used to represent enhanced fractured areas. In these areas, it is assumed that the discontinuous fractures enhance the effective permeability in the range of 2 to 3 times the matrix permeability, and grid blocks with horizontal permeability between 4 to 10 mD are assigned SORM-values of 0.08 which represents the ultimate oil recovery from the discontinuous model. The 3-layer fracture model is used to represent areas with some degree of networks between the fractures. It is believed that such areas have effective permeability ranging between 10 to 90 mD. Grid blocks in the sector model with horizontal permeability between 10 to 90 mD are assigned SORM-values of 0.2 representing the ultimate oil recovery from the layered fracture model. The 9-block fracture model and the 6-layer fracture model are used to represent highly fractured areas. Such areas can have effective permeability above 90 mD, and all grid blocks in the sector model with horizontal permeability above 90 mD is assigned SORM-values of 0.25 based on the average ultimate oil recovery from the 9-block and double layered fracture models.

Table 6.6 summarized how different grid blocks in the sector model are assigned SORM-values based on the horizontal permeability of the grid block.

Table 6.6: Assignment of SORM-values to different grid blocks in sector model based on results from the matrix-fracture mechanistic models

Matrix-fracture system type	Sector model horizontal permeability grid block	SORM-value assigned to grid block
Matrix dominated areas	< 4 mD	0.06
Enhanced fractures areas	4-10 mD	0.09
Fractured dominated areas	10-90 mD	0.20
Highly fractured dominated areas	> 90 mD	0.25

To investigate how the two available SORM options in PSim, described in chapter 4.8, impact oil recovery and how different input SORM-values impact oil saturation in grid blocks, the homogeneous matrix model was used. The model was assumed to be core plug size and slugs of two pore volumes were injected. The reason for this choice is that the interest is to detect how SORM operates at low oil saturations.

The effect the two different options have on oil recovery using input SORM value of 0.2 is compared with a run where SORM options are excluded, shown in figure 6.18.

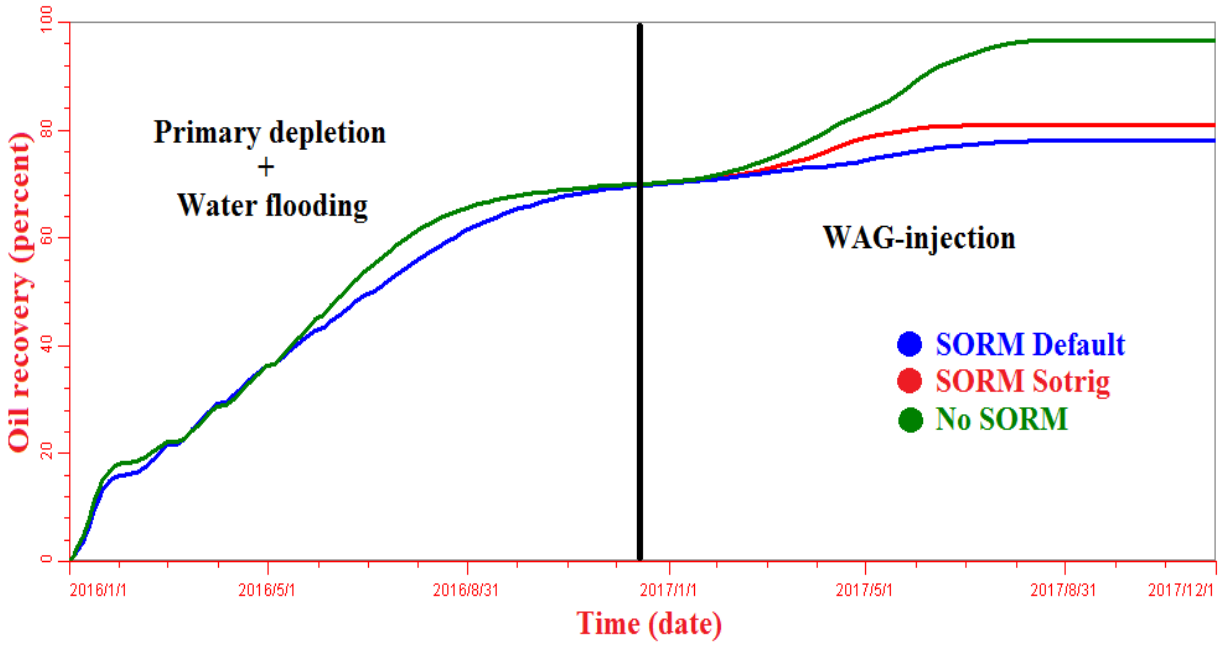

Figure 6.18: Oil recovery for the different SORM options in PSim, and a run without SORM

To get a better understanding how the different options cope with oil saturation, oil saturation as a function of time is plotted for the reference cell (18,1,1), as illustrated in figure 6.19.

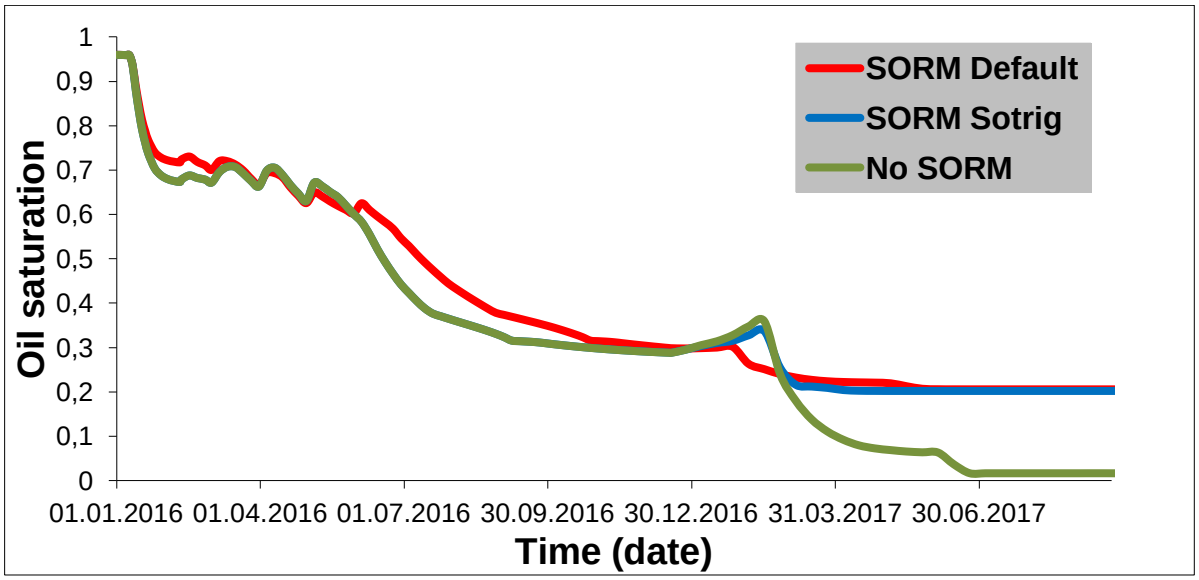

Figure 6.19: Oil saturation as a function of time in the reference grid block (18,1,18) for the two available SORM options in PSim, and the run without SORM

It is observed from, from figure 6.18 and 6.19, that the SORM Sotrig option and the case without SORM are equal for primary depletion and water flooding. The default SORM option though differs from these two cases for the same period. The reason for this is that for the default SORM option, 20 % of the total oil saturation is considered to be isolated in a different medium and this oil will not contribute to phase behavior calculations. This means that mass exchange through vaporization and condensation between the isolated oil and the flowing hydrocarbons is not described as for the other two cases.

The SORM Sotrig option will not affect the performance of primary depletion and water flooding, because SORM first takes effect for a grid block when the oil saturation becomes less than or equals to the input SORM value. This means that all oil contribute to phase behavior calculation until the input SORM value is reached.

Since choice of SORM option should not affect primary depletion and water flooding, rather set a limit for oil depletion from grid blocks, the SORM Sotrig option is chosen for further studies.

The effect on oil recovery and on grid block oil saturation for input SORM values of 0.03 and 0.2 using the SORM Sotrig option is shown in figure 6.20 and figure 6.21 respectively.

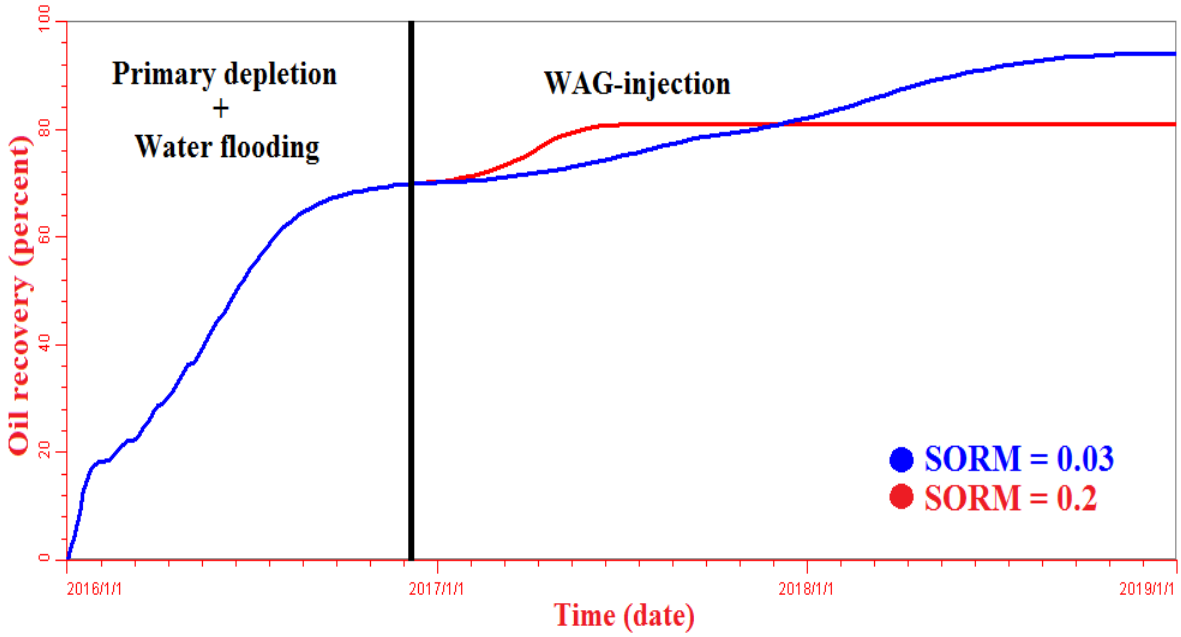

Figure 6.20: Effect of different input SORM values to oil recovery for SORM Sotrig option

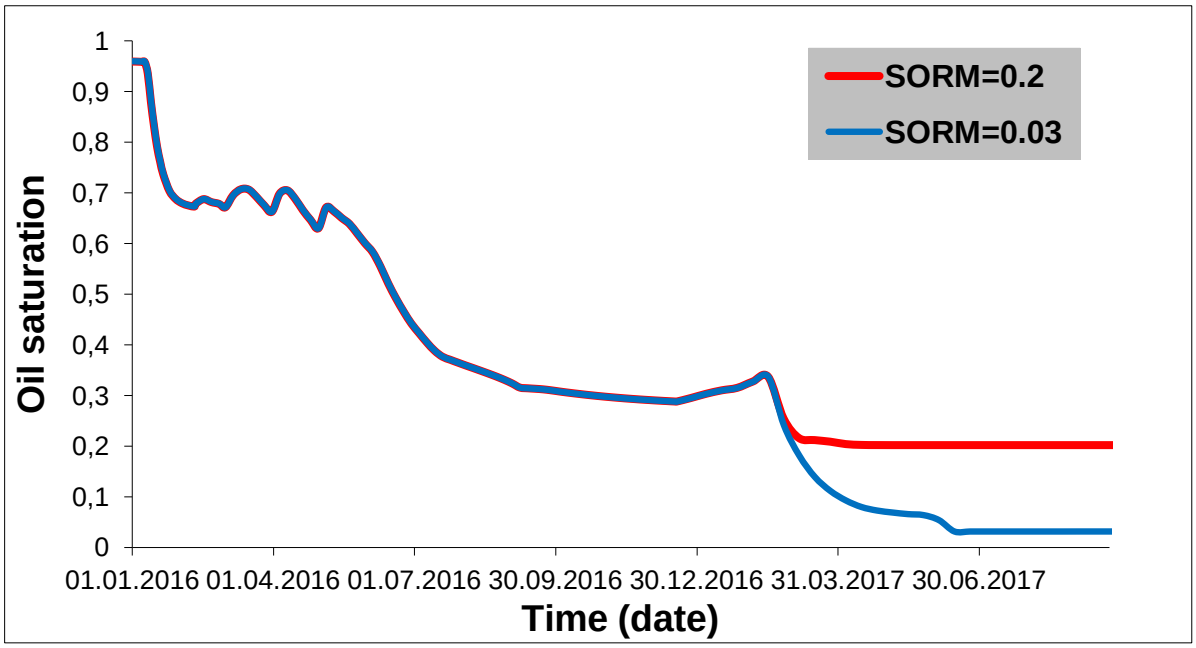

Figure 6.21: Oil saturation as a function of time for different SORM input values for the reference grid block

It is observed that the grid block oil saturations are equal until the oil saturation becomes 0.2. At this saturation SORM will be trigged for the case with user-defined SORM value of 0.2, meaning that further oil depletion from the grid block is not possible. For the case with input SORM value of 0.03, further depletion can occur until the oil saturation reaches 0.03.

7 Sector modeling

A sector model is a section of the Ekofisk full field simulation model. The sector model used in this thesis is shown within the red box on figure 7.1. The sector model uses the same grid blocks, wells, faults and properties as that section of the full field simulation model. The sector model is introduced in this thesis to study how different WAG ratios and half-cycle slug sizes effects production performance and oil recovery on field-scale.

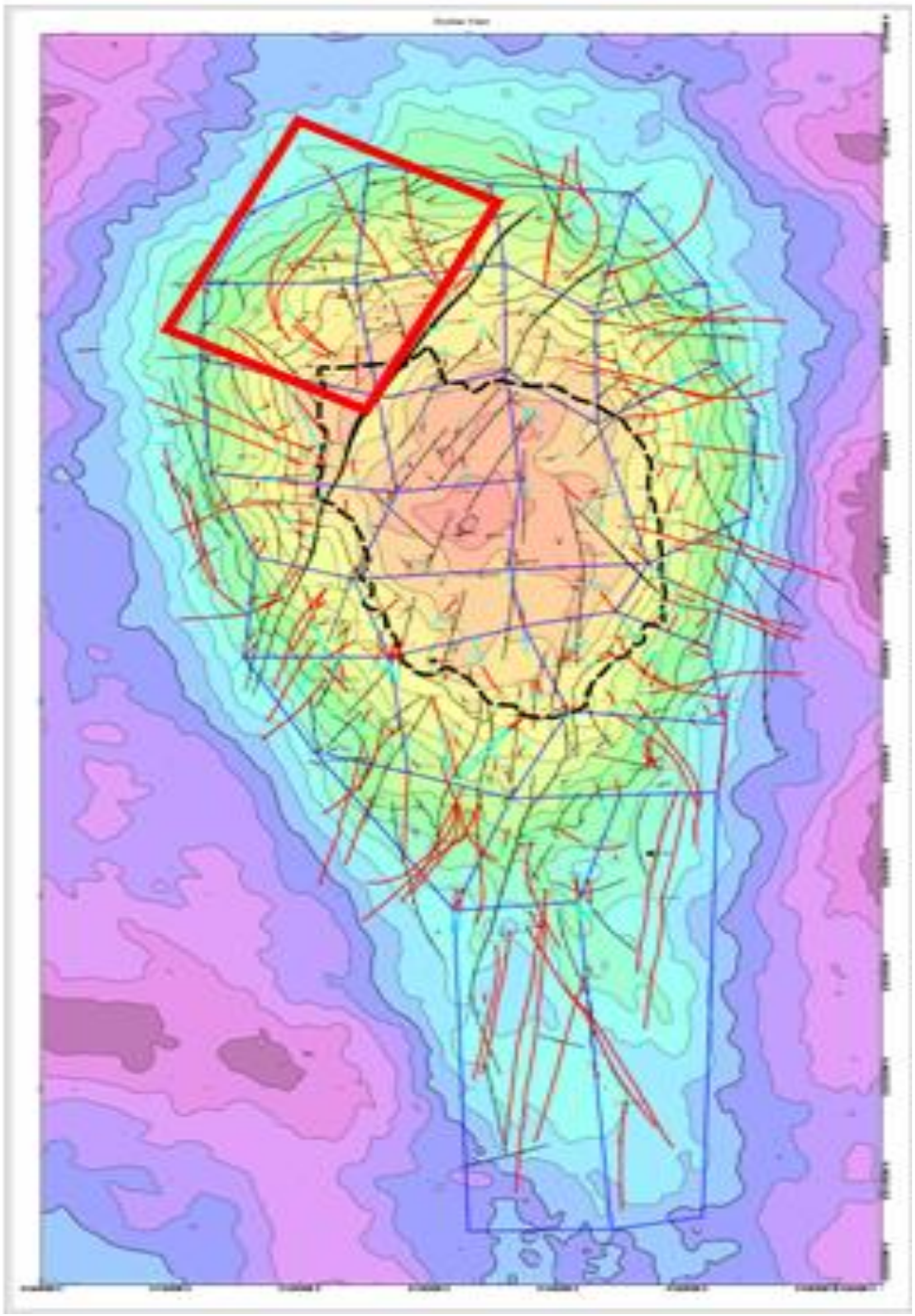

Figure 7.1: Ekofisk full field model, illustrating the location of the sector model within the red square

7.1 Description and methodology for sector model

The sector model comprises a history matched part from 1971 to 2011 and a predictive part from 2011 till end of license in 2028. The history matched part is based on historical data from production and injection wells, on reservoir pressure and fluid flow. Production and injection data are such as rates, pressures, water-cuts, GOR. Knowledge about fluid flow is through tracers, saturation of cores, breakthrough times and 4D seismic. The predictive part gives the opportunity to visualize and compare the continued water flood scenario to WAG scenarios.

Model description

The sector model is a single porosity/single permeability system where the effective porosity and effective permeability are entered for each grid cell. The effective porosity and permeability is calculated from estimated matrix and fracture properties. The model has 22 vertical layers. The division of the Ekofisk formation and Tor formation into the 22 vertical layers is shown in figure 7.2. The sector model is run in compositional mode with the 7-component Peng-Robinson EOS presented in table 6.3 of chapter 6.1.

The sector model consists of 17600 grid blocks, 25·32·22 grids in the x-, y-, z-directions respectively. Only 16244 of the grid blocks are active. Each grid block has size of approximately 225 feet in the x-direction, 240 feet in the y-direction and thickness of average 40 feet. All grid blocks within the sector model have been assigned a set of initial properties such as initial fluid saturations, effective permeability and porosity, and a set of relative permeability curves, stress tables and compaction tables based on upscaling techniques. The stress and compaction tables are used to alter permeability and porosity respectively as a function of pressure to account for the subsidence observed at the Ekofisk field. Three-phase relative permeability data are calculated by Stone's method. Capillary pressure curves are not included in the sector model

The input porosities range from 0.15 to 0.40 with an average of 0.26. The horizontal permeability ranges from zero, in the impermeable tight zone, up to 720 mD, in the most fractured areas. The average horizontal permeability is 6 mD. Input maximum trapped gas saturation is set to 0.35 with trapped gas calculated by Lands correlation, and SORM values are assigned based on horizontal permeability data as discussed in chapter 6.3.3 using the SORM Sotrig option.

The average initial reservoir pressure is 7103 psia and the calculated initial GOR is 1575 SCF/STB. At a reference depth of 10165 ft the initial oil saturation pressure is 5475 psia, the oil viscosity 0.216 cP and oil density of 584 kg/m^3. These fluid parameters change with depth and reservoir pressure.

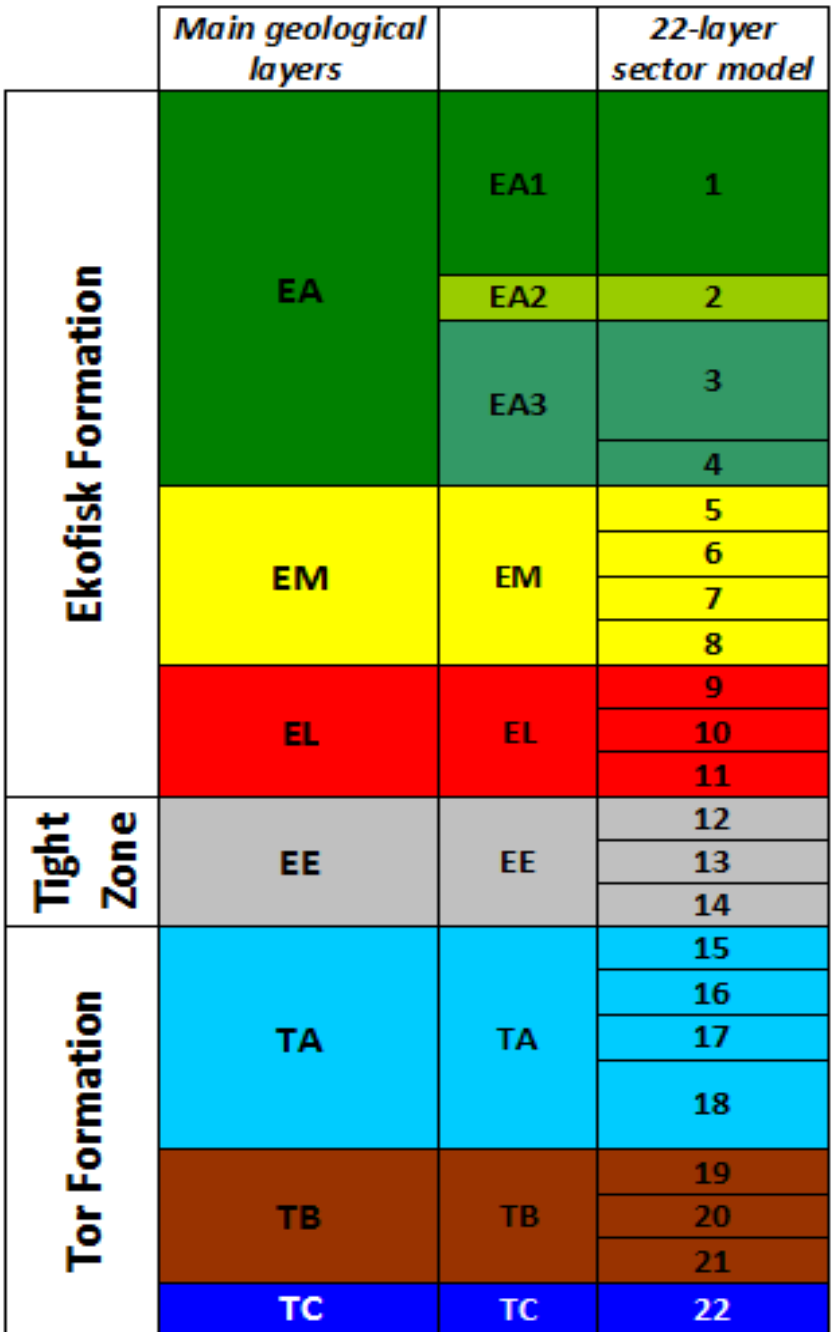

Figure 7.2: The 22 layers of the sector model

Totally 17 wells and 22 faults are included in the sector model. The wells comprise both vertical and horizontal wells. 12 of the wells are production wells which are assumed

operated since 1972 and five are water injection wells assumed operating since 1984. The distribution of the wells and faults in the sector model is shown in figure 7.3, as black dots and black lines between grid blocks. The initial reservoir pressure of the top layer is also illustrated in the figure 7.3.

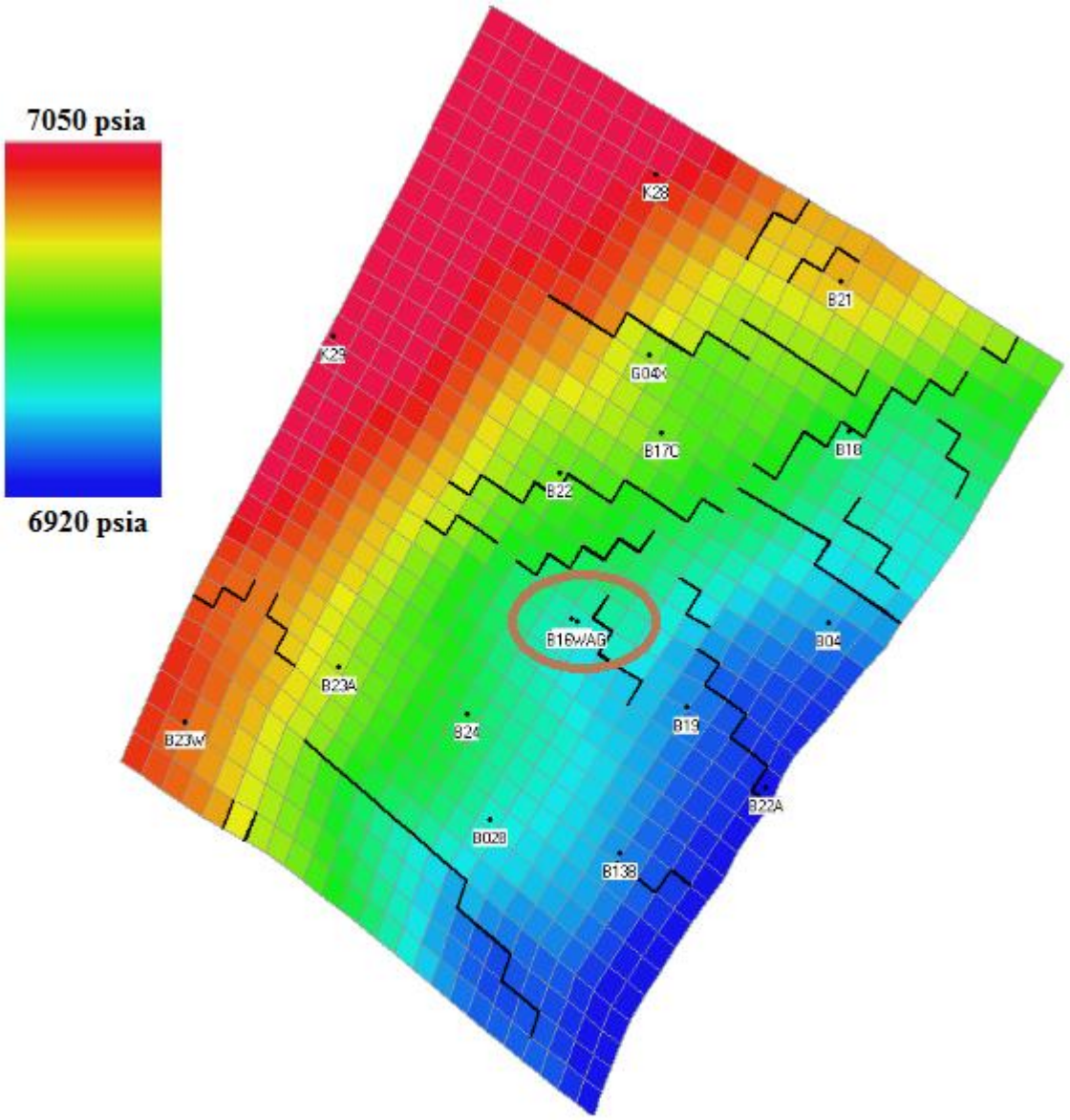

Figure 7.3: Initial reservoir pressures and distribution of wells and faults in the sector models upper layer 1.

Base case simulation

A base case simulation of continued water injection for all the injection wells till the end of license in 2028 is used to compare with different WAG scenarios. All wells are operated with BHP-control and maximum rate limits. The limiting BHP is set to 2 000 psia for production wells and to 7 000 psia for injection wells. The maximum production rate is set to 2 000 STB/D and maximum injection rate to 10 000 BWPD.

The oil recovery and average reservoir pressure as a function of time is shown for the base case simulation in figure 7.4.

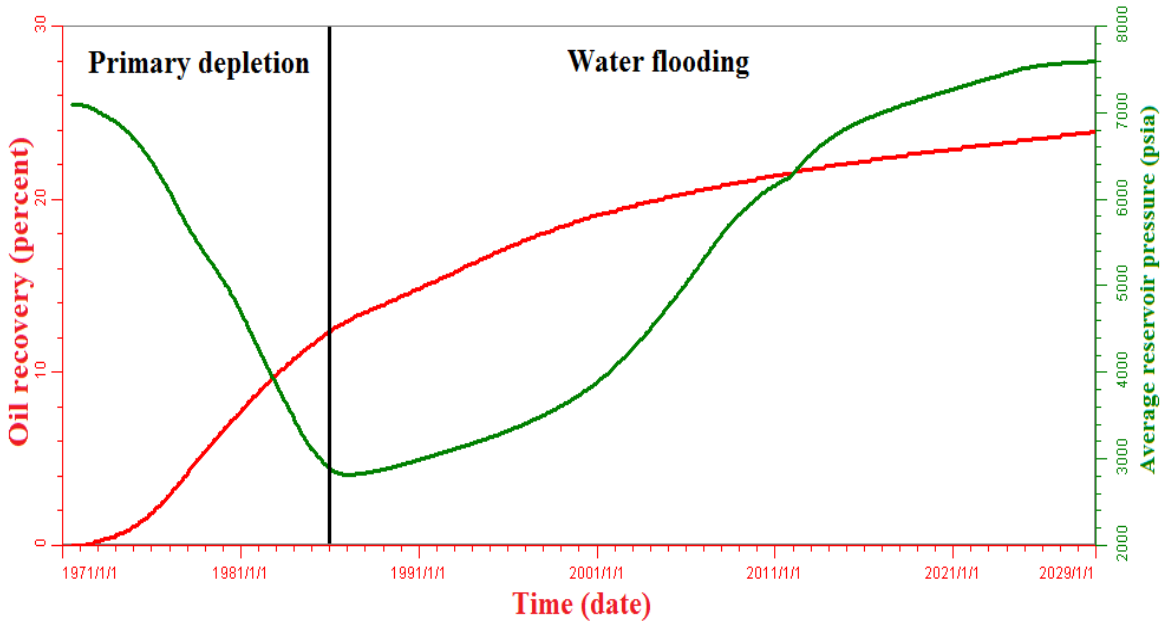

Figure 7.4: Oil recovery and average pressure for the base case simulation in the sector model

The oil recovery after primary depletion is around 12 % and the oil recovery following water flooding till the end of license in 2028 is 23.9 %. These recoveries are a lot lower than what is observed in the field and within the Ekofisk full field simulation model. The reason for the low recoveries in the sector model is that only wells within the region of the sector model are included. In reality, surrounding production and injection well will result in a more extensive water flooding and better depletion than what is modeled within the sector model. However, the sector model can be used to investigate the incremental oil recovery for WAG scenarios within the given model and results can be compared to the water scenario base case. Figure 7.4 further illustrates that if WAG-injection is initiated after water flooding till 2018, the average reservoir pressure would be above 7100 psia. This

reservoir pressure is above the minimum miscibility pressure for all temperatures, presented in chapter 5.3.1, and miscible displacement would likely be achieved.

WAG-injection

For WAG scenarios the former water injection well, well B16W, is changed to a WAG-injection well, B16WAG, for the predictive part starting from 2011. This well is shown in the circle in figure 7.3. The injection well, B16WAG, is a vertical well which is representative for both formations as it is perforated in the Ekofisk formation in layer 1-9 and 11, and in the Tor formation in layer 16-19. Layer 10 and 15 are not represented in the well because of a pinch-out, while layer 12-14 are in the tight zone. All wells are still operated under BHP-control and maximum rate limits, similar to what was presented for the base case. The only difference is that the WAG injection well is switched to a BHP limit of 8 000 psia, which is obtainable, to ensure high injection rates.

Methodology

Methodology WAG-ratios

For the Ekofisk reservoir it is believed that low vertical permeability will result in limited flow in the vertical direction and also that most injected gas flows along fractured areas, which together results in poor macroscopic sweep efficiency. However, optimizing the WAG-ratio, ratio of volume of water injected to gas injected, can result in increased oil recovery. The water slugs stabilizes the gas front by a more favorable displacement mobility ratio, which results in better sweep efficiency, as reduced viscous fingering and postponed gas breakthrough can be obtained.

To study the effect of WAG ratio on recovery for this sector model, four different cases with WAG ratio 4:1, 2:1, 1:1 and 1:2 are simulated and compared with the base case. The gas half-cycle slug sizes are set to 10 % of the pore volume of the grid size which the water injection well, B16W, had swept by 2011. This pore volume equals approximately 100 million barrels and each gas-half cycle equals 10 million barrels or roughly 56 million cubic feet. In each case three WAG-cycles are used, meaning a total of 0.3 pore volumes of gas injected for each case.

Methodology WAG slug sizes

Optimization of the size of injected slugs of water and gas can result in increased oil recovery. Smaller WAG slug sizes will result in an increase zone of three flowing phases, which can result in better displacement efficiency.

To study the effect different slug sizes have on oil recovery, four WAG cases with half-cycle slug sizes of 0.05, 0.1, 0.2 and 0.4 pore volumes are simulated. WAG ratio of 1:1 is used for the different cases. For evaluation the total amount of gas injected should be equal and is set to 0.4 pore volumes, which will control number of WAG-cycles for each case.

7.2 Results and discussion of sector simulations

7.2.1 WAG-ratio

Different WAG-ratios are evaluated by the amount of barrels of oil equivalent (BOE) going to sale, compared to the water flood base case. The BOE to sale is obtained by using a ConocoPhillips tool, based on the simulation output. BOE to sale is calculated based on oil production rates, gas production rates, fuel, gas injection and sales factors and is shown in appendix D for the different WAG ratios. The cumulative incremental BOE to the base case is plotted in figure 7.5 and summarized in table 7.1

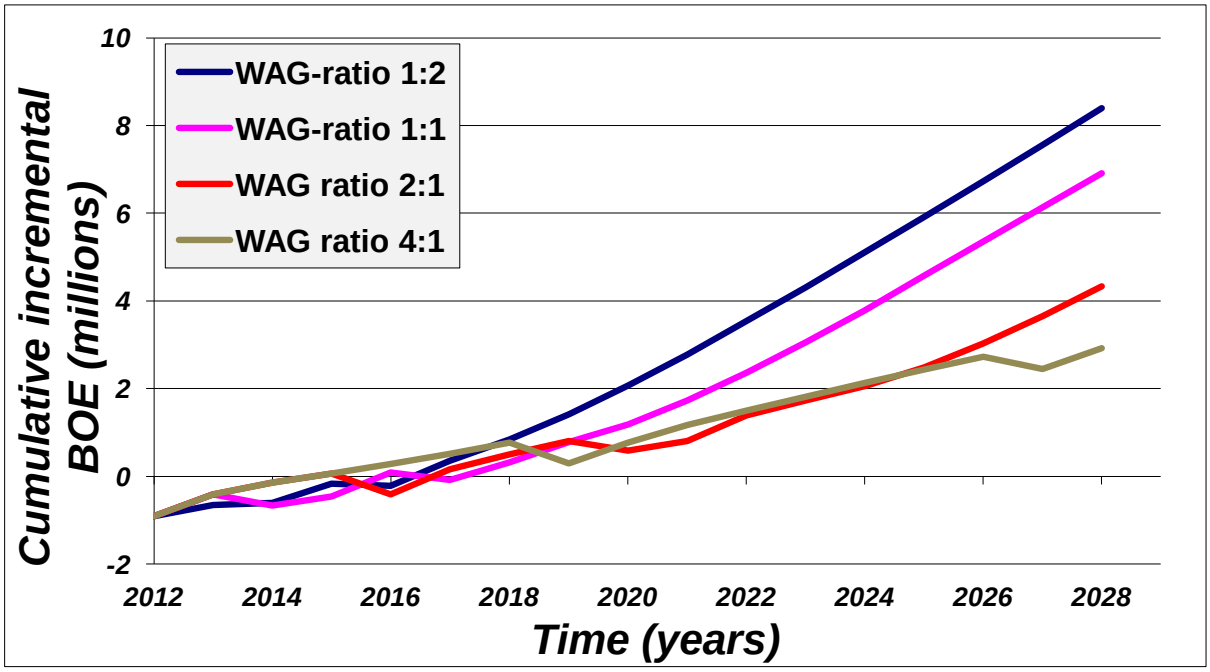

Figure 7.5: Cumulative incremental barrels of oil equivalent to water flood base case for different WAG ratios

Table 7.1: Barrels of oil equivalent and incremental barrels of oil equivalent to base case for different WAG ratios for the predictive part from 2011 to 2028

Scenario	BOE to sale at the end of the predictive period (for year 2011-2028)	Incremental BOE to sale to the base case
Water flood base case	17.5 million BOE	-
WAG ratio 1:1	24.4 million BOE	6.9 million BOE
WAG ratio 2:1	21.8 million BOE	4.3 million BOE
WAG ratio 4:1	20.4 million BOE	2.9 million BOE
WAG ratio 1:2	25.9 million BOE	8.4 million BOE

It is observed that the best WAG scenario is with WAG ratio of 1:2 which gives additional 8.4 million BOE to sale compared to the water flood base case. Figure 7.5 and table 7.1 indicates that decreased WAG-ratios results in increased oil equivalent recovery. For all the WAG scenarios incremental oil equivalent recovery to the water flood base case is observed.

A plot of gas saturation and permeability for layer 8 is given in figure 7.6 to illustrate the flow pattern of injected gas.

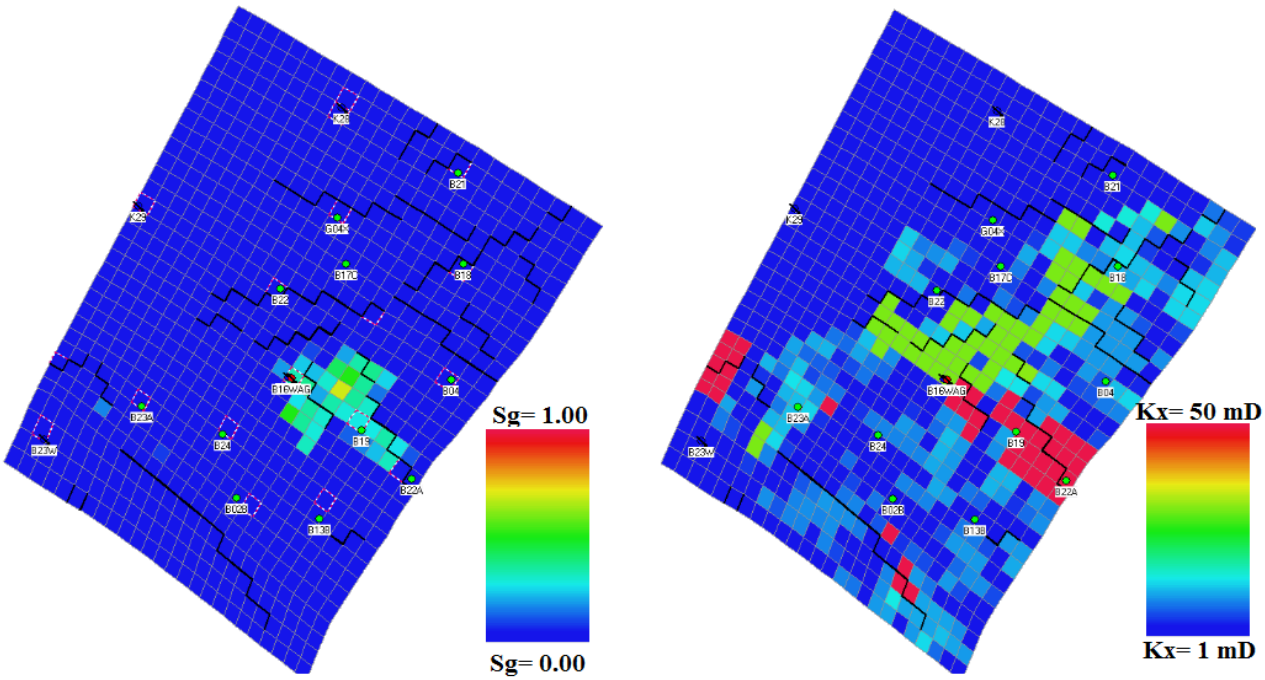

Figure 7.6: Gas saturation and permeability in layer 8 of the sector model during WAG injection

It is seen from figure 7.6 that most of the injected gas will flow in the high permeable grid blocks.

7.2.2 WAG slug sizes

The impact of slug sizes for WAG injection is evaluated by a similar approach as for the WAG ratios, comparing the BOE to sale for the different WAG scenarios against the water flood base case. Calculation of BOE for the different slug sizes is shown in appendix D. The results are plotted as cumulative incremental BOE to the base case in figure 7.7 and summarized in table 7.2

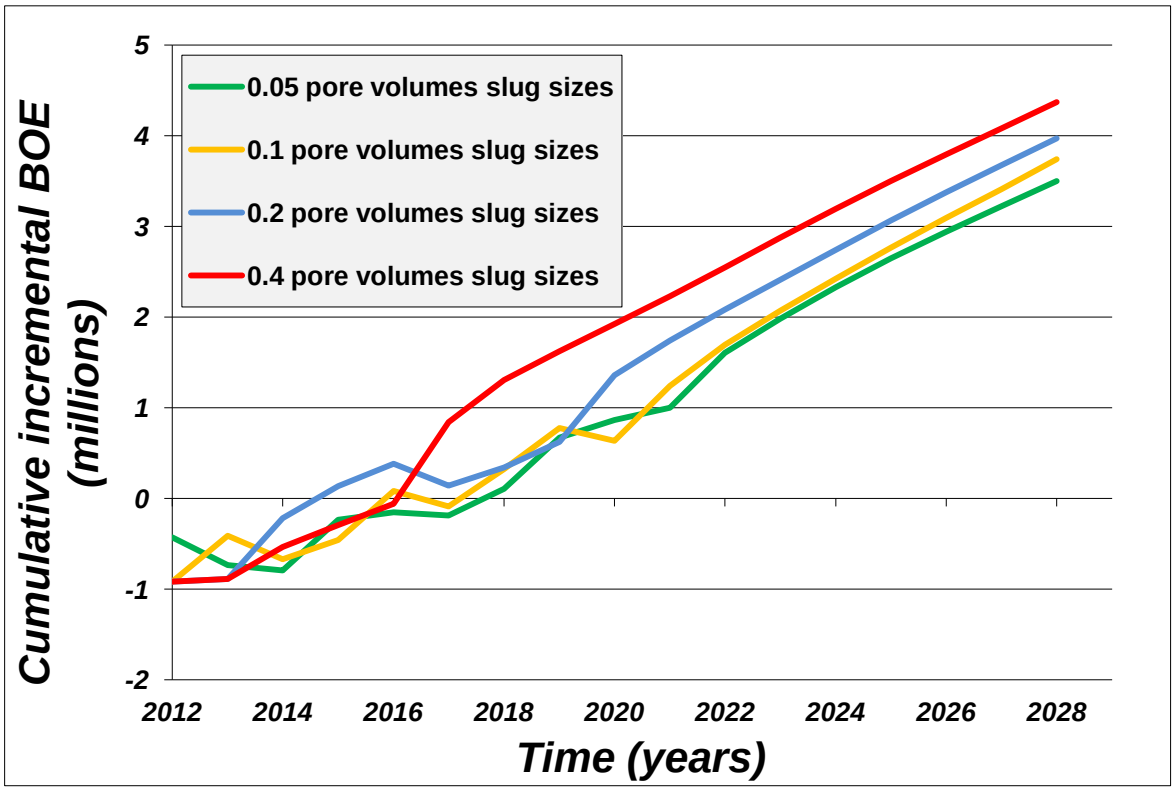

Figure 7.7: Cumulative incremental barrels of oil equivalent to water flood base case for different slug sizes

Table 7.2: Barrels of oil equivalent and incremental barrels of oil equivalent to base case for different slug sizes with WAG ratio 1:1 for the predictive part from 2011 to 2028

Scenario	BOE to sale for predictive period (year 2011-2028)	Incremental BOE to sale to the base case
Water flood base case	17.5 million BOE	-
0.05 pore volumes half-cycle slugs	21.0 million BOE	3.5 million BOE
0.1 pore volumes half-cycle slugs	21.2 million BOE	3.7 million BOE
0.2 pore volumes half-cycle slugs	21.5 million BOE	4.0 million BOE
0.4 pore volumes half-cycle slugs	21.9 million BOE	4.4 million BOE

Figure 7.7 and table 7.2 indicates that increasing the slug size results in increased oil equivalent recovery. The best case was half-cycle slug size of 0.4 pore volumes which gave an incremental 4.4 million BOE to the base case. It is observed that total gas injected of 0.4 pore volumes, give lower BOE than for same WAG ratio with total gas injected of 0.3 pore volumes. Based on this result, the total volume of gas injected is recommended to be investigated and optimized for further studies.

The coarse grid blocks of the sector model may lead to numerical dispersion when implementing a WAG-injection, because of rapidly varying fluid fronts and large differences in reservoir parameters between grid blocks. To avoid numerical dispersion and instability problems caused by coarse gridding in WAG injection, local grid refinement can be applied. The technique can improve grid resolution in particular areas of a model and keep the coarse resolution in other areas. The option will minimize the number of grid blocks and therefore reduce the CPU time of simulation compared to a regular grid refinement option where grids in all areas are refined. The LGR methodology could be useful around the WAG-injection well where fluid saturations change rapidly. The technique is not used in this study because of its complexness, but is recommended to include for further studies to avoid numerical dispersion.

8 Conclusion

The purpose of this thesis was to evaluate hydrocarbon WAG injection at the Ekofisk field. Miscibility evaluation on MMP and MME, and modeling of important reservoir parameters for WAG-displacement, such as trapped gas and hysteresis effect, matrix-fracture mechanisms and SORM was suggested. Also modeling of WAG injection in a sector model to optimize WAG ratios and WAG slug sizes, and to compare against a continuous water flood case was suggested.

The evaluation was performed by running simulations in PSim for various models. The following main conclusion can be drawn from the results from this study:

- At current reservoir pressures at Ekofisk, WAG injection with dry hydrocarbon would most likely be immiscible. This is based on the MMPs for dry hydrocarbon gas with the Ekofisk crude oil determined in the range of 6600 to 7100 psia for different temperatures.

- The results showed that MME decreases with increasing pressures, which agrees with theory. It was found that achieving miscibility by increasing the enrichment was not a solution, because large amounts of NGL were needed. This involves high economical risk because the relative high price NGL is delegated from sales to injection.

- Mechanistic simulations on trapped gas showed that Lands trapped gas correlation with input trapped gas value of 0.35 gave the best match to laboratory and reported trapped gas data for chalks. It was also shown that neglecting trapped gas in simulations gives optimistic predictions.

- Simulations of different matrix-fracture systems gave significant differences in oil recoveries and were used as an argument to introduce SORM for sector modeling, which showed to be best described by the SORM Sotrig option.

- WAG-scenarios in the sector model indicated incremental production to the water flood base case for all cases. The best WAG ratio showed to be 1 to 2, with incremental barrels of oil equivalent of 8.4 million to the base case. The incremental BOE decreased

with increasing WAG ratio. The optimized WAG slug sizes at WAG ratio of 1:1 showed to be 0.4 pore volumes, with incremental BOE of 4.4 million to the base case. Incremental BOE increased with increasing WAG slug sizes.

Recommendation for further work

It is recommended that further research be undertaken in the following areas:

- Laboratory work on miscibility of dry hydrocarbon gas with the Ekofisk crude oil for more accurate and reliable MMP evaluations.

- More research on SORM and more accurate upscaling techniques from mechanistic level to full field level.

- Perform simulation work to investigate the total gas volume injected for WAG scenarios in the sector model.

- Introduction of local grid refinement to avoid numerical dispersion and instability problems in the sector model.

- Investigation of full field WAG potential by running full field simulations.

- Economical study including aspects such as pipeline from production to injection platforms, installation of compression pump, gas and NGL prices, sale of incremental oil and net present value.

9 Abbreviations and symbols

BHP	Bottom-hole pressure
BOE	Barrels of oil equivalent
BWPD	Barrels of water per day
C_{Land}	Lands trapping constant
C	Trapping characteristics of porous rock
CPU	Central processing unit
D	Darcy, unit for permeability
EOR	Enhanced oil recovery
EOS	Equation of state
FCM	First-contact miscibility
FI	Fracture intensity factor
G	Gravitational constant
GOR	Gas to oil ratio
H	Height of matrix blocks
HC-WAG	Hydrocarbon water-alternating-gas
IFT	Interfacial tension
k	Absolute permeability
k_e	Effective permeability
k_{mat}	Matrix permeability from well log porosity or permeability correlations
k_r	Relative permeability
k_{rg}	Relative permeability of gas
k_{ro}	Relative permeability of gas
k_{rog}	Relative permeability of oil in a gas-oil system
k_{row}	Relative permeability of oil in a water-oil system
k_{rw}	Relative permeability of water
k_{well}	Effect permeability from well tests
LGR	Local grid refinement
LPG	Liquefied petroleum gas
MCM	Multi-contact miscibility
MME	Minimum miscibility enrichment
MMP	Minimum miscibility pressure

NGL	Natural gas liquid
OOIP	Original oil place
P_c	Capillary pressure
P_{nw}	Non-wetting phase pressure
PR-EOS	Peng and Robinson equation of state
Psia	Pounds per square inch, absolute pressure
PVT	Pressure-volume-temperature
P_w	Wetting-phase pressure
SCF/D	Standard cubic feet gas per day
SCF/STB	Standard cubic feet gas per standard oil barrel
*Sg**	Total gas saturation
*SgF**	Mobile fraction of gas
*Sgi**	Gas saturation at the start of imbibition process
S_{gc}	Critical gas saturation
S_{gr}	Residual gas saturation
*Sgr**	Residual trapped gas saturation after complete imbibition
Sgr^*_{max}	Maximum obtainable residual gas saturation
*Sgrc**	Current trapped gas fraction of the gas
Som	Mobile oil saturation
S_{org}	Residual oil to gas
SORM	Miscible flood residual oil saturation
S_{orw}	Residual oil to water
S_{orWAG}	Residual oil to WAG
STB/D	Standard oil barrels per day
S_{wr}	Residual water saturation
WAG	Water alternating gas
X_G	Fractional height of gas in the fracture
X_g	Fractional height of the gas in the matrix
X_{WF}	Fractional height of water in the fracture
X_{Wm}	Fractional height of the gas in the matrix
θ	Contact angle
$\in$	Empirically determined pore-size distribution factor
ρ_g	Gas density

ρ_o	Oil density
ρ_w	Water density
σ	Interfacial tension
σ_{os}	Interfacial tension between solid and oil
σ_{ow}	Interfacial tension between water and oil
σ_{ws}	Interfacial tension between solid and water
φ	Rock porosity

10 References

Agarwal, B., Thomas, L.K. and O'Meara, D.J. 1997. Reservoir Charcterization of Ekofisk Field: A Giant, Fractured Chalk Reservoir in the Norwegian North Sea - Upscaling. *SPE 38875.* October 1997.

Ahmed, T. 2000. Minimum Miscibility Pressure from EOS. *Canadian International Petroleum Conference.* 4.-8. June 2000, Paper 2000-01.

Al-Wahaibi, Y.M, Muggeridge, A.H. and C.A.Grattioni. 2007. Experimental and Numerical Studies of Gas/Oil Multicontact Miscible Displacements in Homogeneous and Corssbedded porous Media. *SPEJ 92887.* March, 2007, page 62-76.

Al-Wahaibi, Yahya M. 2009. First-Contact-Miscible and Multicontact Miscible Gas Injection within a Channeling Heterogeneity System. *Energy&fuels article.* 2009, Vol. 2010.

App, J.F. and Mohanty, K.K. 2002. The Benefit of Local Saturation Measurements in Relative Permeability Estimation From Centrifuge Experiments. *SPEJ September 2002.* 2002, page 288-298.

Bark, E. Van den and O.D.Thomas. 1979. Ekofisk: First of the Giant Oil Fields in Western Europe. s.l. : The American Association of Petroleum Geologists, 1979, page 195-223.

Bernudez, L., Johns, R.T. and Parakh, H. 2007. Parametric Inverstigation of WAG Floods Above the MME. *SPEJ.* June 2007, page 224-234.

Bradford, S.A. and Leij, F.J:. 1995. Wettability effect on scaling two- and three-fluid capillary pressure-saturation relations. *Env. Sci. Techn.* 29, 1995, page 1446-1455.

Carlson, F.M. 1981. Simulation of Relative Permeability Hysteresis to the Nonwetting Phase. *SPE 10157.* October 1981.

Christensen, J.R., Stenby, E.H and Skauge, A. 2001. Review of WAG Field Experience. *SPE 71203.* April 2001, page 97-106.

Christian, T.M., et al. 1993. Reservoir Management at Ekofisk Field. *SPE 26623.* October 1993.

Clark, N.J., et al. 1958. Miscible Drive-Its Theory and Application. *SPE 1036-G.* June 1958.

ConocoPhillips Company (1). The Greater Ekofisk Area. [Internett] [Sitert: 04 April 2012.] http://www.conocophillips.no/EN/Norwegian%20shelf/Ekofisk/Pages/index.aspx.

ConocoPhillips Company (2). Worldwide operations: Norway. [Internett] [Sitert: 04 April 2012.] http://www.conocophillips.com/EN/about/worldwide_ops/country/europe/pages/norway.aspx.

ConocoPhillips Company (3). *Discussion and presentations internally in ConocoPhillips*. 2012

ConocoPhillips. January 1994. *Ekofisk WAG Evaluation.* Bartlesville : Phillips Petroleum Company R&S Division, January 1994.

ConocoPhillips Keywords Manual. 2010. PSim Keywords Manual 2010.0. December 2010.

ConocoPhillips Technical Manual. 2010. PSim Technical Manual 2010.0. December 2010. pages 177-202, 140-148, 9-15

Conway, P.I., Damm, M. and Andersen, P.M. 1996. Full Field Dual Porosity Modelling of a Complex Fractured Chalk Oil Reservoir Subject to Both Gas and Water Injection. *SPE 36931*. 22.-24. October 1996.

Dangerfield, J.A and Brown, D.A. 1987. The Ekofisk Field. [bokforf.] Graham Trotman. *The Norwegian Institute of Technology*. 1987, page 3-22.

Donaldson, E.C., Thomas, R.D. and Lorenz, P.B. 1969. Wettability Determination and Its Effect on Recovery Efficiency. *SPEJ*. March, 1969, page 13-20.

Dong, M., et al. 2005. Analysis of Immiscible Water-Alternating-Gas (WAG) Injection Using Micromodel Tests. *Journal of Canadian Petroleum Technology*. February, 2005, page 17-25.

Elsharkawy, A.M., Poettmann, F.H. and Christiansen, R.L. 1992. Measuring Minimum Miscibility Pressure: Slim-Tube or Rising-Bubble Method? *SPE/DOE 24114*. 22-24 April 1992.

Faisal, A., et al. 2009. Injectivity and Gravity Segregation in WAG and SWAG Enhanced Oil Recovery. *SPE 124197*. October 2009.

Firoozabadi, A. and Aziz, K. 1986. Relative permeability From Centrifuge Data. *SPE 15059*. 1986.

Goda, H. and Behrenbruch, P. 2011. A Universal Formulation for the Prediction Of Capillary Pressure. *SPE 147078*. 2011.

Green, D.W. and Willhite, G. P. 1998. *Enhanced Oil Recovery*. Volume 6. 1998. 978-1555630775. pages 12-27, 55-56, 190-196, 198-206

Hallenbeck, L.D, et al. 1989. Implementation of the Ekofisk Waterflood. *SPE 19838*. 1989.

Harpole, K.J., A.Østhus and Jensen, T.B. 2000. Screening for Ekofisk. *SPE 65124.* October 2000.

Heeremans, J.C. and Kruijsdijk, C.P.J.W. van. 2006. Feasibility Study of WAG Injection in Naturally Fractured Reservoirs. *SPE 100034.* 22.-26. April 2006.

Helland, J.O. and Skjæveland, S.M. 2004. Three-Phase Capillary Pressure Correlation for Mixed-Wet Reservoirs. *SPE 92057.* November 2004.

Holm, L.W. 1987. Miscible Displacement. [bokforf.] Howard B. Bradley. *Petroleum Engineering Handbook.* s.l. : Texas: Society of Petroleum Engineers., 1987, 45, ss. 1-9.

Hustad, O.S., et al. 2002. Gas Segregation During WAG Injection and the Importance of Parameter Scaling in Three-Phase Models. *SPE 75138.* 13.-17. April 2002.

Ibrahim, M.N. Mohamad and Koederitz, L.F. 2001. Two-Phase Steady-State and Unsteady-State Relative Permeability Prediction Models. *SPE 68065.* 2001.

Jakobsson, N.M. and Christian, T.M. 1994. Historical Performance of Gas Injection of Ekofisk. *SPE 28933.* September 1994.

Jensen, T.B. 2001. *Ekofisk Field - Simultaneous Water and Gas Injection- SWAG Feasibility Study.* Stavanger : Internal ConocoPhillips report, 2001.

Jethwa, D.J., Rothkopf, B.W. and Paulson, C.I. 2000. Successful Miscible Gas Injection in a Mature U.K. North Sea Field. *SPE 62990.* 2000.

Jewhurst, J. and Wiborg, R. 1987. *Ekofisk reservoir management in a compacting environment.* Sidney Australia : Internal ConocoPhillips report, 1987. page 54-67.

Johnson, J.P, Rhett, D.W. and Slemers, W.T. 1989. Rock Mechanics of the Ekofisk Reservoir in the Evaluation of Subsidence. *Journal of Petroleum Technology.* July 1989, page 717-722.

Kalam, Z., et al. 2011. Miscible Gas injection Tests in Carbonates and its Impact on Field Development. *SPE 148374.* October 2011.

Keelan, Dare K. and J.Pugh, Virgil. 1975. Trapped-Gas Saturations in Carbonate Formations. *SPEJ.* April 1975, page 149-160.

Killough, J.E. 1976. Reservoir Simulation With History-Dependent Saturation Functions. *SPEJ.* February 1976, ss. 37-48.

Kleppe, Hans. 2011. Reservoir simulation course MPE750 at UiS, autumn 2011. University of Stavanger : s.n., 2011. Chapter 6.

Kleppe, J., Teigland, R. and Awan, A.R. 2006. A Survey of North Sea Enhanced-Oil-Recovery Projects Initiated During the Years 1975 to 2005. *Revised SPE 99546.* 2006, Vol. 2008, page 497-512.

Kossack, C.A. 2000. Comparison of Reservoir Simulation Hysteresis Options. *SPE 63147.* October 2000.

Land, Carlon S. 1968. Calculation of Imbibition Relative Permeability for Two- and Three-Phase Flow From Rock Properties. *SPEJ.* June 1968, page 149-156.

Land, Carlson S. 1971. Comparison of Calculated with Experimental Imbibition Relative Permeability. *SPE 3360.* December 1971, page 419-425.

Larsen, J.A and Skauge, A. 1998. Methodology for Numerical Simulation With Cycle-Dependent Relative Permeabilities. *SPEJ.* June 1998, page 163-173.

Larsen, J.A. and Skauge, A. 1995. Comparing hysteresis models for relative permeability in WAG studies. *SCA 9506.* 1995.

Lekvam, Surgucchev and Ekrann. 1997. *Hydrate Control for WAG injection in the Ekofisk Field.* Rogaland Research Institute, 1997. RF. 97/165.

Li, D., Kumar, K. and Mohanty, K.K. 2003. Compositional Simulation of WAG Processes for a Viscous Oil. *SPE 84074.* 5.-8. October 2003.

Maloney, D.R. 2003. *Consistency of Eldfisk, Ekofisk, and literature trapped gas results.* Upstream Reservoir Technology Report #17129. Bartlesville : ConocoPhillips, 2003.

Morrow, N.R. 1979. Interplay of capillary, viscous and buoyancy forces in the mobilization of residual oil. *Journal of Canadian Petroleum Technology (JCPT 79-03-03).* July-September, 1979.

Norsk Teknisk Museum. Det norske olje-eventyret 1965-2000. [Internett] [Sitert: 04 April 2012.] http://tekniskmuseum.no/gamlewebben/no/utstillingene/Jakten_oljen/historie.htm.

Pow, M., et al. 1997. Production of Gas From Tight Naturally-fractured Reservoirs With Active Water. *SPEJ 97-03.* 1997. Annual Technical Meeting, Jun 8 - 11, 1997 , Calgary, Alberta.

Ramachandran, K.P., Gyan, O.N. and Sur, S. 2010. Immiscible Hydrocarbon WAG:Laboratory to Field. *SPE 128848.* 20.-22. January 2010.

Randall, T.E. and Bennion, D.B. 1988. Recent developments in slim tube testing for hydrocarbon-miscible flood (HCMF) solvent design. *Journal of Canadian Petroleum Technology.* Volume 27, No.6, November-December 1988, JCPT88-06-02, page 33-44.

Reservoir Laboratories AS. 1995. *Tertiary gas injection following imbibition in a long chalk sample.* s.l. : ConocoPhillips in cooperation with Reservoir Laboratorias AS, as part of "Ruth research program, WAG subprogram", 1995.

Sanchez, N.L. 1999. Management of Water Alternating Gas (WAG) Injection Projects. *SPE 53714.* 21.-23. April 1999.

Shyeh-Yung, J-G.J. 1991. Mechanisms of Miscible Oil recovery: Effect of Pressure and Miscible and Near-Miscible Displacement of Oil by Carbon Dioxide. *SPE 22651.* 1991.

Skauge, A. and Dale, E.I. 2007. Progress in Immiscible WAG Modeling. *SPE 111435.* October 2007.

Skauge, A. and J.A.Larsen. 1994. Three-phase relative permeabilities and trapped gas measurements related to WAG processes. *SCA 9421.* September 1994, page 227-236.

Sohooli, Kh. 2012. Fracture Network Parameters in Dynamic Models of Fractured Reservoir and Its Upscaling. *SPE 151667.* 20.-22. February 2012.

Spiteri, Elizabeth J. and Juanes, Ruben. 2004. Impact of Relative Permeability Hysteresis on the Numerical Simulation of WAG injection. *SPE 89921.* September 2004.

Spronsen, E.V. 1982. Three-Phase Relative Permeability Measurements Using the Centrifuge Method. *SPE/DOE 10688.* 1982.

Stone, H.L. 1970. Probability Model for Estimating Three-Phase Relative Permeability. *Journal of Petroleum Technology (2116).* February 1970, ss. 214-218.

Stone, H.L. 1973. Estimation of Three-Phase Relative Permeability. *Journal of Canadian Petroleum Technology (JCPT73-04-06).* October-December 1973, No.4, ss. 53-63.

Suicmez, V.S, Piri, M. and Blunt, M.J. 2006. Pore-Scale Modeling of Three-Phase WAG injection: Prediction of Relative Permeabilities and Trapping for Different Displacement Cycles. *SPE 95594.* April 2006.

Sulak, R.M. 1990. Ekofisk Field: The First 20 Years. *SPE 20773.* September 1990.

Sulak, R.M and Danielsen, J. 1989. Reservoir Aspects of Ekofisk Subsidence. *Journal of Petroleum Technology.* July 1989, page 709-716.

Sylte, J.E, et al. 1999. Water Induced Compaction in the Ekofisk Field. *SPE 56426.* October 1999.

Sylte, J.E, Hallenbeck, L.D. and Thomas, L.K. 1988. Ekofisk Formation Pilot Waterflood. *SPE 18276.* October 1988.

Takla, L.A. and Sulak, R.M. 1989. Production Operations and Reservoir Aspets - Ekofisk Area. October 1989. paper presented at the Integrated Petroleum Resource Management Seminar and Workshop, Phillips, Stavanger, Norway.

Thomas, L.K, et al. 1987. Ekofisk Waterflood Pilot. *Journal of Petroleum Technology.* February 1987, ss. 221-232.

Ursin, J.R. and Zolotukhin, A.B. 1997. *Introduction to ResTek.* Stavanger : UiS, 1997. Pages 63, 67, 87-110, 115-118. Part of Reservoir Engineering Course BIP 140 autumn 2009.

Warren, J.E. and Root, P.J. 1963. The Behavior of Naturally Fractured Reservoirs. *SPEJ (SPE 426).* September, 1963, page 245-255.

Wegener and Allred. 1997. *Hydrate Formation Tendencies, Lean Gas, Water, Thermodynamic Inhibitors. Predictions: Models versus Lab.* Bartlesville : Phillips, 1997. Presented Material.

Wegener, D.C and K.J.Harpole. 1996. Determination of Relative Permeability and Trapped Gas Saturation for Predictions of WAG Performance in the South Cowden CO2 Flood. *SPE 35429.* April 1996, page 273-285.

Wu, R.S. and Batycky, J.P. 1990. Evaluation of miscibility from slim tube tests. *The Journal of Canadian Petroleum Technology.* Volume 29, No.6, November-December 1990, JCPT90-06-06, page 63-70.

Wu, X., et al. 2004. Critical Design Factors and Evaluation of Recovery Performance of Miscible Displacement and WAG Process. *Canadian International Petroleum Conference.* 8.-10. June 2004, Paper 2004-192.

Zick, A.A. 1986. A Combined Condensing/Vaporizing Mechanism in the Displacement of Oil by Enriched Gases. *SPE 15493.* October 1986.

Østhus, A. 1998. *Ekofisk Whiskey WAG pilot.* Stavanger : Internal ConocoPhillips report, 1998.

Øyno, Lars. 1995. *Tertiary Gas injection Following Imbibition in a Long Chalk Sample.* Reservoir Laboratories AS. 1995. Report 344/10-96 for ConocoPhillips.

11 Appendices

Appendix A - Slim tube

MMP

268 F	
Pressure	Oil recovery at 1.2 PV gas injected
3500	54,36
4000	57,72
4500	61,57
5000	66,48
5500	73,78
6000	81,32
6500	89,18
6800	94,26
6850	95,12
6900	95,84
6950	96,33
7000	96,67
7050	96,91
7100	97,11
7500	97,93
8000	98,43
9000	98,99

Oil recovery as a function of operating pressure at 268˚ F

200 F	
Pressure	Oil recovery at 1.2 PV gas injected
3500	53,51
4500	60,99
5500	73,65
6000	80,79
6500	88,09
6900	94,35
7000	95,61
7100	96,26
7500	97,3
8000	97,83

Oil recovery as a function of operating pressure at 200˚ F

150F	
Pressure	Oil recovery at 1.2 PV gas injected
3500	53,8
4500	61,93
5500	75,37
6000	82,32
6500	89,22
6800	93,63
6900	94,86
7000	95,59
7100	96,02
7500	96,87
8000	97,36

Oil recovery as a function of operating pressure at 150˚ F

100F	
Pressure	Oil recovery at 1.2 PV gas injected
3500	55,5
4500	65,61
5500	78,96
6000	85,21
6500	91,19
6600	92,42
6700	93,55
6800	94,44
6900	94,99
7000	95,38
7500	96,3
8000	96,73

Oil recovery as a function of operating pressure for 100˚ F

60 F	
Pressure	Oil recovery at 1.2 PV gas injected
3500	58,68
4500	70,2
5500	82,04
6000	86,58
6250	88,73
6500	90,87
6750	92,87
7000	94,34
7250	95,05
7500	95,45
8000	95,92

Oil recovery as a function of operating pressure for 60˚ F

MME

	0 % NGL	2 % NGL	5 % NGL	8 % NGL	10 % NGL	12 % NGL	15 % NGL	20 % NGL
N2	0,28 %	0,27 %	0,27 %	0,26 %	0,25 %	0,25 %	0,24 %	0,22 %
CO2	2,65 %	2,62 %	2,58 %	2,53 %	2,50 %	2,47 %	2,43 %	2,35 %
C1	84,02 %	82,38 %	79,92 %	77,46 %	75,81 %	74,17 %	71,71 %	67,61 %
C2	9,41 %	9,59 %	9,87 %	10,14 %	10,33 %	10,51 %	10,79 %	11,25 %
C3	2,94 %	3,45 %	4,23 %	5,00 %	5,51 %	6,03 %	6,80 %	8,09 %
iC4	0,22 %	0,35 %	0,54 %	0,73 %	0,85 %	0,98 %	1,17 %	1,49 %
C4	0,41 %	0,79 %	1,36 %	1,92 %	2,30 %	2,68 %	3,25 %	4,19 %
iC5	0,04 %	0,17 %	0,37 %	0,56 %	0,70 %	0,83 %	1,02 %	1,35 %
C5	0,03 %	0,18 %	0,40 %	0,62 %	0,76 %	0,91 %	1,13 %	1,49 %
C6	0,00 %	0,15 %	0,36 %	0,58 %	0,73 %	0,87 %	1,09 %	1,46 %
C7P1	0,00 %	0,05 %	0,12 %	0,20 %	0,25 %	0,29 %	0,37 %	0,49 %
C7P2	0,00 %	0,00 %	0,00 %	0,00 %	0,01 %	0,01 %	0,01 %	0,01 %
C7P3	0,00 %	0,00 %	0,00 %	0,00 %	0,00 %	0,00 %	0,00 %	0,00 %
C7P4	0,00 %	0,00 %	0,00 %	0,00 %	0,00 %	0,00 %	0,00 %	0,00 %
C7P5	0,00 %	0,00 %	0,00 %	0,00 %	0,00 %	0,00 %	0,00 %	0,00 %

Total composition of injected gas with different degree of enrichment

268 F, 6000 psia	
Enrichment (NGL added)	**Oil recovery at 1.2 PV gas injected**
0 %	81,32
2 %	82,56
5 %	85,6
8 %	90,25
10 %	93,43
12 %	95,82
15 %	97,72
20 %	99,47

Oil recovery as a function of enrichment level at 268˚F and 6000 psia

268F, 5000 psia	
Enrichment (NGL added)	**Oil recovery at 1.2 PV gas injected**
0 %	66,48
2 %	67,59
5 %	70,36
8 %	75,34
10 %	79,73
12 %	84,48
15 %	91,24
20 %	97,4

Oil recovery as a function of enrichment level at 268˚F and 5000 psia

150 F, 6000 psia	
Enrichment (NGL added)	Oil recovery at 1.2 PV gas injected
0 %	82,32
2 %	83,66
5 %	86,69
8 %	91,1
10 %	93,78
12 %	95,53
15 %	97,16
20 %	98,89

Oil recovery as a function of enrichment level at 150˚F and 6000 psia

60 F, 6000 psia	
Enrichment (NGL added)	Oil recovery at 1.2 PV gas injected
0 %	86,58
2 %	87,22
5 %	88,32
8 %	89,71
10 %	90,93
12 %	92,3
15 %	94,27
20 %	96,79

Oil recovery as a function of enrichment level at 60˚F and 6000 psia

Appendix B – Test of EOS for immiscible conditions

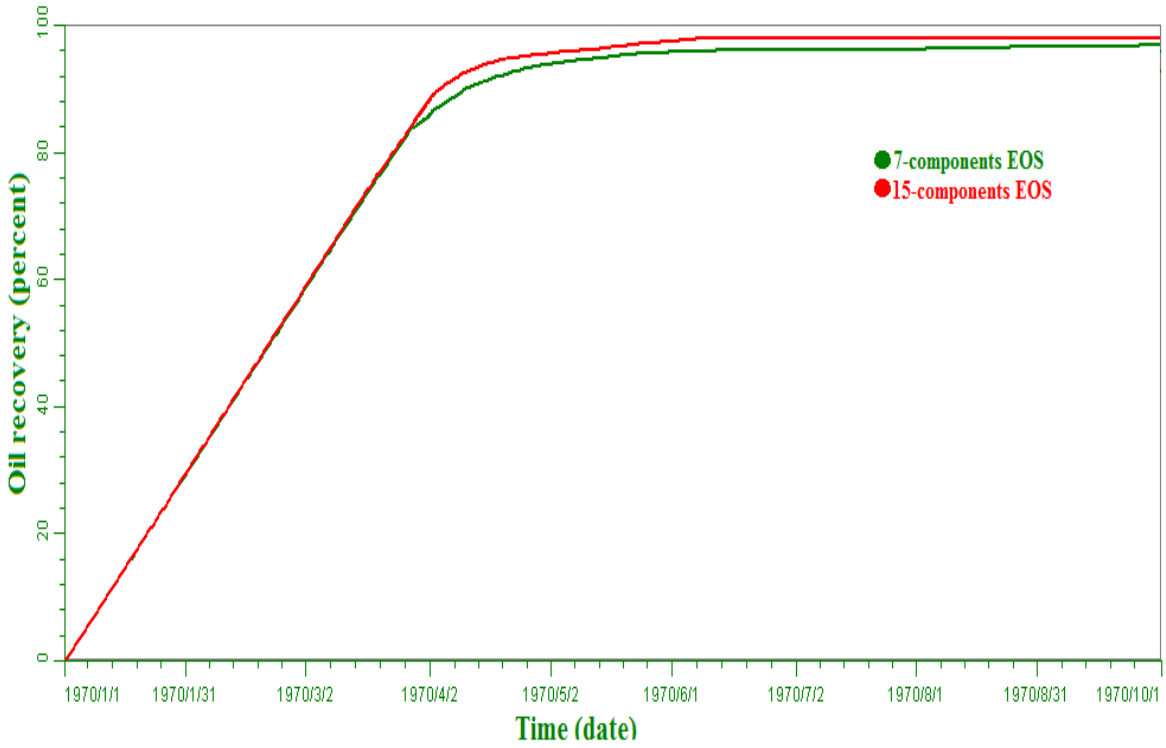

Oil recovery from a slim-tube simulation for a 7-components EOS compared to a 15-components EOS at operating pressure of 6500, which is close to miscible condition

Appendix C – trapped gas saturation and hysteresis effect

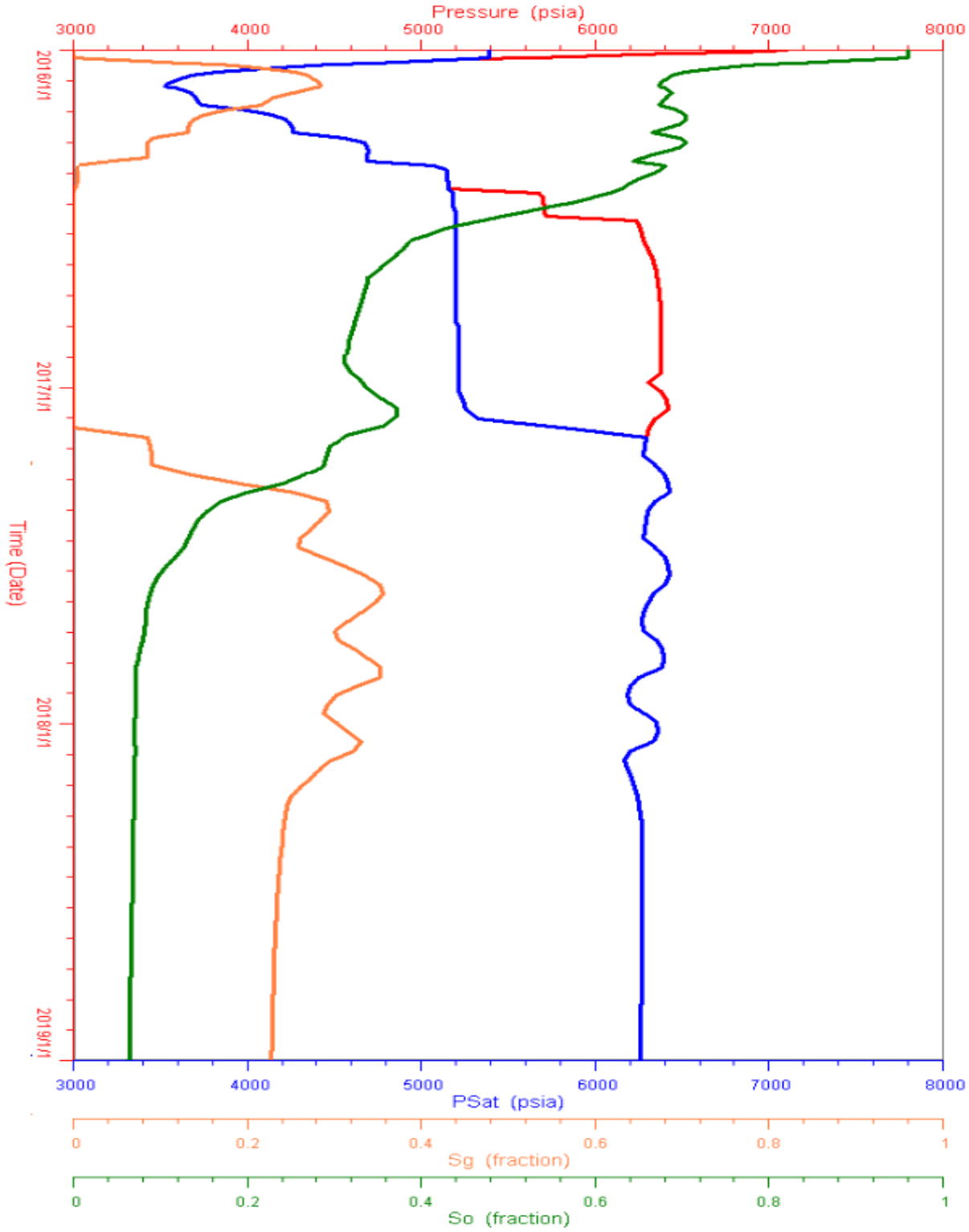

Oil saturation, gas saturation, pressure and oil saturation pressure as a function of time in reference grid block (18,1,18) of the homogeneous matrix model for a run with input trapped gas of 0.35

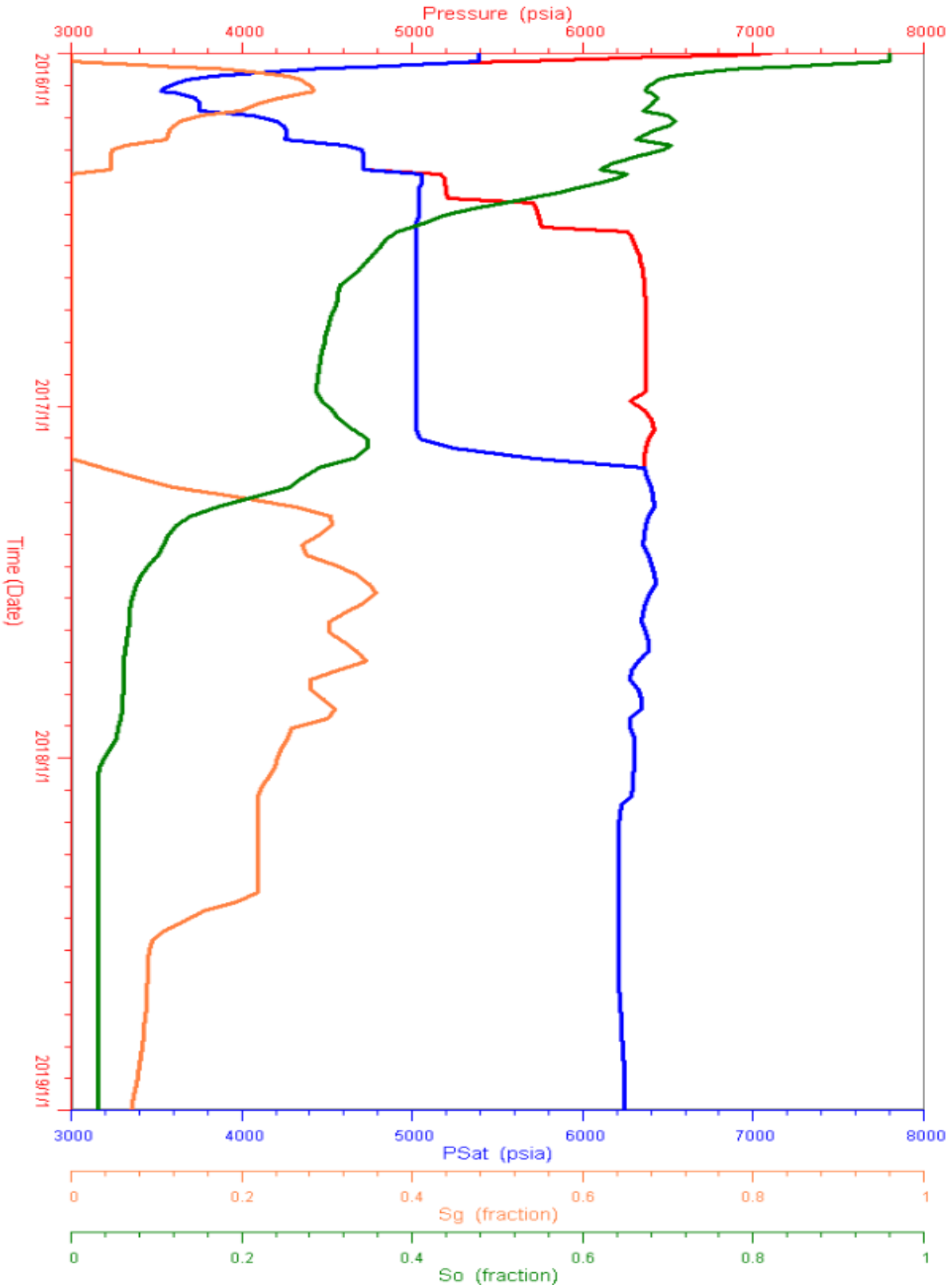

Oil saturation, gas saturation, pressure and oil saturation pressure as a function of time in reference grid block (18,1,18) of the homogeneous matrix model for a run with negligible trapped gas saturation

Appendix D – sector model

WAG-ratio

Year	Sales Oil	Sales Net gas	Sales NGL	Sales BOE	Fuel	Cumulative BOE sale
	BBL/yr [1000s]	SCF/yr [millions]	BBL /yr [1000s]	BBL/yr [1000s]	SCF/yr [millions]	BBL [1000s]
2012	419,06	-6000,17	-220,81	-914,7	106,91	-914,7
2013	360,1	-320,93	-12,64	260,23	97,35	-654,47
2014	593,89	-2145,28	-85,45	42,97	194,16	-611,5
2015	444,9	194,31	7,45	441,69	93,69	-169,81
2016	479,15	-1866	-72,2	-46,72	171,89	-216,53
2017	487,02	625,74	24,86	576,45	100,02	359,92
2018	394,22	425,69	16,69	481,87	39,51	841,79
2019	475,39	463,25	18,87	571,47	46,86	1413,26
2020	543,74	557,25	22,28	658,89	54,03	2072,15
2021	590,52	563,06	22,57	706,93	60,8	2779,08
2022	631,59	616,44	25,04	759,37	75,18	3538,45
2023	655,38	582,6	23,41	775,89	80,69	4314,34
2024	676,93	579,19	23,19	796,65	89,22	5110,99
2025	681,67	574,12	23,14	800,5	109,67	5911,49
2026	690,5	591,33	24,68	813,74	125,32	6725,23
2027	703,85	597,17	26,03	829,4	155,93	7554,63
2028	716,7	614,61	27,38	846,51	193	8401,14
	9544,61	-3347,61	-105,5	8401,15	1794.24	

Calculation of BOE to sale for the WAG ratio 1:2 case

Year	Sales Oil	Sales Net gas	Sales NGL	Sales BOE	Fuel	Cumulative BOE sale
	BBL/yr [1000s]	SCF/yr [millions]	BBL /yr [1000s]	BBL/yr [1000s]	SCF/yr [millions]	BBL [1000s]
2012	419,06	-6000,17	-220,81	-914,7	106,91	-914,7
2013	356,87	818,46	32,24	504,66	98,02	-410,04
2014	273	-2368,14	-94,33	-259,17	50,56	-669,21
2015	599,78	-1213,67	-46,56	214,36	190,45	-454,85
2016	353,54	895,07	34,63	537,35	48,9	82,5
2017	359,76	-2167,95	-86,12	-170,31	90,27	-87,81
2018	506,41	11,84	0,46	410,91	153,92	323,1
2019	376,89	370,03	15,07	453,64	37,2	776,74
2020	333,98	347,94	13,91	405,88	33,28	1182,62
2021	461,19	441,57	17,7	552,49	47,51	1735,11
2022	527,44	479,92	19,5	626,92	62,07	2362,03
2023	573,82	576,02	23,14	692,96	72,07	3054,99
2024	615,02	577,28	23,12	734,35	82,25	3789,34
2025	647,22	658,38	26,54	783,49	107,34	4572,83
2026	656,08	577,64	24,11	776,46	119,57	5349,29
2027	655,87	591,06	25,76	780,14	146,67	6129,43
2028	659,82	591,59	26,35	784,77	178,93	6914,2
	8375,75	-4813,13	-165,27	6914,19	1625,92	

Calculation of BOE to sale for the WAG ratio 1:1 case

Year	Sales Oil	Sales Net gas	Sales NGL	Sales BOE	Fuel	Cumulative BOE sale
	BBL/yr [1000s]	SCF/yr [millions]	BBL /yr [1000s]	BBL/yr [1000s]	SCF/yr [millions]	BBL [1000s]
2012	419,06	-6000,17	-220,81	-914,7	106,91	-914,7
2013	356,87	818,46	32,24	504,66	98,02	-410,04
2014	218,32	204,47	8,14	260,55	25,53	-149,49
2015	181,25	155,02	5,95	213,04	19,17	63,55
2016	396,86	-3635,74	-140,67	-473,46	109,62	-409,91
2017	531,04	498,98	19,82	564,52	136,8	154,61
2018	290,74	276,69	10,85	347,71	28,51	502,32
2019	259,32	225,32	9,18	306,05	25,10	808,37
2020	297,28	-2220,41	-88,77	-219,27	48,22	589,1
2021	530,54	-818,56	-32,82	213,72	182,7	802,82
2022	397,64	906,89	36,84	585,63	57,98	1388,45
2023	289,71	275,43	11,07	346,68	36,05	1735,13
2024	274,76	255,4	10,23	327,55	36,69	2062,68
2025	344,73	343	13,83	415,73	56,95	2478,41
2026	459,92	429,52	17,93	549,43	84,61	3027,84
2027	519,31	495	21,57	623,38	117,2	3651,22
2028	557,23	568,29	25,31	677,26	154,41	4328,48
	6324,59	-7222,41	-260,11	4328,47	1324.49	

Calculation of BOE to sale for the WAG ratio 2:1 case

Year	Sales Oil	Sales Net gas	Sales NGL	Sales BOE	Fuel	Cumulative BOE sale
	BBL/yr [1000s]	SCF/yr [millions]	BBL /yr [1000s]	BBL/yr [1000s]	SCF/yr [millions]	BBL [1000s]
2012	419,06	-6000,17	-220,81	-914,7	106.91	-914,7
2013	356,87	818,46	32,24	504,66	98.02	-410,04
2014	218,32	204,47	8,14	260,55	25.53	-149,49
2015	181,25	155,02	5,95	213,04	19.17	63,55
2016	185,05	152,92	5,92	216,46	19.70	280,01
2017	203,2	161,5	6,42	236,54	20.34	516,55
2018	216,63	169,81	6,66	251,59	20.63	768,14
2019	306,91	-3370,07	-137,28	-473,48	53.33	294,66
2020	616,63	-145,51	-5,82	471,9	170.24	766,56
2021	331,18	377,07	15,12	409,14	35.19	1175,7
2022	275,17	239,39	9,72	324,8	32.15	1500,5
2023	269,54	229,44	9,22	317	32.97	1817,5
2024	266,76	224,26	8,98	313,12	35.07	2130,62
2025	259,74	217,5	8,77	304,76	41.75	2435,38
2026	252,42	211,63	8,83	296,52	45.66	2731,9
2027	343,92	-2872,15	-125,17	-289,05	160.11	2442,85
2028	515,73	-68,73	-3,06	476,06	468.49	2918,91
	5218,4	-9295,18	-366,17	2918,89	1385.28	

Calculation of BOE to sale for the WAG ratio 4:1 case

WAG slug sizes

Year	Sales Oil	Sales Net gas	Sales NGL	Sales BOE	Fuel	Cumulative BOE sale
	BBL/yr [1000s]	SCF/yr [millions]	BBL /yr [1000s]	BBL/yr [1000s]	SCF/yr [millions]	BBL [1000s]
2012	330,59	-3449,96	-126,96	-429,63	59,53	-429,63
2013	347,08	-2799,91	-110,31	-303,05	115,74	-732,68
2014	396,24	-1974,63	-78,65	-57,88	75,94	-790,56
2015	470,06	609,56	23,38	557,44	97,29	-233,12
2016	459,80	-1350,97	-52,27	82,85	130,40	-150,27
2017	419,00	-1839,61	-73,08	-38,93	96,02	-189,20
2018	446,56	-549,10	-21,53	294,49	72,04	105,29
2019	527,64	510,97	20,81	564,47	124,53	669,76
2020	499,13	-1013,48	-40,52	193,50	126,22	863,26
2021	449,47	-1221,14	-48,96	135,41	80,21	998,67
2022	473,39	840,58	34,15	605,91	114,15	1604,58
2023	312,40	330,27	13,27	380,72	39,59	1985,30
2024	282,56	287,74	11,52	342,03	38,31	2327,33
2025	262,79	264,76	10,67	317,59	43,51	2644,92
2026	244,26	242,30	10,11	294,76	45,39	2939,68
2027	232,13	243,87	10,63	283,40	53,28	3223,08
2028	226,72	244,27	10,88	278,31	63,46	3501,39
	6379,82	-10624,46	-406,85	3501,40	1375,59	

Calculation of BOE to sale for the case of 0.05 pore volumes slug sizes

Year	Sales Oil	Sales Net gas	Sales NGL	Sales BOE	Fuel	Cumulative BOE sale
	BBL/yr [1000s]	SCF/yr [millions]	BBL /yr [1000s]	BBL/yr [1000s]	SCF/yr [millions]	BBL [1000s]
2012	419,06	-6000,17	-220,81	-914,70	106,91	-914,70
2013	356,87	818,46	32,24	504,66	98,02	-410,04
2014	273,00	-2368,14	-94,33	-259,17	50,56	-669,21
2015	599,78	-1213,67	-46,56	214,36	190,45	-454,85
2016	353,54	895,07	34,63	537,35	48,90	82,50
2017	359,76	-2167,95	-86,12	-170,31	90,27	-87,81
2018	506,41	11,84	0,46	410,91	153,92	323,10
2019	376,89	370,03	15,07	453,64	37,20	776,74
2020	463,85	-2338,89	-93,51	-141,78	128,68	634,96
2021	544,14	676,59	27,13	608,95	135,97	1243,91
2022	373,47	379,55	15,42	452,15	44,76	1696,06
2023	313,85	297,77	11,96	375,44	39,05	2071,50
2024	298,67	269,14	10,78	354,31	39,68	2425,81
2025	287,81	259,00	10,44	341,41	46,77	2767,22
2026	273,55	245,74	10,26	324,76	50,01	3091,98
2027	268,99	255,04	11,12	322,61	60,65	3414,59
2028	268,51	261,88	11,16	323,82	73,83	3738,41
	6338,17	-9348,72	-350,15	3738,41	1395,65	

Calculation of BOE to sale for the case of 0.10 pore volumes slug sizes

Year	Sales Oil	Sales Net gas	Sales NGL	Sales BOE	Fuel	Cumulative BOE sale
	BBL/yr [1000s]	SCF/yr [millions]	BBL /yr [1000s]	BBL/yr [1000s]	SCF/yr [millions]	BBL [1000s]
2012	419,06	-6000,17	-220,81	-914,70	106,91	-914,70
2013	475,46	-1675,02	-65,99	26,95	213,52	-887,75
2014	657,35	359,59	14,32	671,80	171,10	-215,95
2015	294,44	283,49	10,88	352,57	31,73	136,62
2016	208,78	189,83	7,34	247,77	22,55	384,39
2017	342,12	-2447,80	-97,23	-242,18	79,61	142,21
2018	528,00	-974,84	-38,23	197,51	175,51	339,72
2019	572,80	-712,66	-29,03	286,69	180,00	626,41
2020	525,87	1103,96	44,14	732,82	84,38	1359,23
2021	323,48	293,69	11,77	384,20	33,04	1743,43
2022	286,09	266,62	10,83	341,36	33,79	2084,79
2023	274,78	240,71	9,67	324,57	33,76	2409,36
2024	280,67	244,67	9,80	331,24	37,10	2740,60
2025	274,40	244,17	9,84	324,93	44,52	3065,53
2026	262,91	232,52	9,70	311,36	47,95	3376,89
2027	252,60	231,21	10,08	301,22	56,63	3678,11
2028	246,95	222,58	9,91	293,96	67,02	3972,07
	6225,75	-7897,46	-293,00	3972,07	1419,12	

Calculation of BOE to sale for the case of 0.20 pore volumes slug sizes

Year	Sales Oil	Sales Net gas	Sales NGL	Sales BOE	Fuel	Cumulative BOE sale
	BBL/yr [1000s]	SCF/yr [millions]	BBL /yr [1000s]	BBL/yr [1000s]	SCF/yr [millions]	BBL [1000s]
2012	419,06	-6000,17	-220,81	-914,7	106,91	-914,7
2013	475,46	-1675,02	-65,99	26,95	213,52	-887,75
2014	670,48	-1030,82	-41,06	352,58	219,43	-535,17
2015	544,41	-827,41	-31,74	240,94	189,39	-294,23
2016	573,57	-964,1	-37,3	238,96	190,41	-55,27
2017	678,08	1241,93	49,33	896,34	125,42	841,07
2018	392,17	343,31	13,46	462,85	37,95	1303,92
2019	270,75	245,18	9,99	321,6	26,37	1625,52
2020	253,67	230,91	9,00	301,38	24,71	1926,9
2021	258,32	230,24	9,23	305,93	26,31	2232,83
2022	267,16	239,18	9,72	316,74	31,36	2549,57
2023	274,14	244,87	9,84	324,79	33,78	2874,36
2024	272,68	229,15	9,18	320,05	35,85	3194,41
2025	260,56	215,05	8,67	305,07	41,79	3499,48
2026	250,27	205,61	8,58	293,12	45,14	3792,6
2027	244,9	211,65	9,22	289,39	54,41	4081,99
2028	240,47	212,66	9,47	285,38	65,07	4367,37
	6346,16	-6647,8	-240,98	4367,38	1467,84	

Calculation of BOE to sale for the case of 0.40 pore volumes slug sizes